8-2021

Effect of Additional Weight on Stability of Human Squat Exercise

Jose De Jesus Galarza Lozano
The University of Texas Rio Grande Valley

EFFECT OF ADDITIONAL WEIGHT ON STABILITY OF HUMAN SQUAT EXERCISE

A Thesis

by

JOSE DE JESUS GALARZA LOZANO

Submitted to the Graduate College of
The University of Rio Grande Valley
In partial fulfillment of the requirements for the degree of

MASTER OF SCIENCE IN MECHANICAL ENGINEERING

August 2021

Major Subject: Mechanical Engineering

EFFECT OF ADDITIONAL WEIGHT ON STABILITY OF HUMAN SQUAT EXERCISE

A Thesis
by
JOSE DE JESUS GALARZA LOZANO

COMMITTEE MEMBERS

Dumitru I. Caruntu, PhD, PE
Chair of Committee

Alley Butler, PhD
Committee Member

Robert Freeman, PhD
Committee Member

Paul Choi, PhD
Committee Member

August 2021

ABSTRACT

Galarza, Jose, Effects of Additional Weight on Ground Reaction Forces and Center of Pressure for Human Squat Exercise. Master of Science in Engineering (MSE), August, 2021, 111 pp., 2 tables, 166 figures, 74 references, 37 titles.

The main focus of the study is to analyze the stability of the squat exercise. The squat is a human common exercise. The study analyzes the time series of the normal component of the ground reaction forces, each coordinate of the center of pressure, and knee flexion angle. Theses time series are used to estimate the Lyapunov Exponents using Rosenstein method. MATLAB from Mathworks is used to calculate the graphs and program the methods. We compare this result with the literature and previous experiments. This work gives more information relating the safety of the squat exercise when adding additional weight.

DEDICATION

I would like to dedicate this work to my family which were very supportive. My father Jesus Galarza and my mother Anita Galarza.

ACKNOWLEDGMENT

I would like to thank my advisor Dr. Dumitru Caruntu for all the advice and guidance for this research. He taught me to become a better engineer and professional researcher. Thanks to his mentorship is that I was able to finish.

TABLE OF CONTENTS

Page

LIST OF TABLES

Page

LIST OF FIGURES

Page

CHAPTER I

INTRODUCTION

Human gait and stability has been the focus of studies in the past. Instability has been associated with variability and how the system will never make the same movement [1]. Here we defined that stability is the inverse rate of divergence of two trajectories. This definition is called local stability and the measure used are the Largest Lyapunov Exponent. Lyapunov Exponents are the exponential rate of divergence of neighboring trajectories which is used to measure local stability. Recent studies focus on understand how gaits differ in healthy subjects [1], how age affects the stability of the gait [2] or how the stability of the walking gait is affected by a treadmill [3].

It has been observed that the cycle-to-cycle motion has inherent variability. Stergiou et al. [1] in their paper discussed and reviewed several points of view were the previous paradigm tells us that variability in general was associated with instability in dynamical systems. However, Dingwell et al. [3], also discussed that there are various cases which the variability is in fact better for a stable movement, this being observed in professional athletes and in learning of movement experiments. The case of elderly people or neuropathic patients has reduced variability from the normal variable data taking from the walking measurements, and the increase of variability results in a fall. In this sense, there is a view that for an optimal movement there should be certain amount of variability.

Stergiou et al. [1] stated that variability on the movement and stability are related. However, they stated that it is preferable to see variability as adaptability of the system and not noise. Dingwell et al. [3] commented that variability could be chaotic in nature and would be corrective adjustments to maintain the movement and balance of the gait. Emmerik et al. [4] explains that variability appears in healthy subjects. Cavanaugh et al. [5] summarizes these points in his paper, see Table 1.

Table 1 Cavanaugh's [5] summary of most important points.

Characteristic	Linear model	Nonlinear model
Paradigm	Stimulus response	Self-organisation
Degree of postural control reflected in the output signal	Predicted based on input (perturbation) parameters and known linear relationships among system components	Dependent on initial conditions and nature of multi-linked interactions among system components. Predicted over various time scales
Signal variability	Random error	Can contain temporal structure that reflects the organisation of the underlying control system
Measurement implications	Error magnitude is proportional to the intensity of the perturbation or the severity of disruption in the feedback loop	Error magnitude is irrelevant. Temporal structure is measured as patterns of variability

In this sense we can say that variability is in a sense necessary in order to have an optimum movement. Stergiou et al. commented that is preferable to see it as the adaptability of the system. Dingwell et al. in [3] commented that it is important to see that this variability is not noise, instead we need to see them as corrective adjustments which were created to maintain the balance and the ongoing movements of the gait. So, it is important not to discard that this variability in the movement could be chaotic in nature [3], and further study is needed. On a related commentary, Emmerik et al. emphasizeed that varialibility should not be regarded as instability, as variability inherently appears in healthy subjects as an example in Fig. 1, [4].

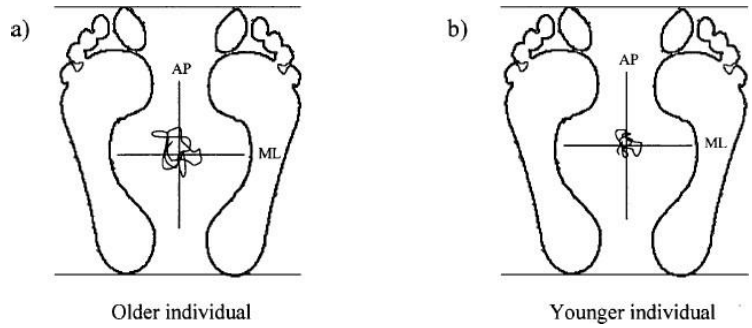

Figure 1 Emmerik's [4] example of the center of pressure between a healthy adult a) and a healthy younger subject b)

Frequency couplings as defined by Van Emmerik et al. [6] is the ratio of two different movements, for example breathing rhythm and breathing rhythm. In the review Van Emmerik made [6] one can see the relationship of the number of breaths taken by the runner per stride. These frequency couplings have ratios like 1:1,2:1,3:1, etc. These frequency couplings for an overall speed can be seen in Fig. 2. Stability in this case in his study is a prefer coupling, in particular 2:1 in which the runners (R1 and R4) tend to adopt in contrast to the non runner (NR1).

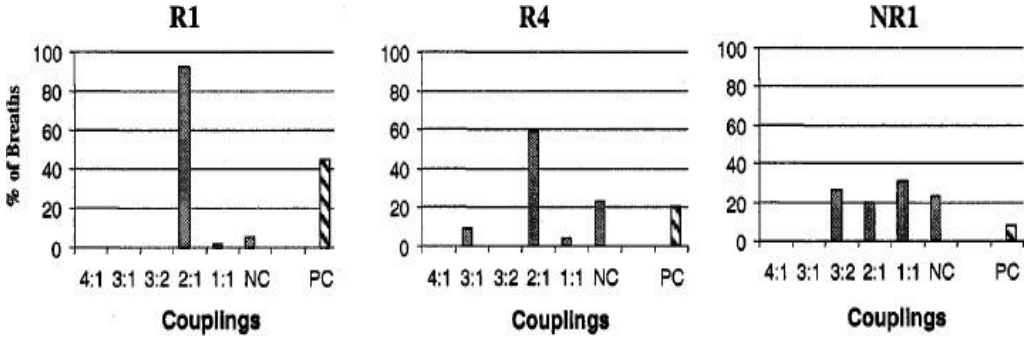

Figure 2 Van Emmerik's [6] results of the difference between frequency couplings of runner 1 (R1), runner 2 (R4) and a non runner (NR1)

The approximate entropy (ApEn) is another parameter that is used to quantify the regularity of a time series [1]. Cavanaugh et al [5] explained the ApEn algorithm, which gives you a dimensionless parameter that estimates the probability of a time series to repeat itself..

Dingwell et al. [7] investigated the stability of walking on a treadmill. The result were conclusive, it does increase stability. They reported a decrease of Lyapunov Exponents values, which means that walking in a treadmill actually makes walking more stable. Notice that every subject choose their own speed they were they felt comfortable. Interesting enough, now the question is, does this in general work for all different range of subjects and treadmills.

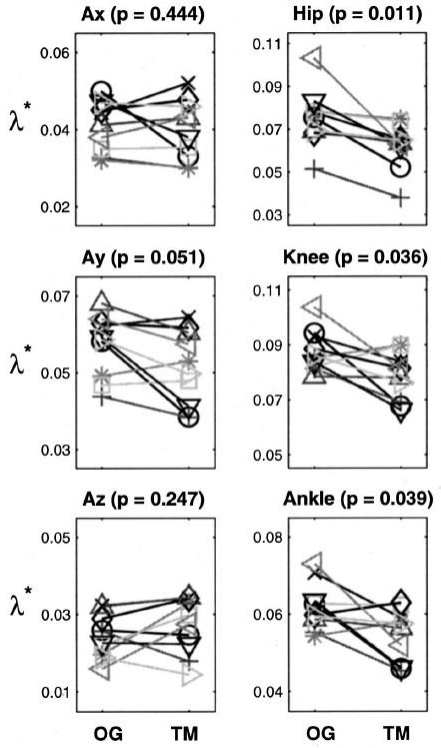

Figure 3 Dingwell's [7] value comparison of the LyEs with normal walking (OG) and treadmill walking (TM).

In another interesting subject was: does age affect the stability of the Gait? This question was the topic of research of the teams Buzzi and Lochckhart [2, 8]. Dingwell et al. [9] demonstrate that patients with Neuropathic disease tend to have slower speeds to maintain local

stability in walking. Also, as the speed increases the stability decreases as demonstrated by Dingwell et al. [10].

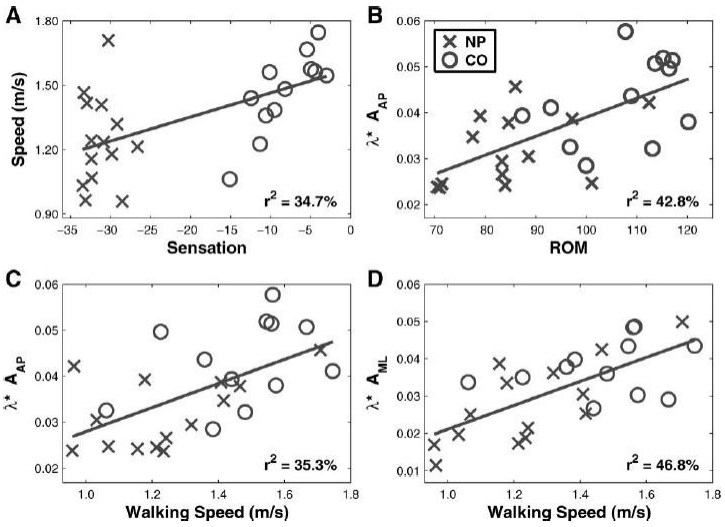

Figure 4 Dingwell's [9] values on LyE for Neuropathic patients (NP) and control (CO) subjects.

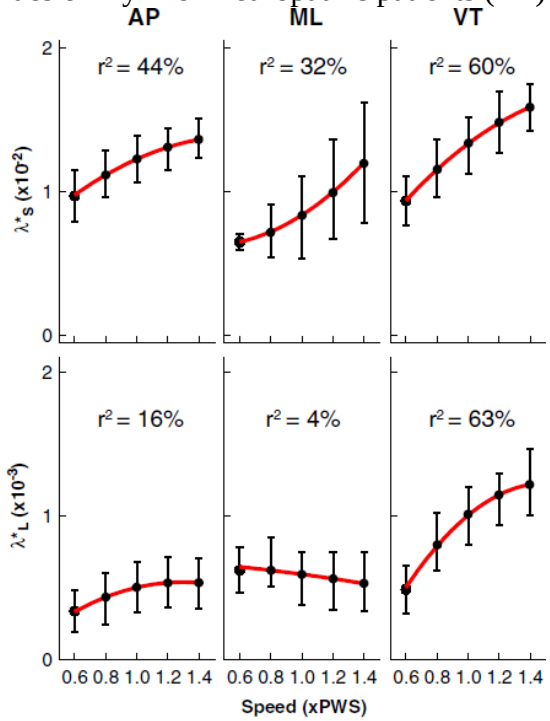

Figure 5 Dingwell's [10] result in Lyapunov Exponents values as speed changes.

In this work we investigate the effect of added weight on the stability of the human squat exercise. A similar study done by Zink et al. [11] measured the mean myoelectric activity on the muscles of the leg. The novelty of the present investigation is that the Largest Lyapunov Exponent of the normal ground reaction forces and coordinates of the center of pressure are used to assess the stability of the squat exercise. The cases to be studied are no additional weight, and additional weights of 10, 20, and 32 kg. This study can give qualitative insight on how safe the exercise is performed with added weight.

CHAPTER II

METHODOLOGY

Data Acquisition

The data acquisition system in the lab are 10 Vicon Cameras and 2 AMTI OR6 Series Force Plates as in Fig. 6. The cameras need to be calibrated each time with the Vicon system is turned on. The force plates are used to capture the ground reaction forces during the exercise. The software that is used to obtain the center of pressure's coordinates is software Nexus.

Figure 6 Vicon Cameras and Force plates setup.

The subject is positioned as seen in Fig. 7. The subject for the trials has a height of 1.70 meters and a mass of 77 Kg. The origin of the global coordinate system is positioned in the posterior and lateral corner (with respect to the subject) of the plate of the right foot of the subject.

Figure 7 Subject on the force Plates.

Data Filtering

The double pass Butterworth filter will be used as in previous studies, Caruntu et al. [12] The formulas used are as follows.

$$\omega = \frac{tan\frac{\pi f_c}{f_s}}{c},\ K = \sqrt{2}\omega,\ K_2 = \omega^2,\ K_3 = \frac{2a_0}{K_2} \tag{1}$$

$$a_0 = \frac{K_2}{(1+K+K_2)},\ a_1 = 2a_0,\ a_2 = a_0 \tag{2}$$

$$b_1 = -2a_0 + K_3,\ b_2 = 1 - 2a_0 + K_3 \tag{3}$$

The process is to first calculate the parameter ω, in which f_c is the cutoff frequency and f_s is the sampling frequency in which in our case is 1000 Hz for force plates and a correction

factor C = 0.802. The Cutoff frequency can be sought between 1 and 15Hz. The residuals are calculated in accordance to Winter et al.[13] in order to filtered out the noise. Equations 1-3 give the coefficients $a_0, \dots, b_2$. Having these coefficients the following formula is used:

$$X^1(nT) = a_0X(nT) + a_1X(nT - T) + a_2X(nT - 2T) + b_1X^1(nT - T) + b_2X^1(nT - 2T) \quad (4)$$

where X^1 filtered output coordinates, X unfiltered data coordinates, nT is the nth sample, $(nT - T)$ is (n-1)th sample, $(nT - 2T)$ is the (n-2)th sample and $a_0 \dots b_2$ are the filter coefficients as already mentioned [13] The Root Mean Square Error (RMS) of the residuals are calculated as follows:

$$RMS = \sqrt{\frac{1}{N}\sum_{i=1}^{N}(X_i - \widehat{X}_\iota)^2} \quad (5)$$

where X_i ith value of the sample and $\widehat{X}_\iota$ is the filtered data ith value of the sample.

Stability Analysis

Stability of a movement has been a focus of study for several years. Orbital stability has been used in the past by Hurmuzlu and Basdogan [14]. They used Floquet multipliers (eigenvalues of the Jacobian Matrix) for analyzing the system of equations and by Dingwell et al., [15]. This work used the Largest Lyapunov Exponent.

Stability can be measured as the inverse rate of the average exponential rate divergence in a trajectory, Stegiou [1,2] and Dingwell et al. [3,9]. The formal definition can be seen in this papers. The state space reconstruction is done from the data obtained experimentally [9]. As such the state space can be defined as:

$$X(t) = [x(t), x(t + T), \dots, x(t + (d_E - 1)T] \quad (6)$$

where $X(t)$ is the d_E - dimensional state vector, with $x(t)$ one-dimensional data, T time delay, and d_E embedding dimension [13]. The time delay for the reconstruction can be chosen as the minimum of the mutual information function [16]. However, one should analyze ranges in order to choose an appropriate time delay. For the embedding dimension we can use the Kenel et al. approach [17]. We choose to use the embedding dimension of 3, since we have convergent results as recommended by Rosenstein [18] paper. From experiments the mean separation or divergence $d(t)$ calculated from the neighboring points in the state space is as follows

$$d(t) = d_0 e^{\lambda_1 t} \tag{7}$$

For a positive time the two neighboring points will exponentially diverge at a rate λ_1.
The distance of the nearest neighbors given by Rosenstein [18], is defined as:

$$d_j(i) = \min_{X_k} \|X_j - X_k\| \tag{8}$$

One finds the minimum distance between point X_j and points X_k and call it $d_j(i)$ at time , where the absolute value of the difference between j and k needs to be greater that the mean period.

$$|j - k| > \text{mean period} \tag{9}$$

The idea is that we record these distances as such the distances should diverge according to:

$$d_j(i) \approx C_j e^{\lambda_1 (i \cdot \Delta t)} \tag{10}$$

The idea is to get the least square regression line in the most linear part of the curve defined as:

$$y(i) = \frac{1}{\Delta t}\langle \ln d_j(i) \rangle \tag{11}$$

where $\langle \cdot \rangle$ denotes the averages across all j. The slope that is defined in Rosenstein method at the end of the algorithm is a topic that need to be discussed We are going to show how some authors tackle with the problem, since it is not defined.

Rosenstein ended his algorithm stating that you can obtain the Lyapunov Exponent via taking the slope of least regression line vs time in his paper. The idea is to try to choose a good linear region. Rosenstein explains that a range between $0.6 \leq i\Delta t \leq 1.6$ or in other words in between 600 and 1600 time steps. However this only true for the Lorentz attractor and in this range our data set reaches plateau. As such it leaves open to choose.

In order to check our results, we will also use Wolf's algorithm . The algorithm is similar to Rosenstein in which you need to use the reconstructed state space. The algorithm states that you follow a reference trajectory and measure the divergence of the nearest neighbor. The first step is to find the distance between the point and the nearest neighbor. After some fixed time that you choose, call the evolution time, we calculate the distance again. This divergence between these two distances is measured. The procedure is then repeated picking a new nearest neighbor and doing the previous steps.

$$\lambda_1 = \frac{1}{T_{\mathrm{M}} - T_0}\sum_{k=0}^{n} \log_2 \frac{L'_{k+1}}{L_k} \tag{12}$$

where M is the total number of time steps performed. L_k is the distance to the nearest neighbor and L'_{k+1} is the distance to the nearest neighbor after a fixed time.

Dingwell et al. [3, 9] choose to calculate the Lyapunov Exponent using Rosenstein method between 4 and 10 strides for all curves. A stride is approximately .83 seconds. The explanation is that around this range for all curves it is more linear. However in Refs. [7, 9-10, 15, 19], Dingwell et al. changed the interval for which he calculates Lyapunov Exponents in between 0-1 strides and also 4-10 strides.

Bruijin et al. [20] changed the range to fit his data, expressing that his data clearly non-linear after 75 samples. He changed the range to calculate the Lyapunov Exponent to between approximately 0 to 50 time steps, or in other words between 0 to 0.5 strides. Stating that the curve is different, there was a need to change the range in order to get a more linear part of the curve. Graham [22,23] uses this approach as well.

This strategies can change. Look et al. [21] commented that depending of the gait, they cannot use the previous criteria. Their plateau of the divergence curve was reached in between 11 and 20 time intervals or 0.033 and 0.067 seconds. This on average a stride is 18 times larger than that, as such they choose depending on the geometry and not a fixed interval as the case of Dingwell [8, 10-11, 15, 19], Bruijin [20] and Graham et al. [22,23]. Similarly, Lee et al. [24] had the same approach.

Regarding choosing of the slope, one takes into consideration the signal-to-noise ratio (SNR). This was defined with several other alternatives first by Box et al. [25] and later on more detail by Haralick et al. [26] as follows:

$$SNR = 10 \log_{10}\left(\frac{\mu^2}{\sigma^2}\right) \tag{13}$$

where μ is the mean of the signal, and σ is the standard deviation of the noise. We see that this has been used before in different studies to quantify noise as an example in Alexander et al. [27] MR images and Ducros' work on tomography [28]. The reasoning behind this is that we need to

choose a suitable cutoff frequency since the filtering alters the log divergence curve. This affect the calculation of the Lyapunov Exponent since it depends on the Least Square Regression Line. The effect of the filtering on the log divergence curve can be seen in Figs. 8 and 9. One can see that the initial section of the curve with low cutoff frequency will tend to be more non-linear than at higher frequencies. In fact, one can see how the curves will try to converge to the unfiltered divergence curve which is what is expected since at higher frequencies there is almost not noise filtered.

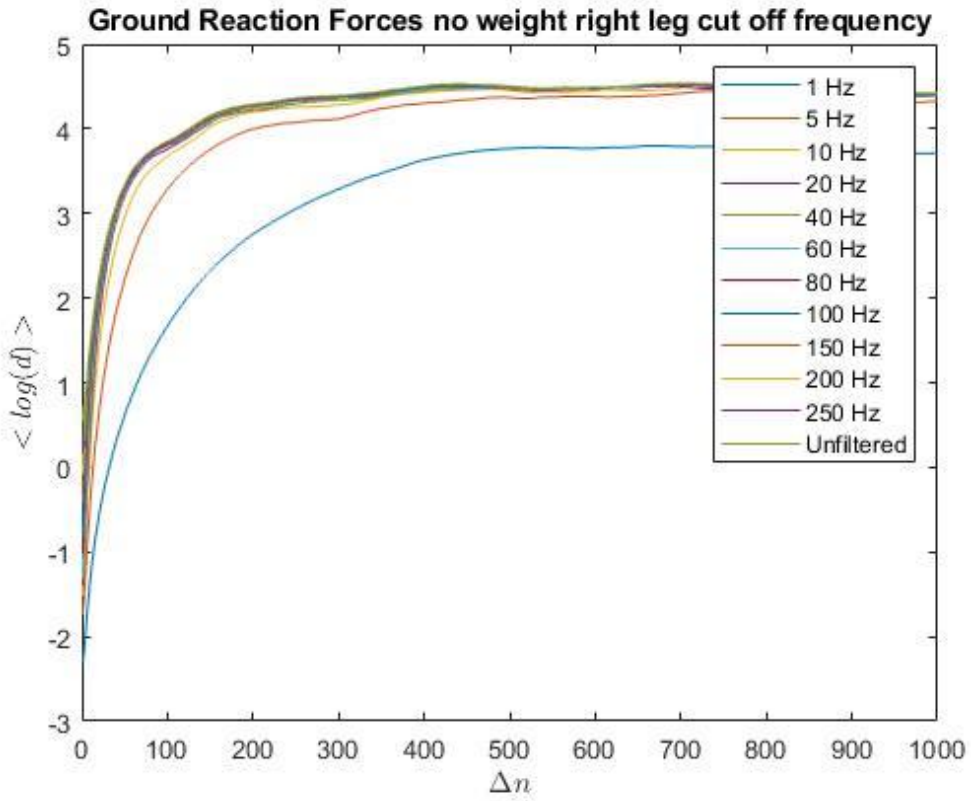

Figure 8 Ground Reaction Forces no weight right leg divergence curves filtered at high cut off frequencies (1-250 Hz).

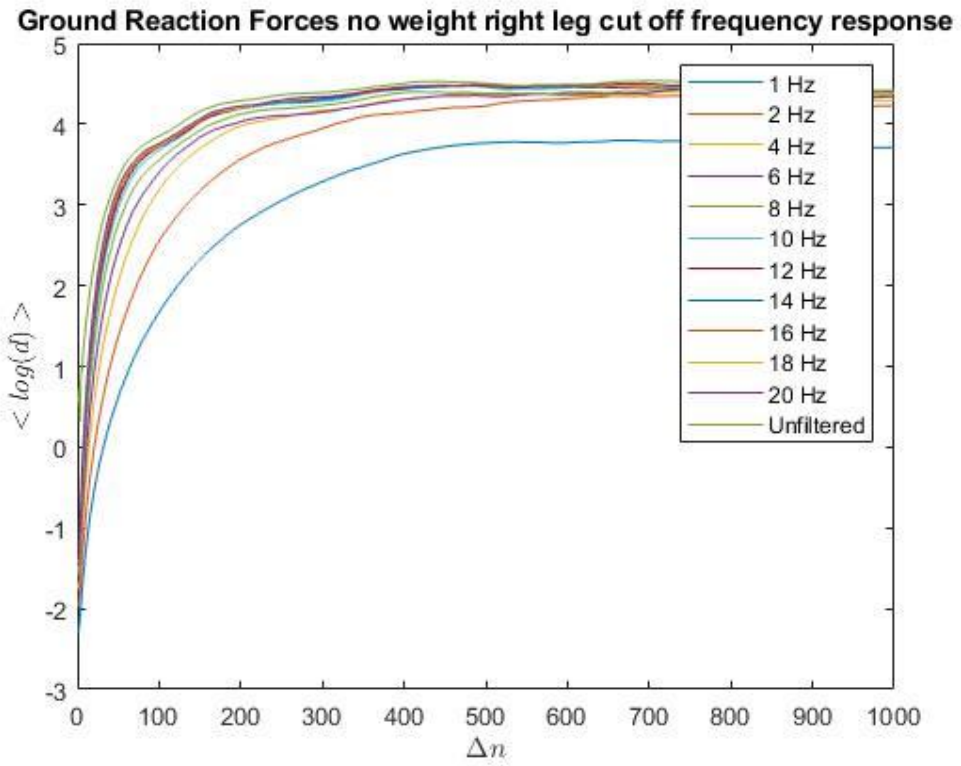

Figure 9 Ground Reaction Forces no weight right leg divergence curve per cut off frequency (1-20 Hz).

We notice that as n is large the Root Mean Square Error (RMSE) method of Winter [13] can be associated with the SNR. This can also be seen for example in Fig. 10 where the square of the RMS and the SNR for the case of ground reaction forces are plotted.

$$\sigma^2 = \frac{1}{n-1}\sum_{1=1}^{n}(x_i - \hat{x}_i)^2 \approx \frac{1}{n}\sum_{1=1}^{n}(x_i - \hat{x}_i)^2 = RMS^2 \tag{14}$$

$$SNR = 10\log_{10}\left(\frac{\mu^2}{\sigma^2}\right) \approx 10\log_{10}\left(\frac{\mu^2}{RMS^2}\right) \tag{15}$$

Noticing this relationship, we now see that we can apply a similar procedure from Winter and draw a line from the “linear part”. This is to get the correct cutoff frequency.

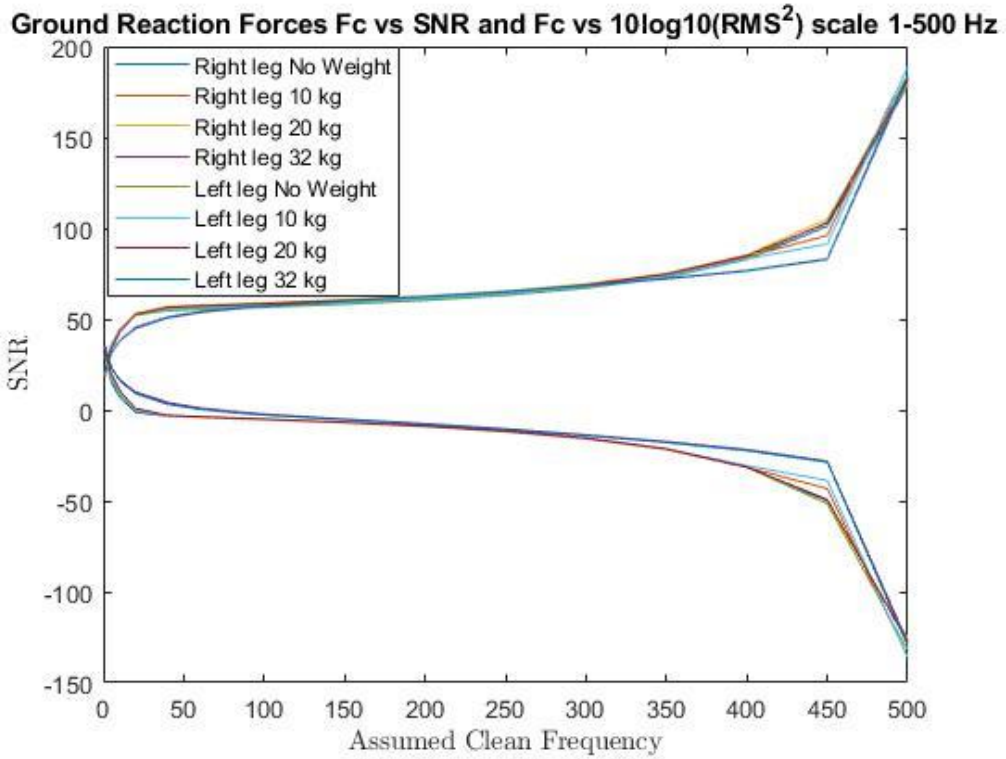

Figure 10 Ground Reaction Forces Fc vs SNR and Fc vs $10Log_{10}(RMS^2)$ for Ground Reaction Forces High Frequency.

However, in order to choose the segment we need to try to find the “most linear” part on our divergence curve. To do this, we choose the approach to get the best Pearson Correlation Coefficient. The Pearson’s correlation coefficient, sometimes simply called the correlation coefficient, describes the linear association between two variables. In this case we can use this coefficient to determine how linear a segment is. Onwuegbuzie [29] mentions that a correlation coefficient of 0.8 is often used and recommends 0.9. Schober [30] however mentions that a very strong linear association would be 0.9 or above. We can see that this in Fig. 11 in which this is

done so for the case of the ground reaction forces with no weight. This procedure is done for each case and we can see each filter frequencies in Table 2.

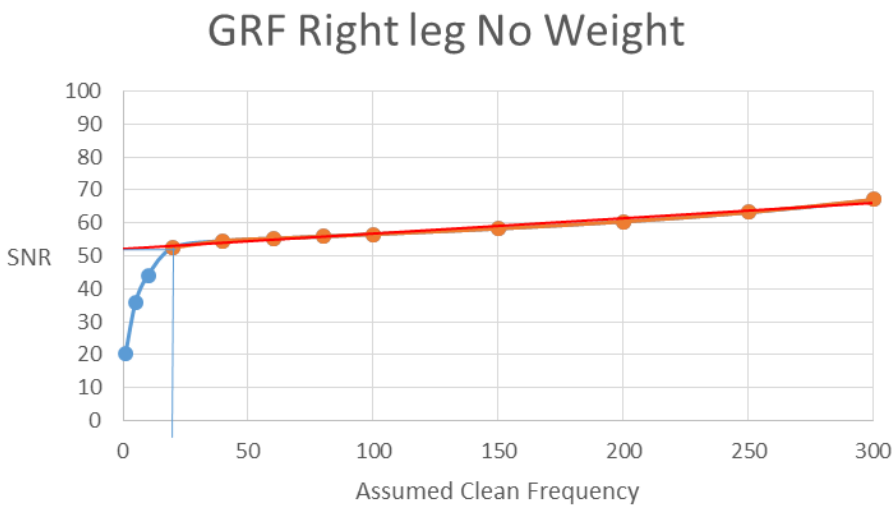

Figure 11 SNR vs Assumed Clean Frequency Ground Reaction Forces of right leg with no additional weight.

	NW	10kg	20kg	32kg
GRF Right	20	20	20	28
GRF Left	20	20	20	28
COPX Right	15	15	15	28
COPX Left	15	15	15	28
COPY Right	8	10	10	18
COPY Left	10	15	10	20

Table 2 Cutoff Frequencies for Filtering of Ground Reaction Forces and Center of Pressure

As such we are going to use segments from the initial part of the divergence curve that gives a correlation of 0.9. To do this, we fixed the starting point at the first point of the divergence curve. We then choose a point that is near the start of the saturation. If the correlation of this segment is bigger that 0.9 we use it to calculate the Lyapunov Exponent. If it's not, then change the end point to the preceding point and calculate again. This process is repeated until you get the segment with a correlation at or above 0.9 in order to calculate the Lyapunov

Exponent. We can see an example of the correlation line, Fig. 12, with correlation of 0.9 graphed in the same plot as the divergence curve. The curves of the other cases are in the Appendix A.

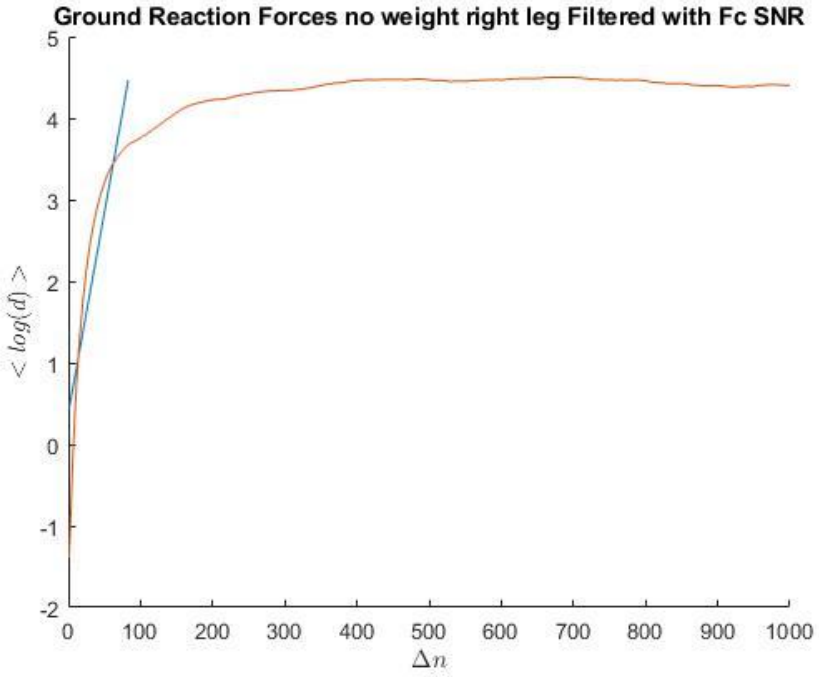

Figure 12 Divergence Curve of Ground Reaction Forces no weight right leg Filtered 0.9 Correlation Coefficient Regression Line.

Method Verification with stability of Treadmill and Overground Walking

We are going to check that the procedure with the Lyapunov Exponents is correct and consistent with the literature in order to make sure that the methodology is reliable.

Taking this into consideration we are going to check stability of treadmill walking and overground walking with another method to measure stability and compare it with the Lyapunov Exponent approach.

First attempts to measure the stability with Floquet Multipliers was done by Hurmuzlu and Basdogan [14]. They are used to measure orbital stability in which are the eigenvalues of the Jacobian (Floquet Multipliers) which measure how far apart the orbits are evolving. Is important

to notice that if the magnitude of the eigenvalues are less or equal to 1 that means that the orbits are stable [14]. Dingwell et al. used in Ref. [15] corroborated previous studies made in Refs. [3,9]. Hurmuzlu used a matrix for the state space representation of the system using position and velocities. Here, however we are going to use the approach that Dingwell et al. used. For Floquet Multipliers, we use the state space reconstruction that we used for the Lyapunov Exponent.

Let's call the state of the vector in the kth time as S_k. Let's define the average orbit S^* to be our stable fix behavior in which we are going to find our Jacobian Matrix. Thus we have the following relation [14, 15]:

$$S_{k+1} - S^* = J(S^*)[S_k - S^*] \tag{16}$$

Notice that we have a series of column vectors in this relationship with size d_E which is the embedding dimension. Thus it follows that $J(S^*) \in \mathbb{R}^{d_E \times d_E}$. Notice that we can define the following:

$$\boldsymbol{S_k} = \begin{bmatrix} S_k - S^* & S_{k+1} - S^* & \cdots & S_{k+d_E-1} - S^* & S_{k+d_E} - S^* \end{bmatrix} \tag{17}$$

$$\boldsymbol{S_{k+1}} = \begin{bmatrix} S_{k+1} - S^* & S_{k+2} - S^* & \cdots & S_{k+d_E} - S^* & S_{k+d_E+1} - S^* \end{bmatrix} \tag{18}$$

Thus we have the following:

$$\boldsymbol{S_{k+1}} = J(S^*)\boldsymbol{S_k} \tag{19}$$

Which then we can find the Jacobian as:

$$J(S^*) = \boldsymbol{S_{k+1}}\boldsymbol{S_k^{-1}} \tag{20}$$

With his we can obtain the eigenvalues. We use the α measure defined by Hurmuzlu in [9] as:

$$\alpha = \frac{1}{n}\sum_{i}^{n} |\lambda_i| \tag{21}$$

Here we tested the Floquet multipliers for Overground Walking and Treadmill Walking in order to verify that are consistent with the Lyapunov Exponent and with the study that Dingwell et al. [15].

The orbits were taken from the treadmill and overground walking knee flexion angle were the heel strike starts. As such we obtain the graphs as see in Figs 13 and 14. Is important to notice that the subject has a hernia between disk L5-S1. We took the state pace vector when the orbit is around 30% with an embedding dimension of 5 and a delay of 0.1 second. The α measure, i.e. the average of the absolute values of Floquet Multipliers, obtained from the data are *0.8879 for Treadmill Walking* and *0.9506 for Overground Walking*. *This indicates that the orbital stability of Treadmill Walking is higher than the Overground Walking.* This is in agreement with Dingwell et al. [15]. Also, we can see how the orbits are very consistent with each stride as seen in the previous figure.

The same investigation is conducted using Lyapunov Exponents, to compare the stability of Treadmill Walking and Overground Walking. One can see the divergence curves in Figs 15 and 16. The Lyapunov Exponents were taken from the 0.9 Regression Line of the linear part of the divergence curve. The *Lyapunov Exponents of the curves are 0.0205 for Treadmill Walking* and *0.0240 for Overground Walking. This indicates that the stability of Treadmill Walking is higher than the Overground Walking.* This is in agreement with the predictions from α measure obtained from Floquet Multipliers and data reported in the literature [15]. In other words, both Floquet Multipliers and Lyapunov Exponents predicted that treadmill walking is more stable than the Overground Walking for the knee flexion angle between heel strikes.

As such we will proceed analyzing the knee flexion angle of squatting using the Lyapunov Exponent method that was also verified with the Floquet Multipliers.

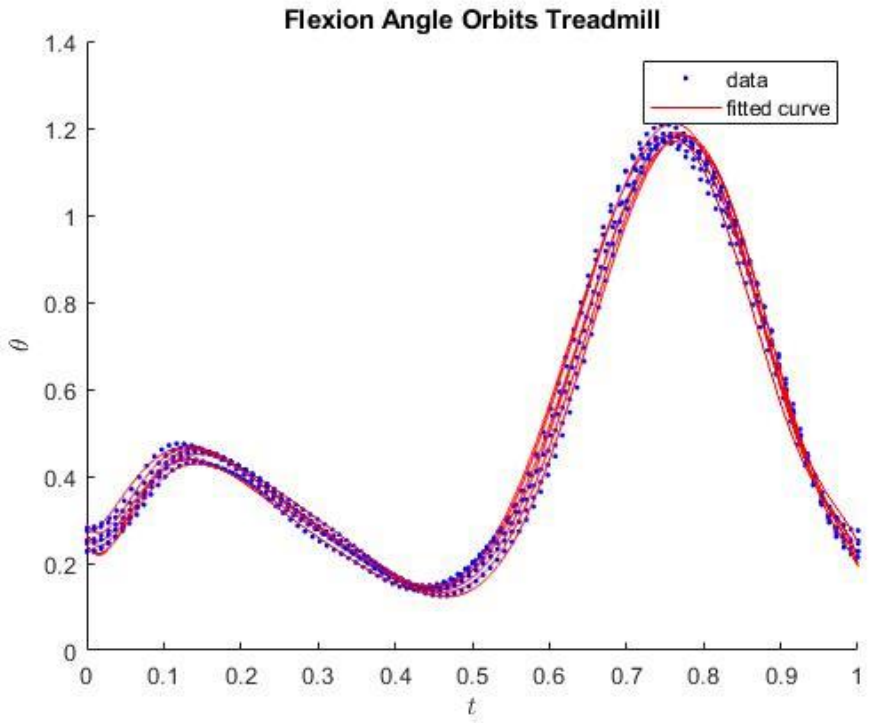

Figure 13 Flexion Angle Orbits walking over the treadmill

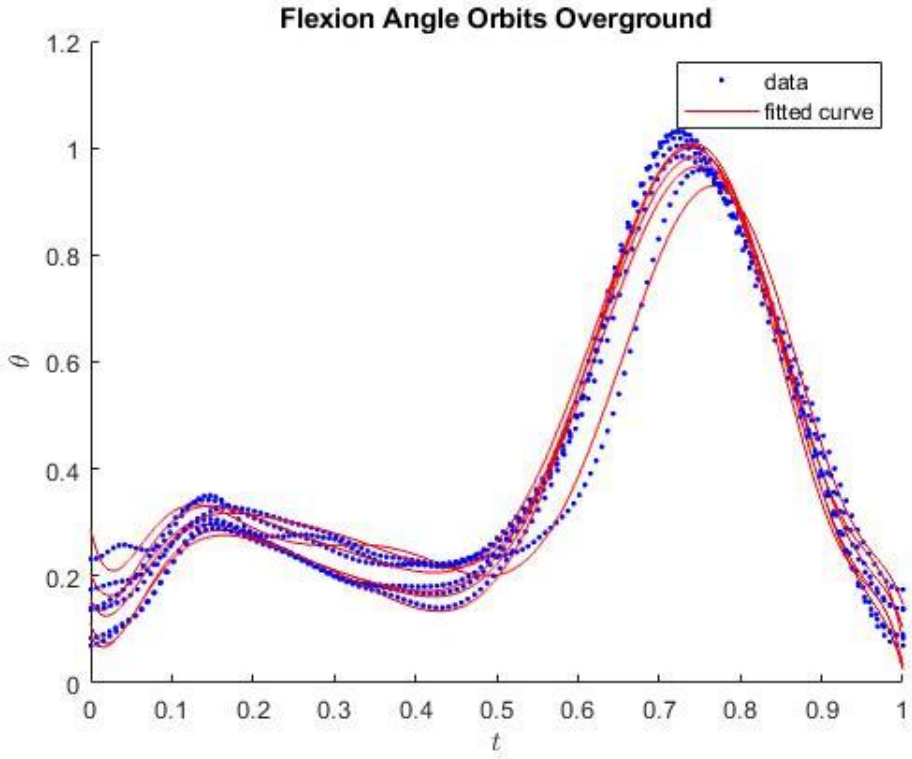

Figure 14 Flexion Angle Orbits walking overground

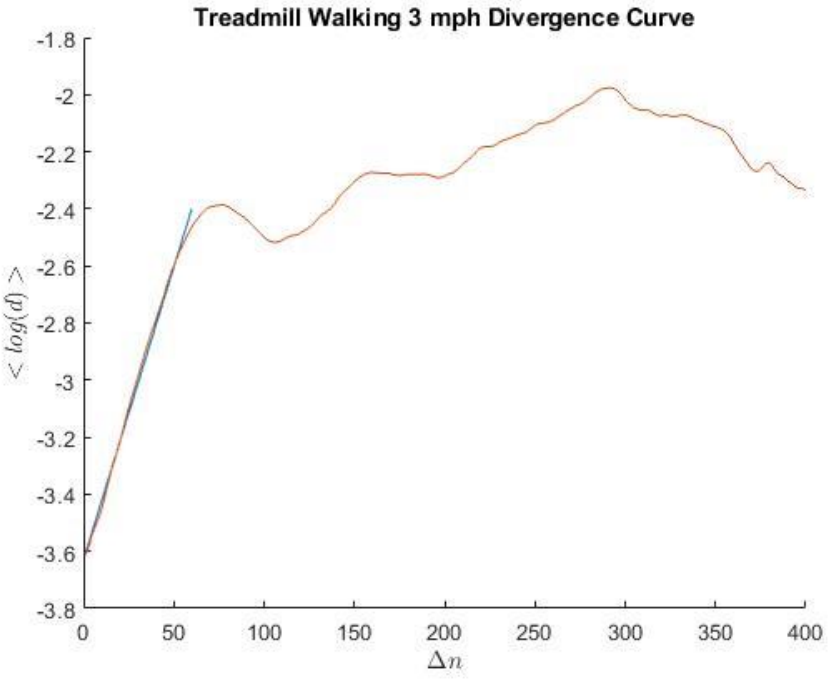

Figure 15 Divergence Curve for Walking at 3 mph on the Treadmill

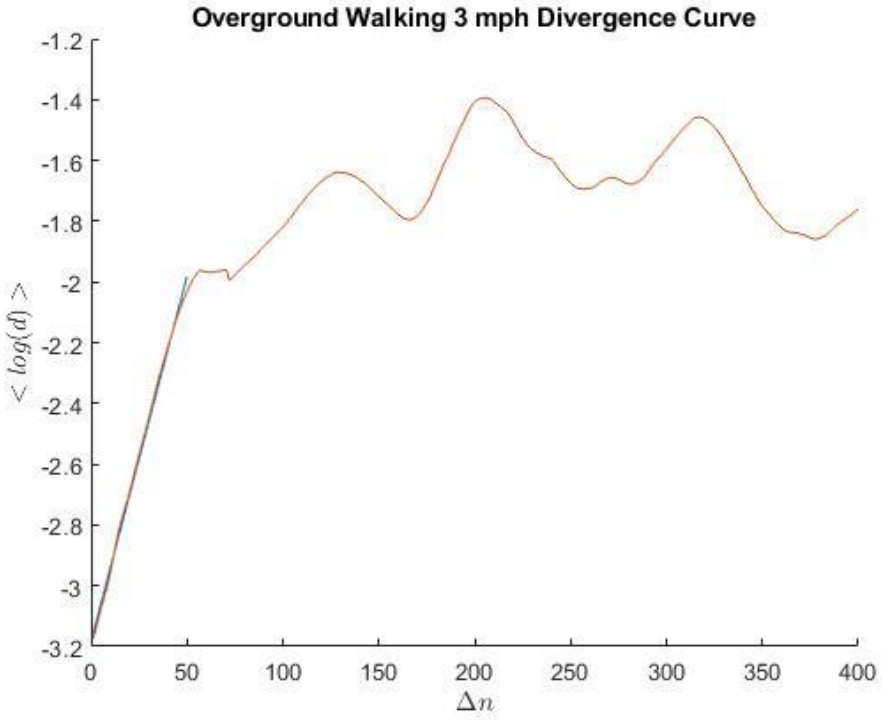

Figure 16 Divergence Curve for Walking at 3 mph Overground

CHAPTER III

EXPERIMENTAL PROTOCOL

Warm up Procedure

The subject will do the warm as previously explained in [31]. Doing squats for 5 minutes and resting for 3 minutes before the trials began.

Exercise Technique and procedure

Squat exercises are performed in the experimental trials. The origin of the global coordinate system is positioned in the posterior and lateral corner of the plate of the right foot of the subject. The anterior direction is the positive direction. The y-axis is the lateral-medial direction. A block was positioned so the subject can maintain a regular squat depth at all times and also the subject arms are in front at all times. We can see this in Fig. 17.

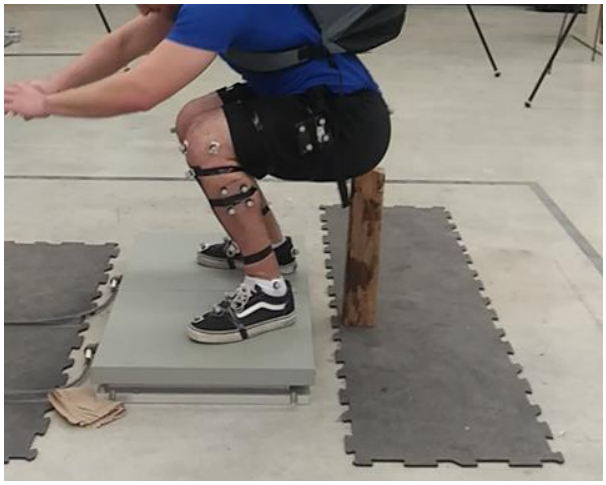

Figure 17 Subject squat configuration

The experiment consists of 4 trials with 5 minutes rest in between with various weights. The first trial is with the subject bodyweight only and subsequent trials are added weight of 10.16, 20.69 and 32 Kgs. With 10.16 Kg a backpack was used. A vest and backpack was used for 20.69 Kg and 32 Kg.

CHAPTER IV

RESULTS

Center of Pressure Trajectories

The center of pressure in the right leg with no additional mass ranges from no additional mass from in the x-axis from 100 mm to 160 mm and in the y-axis that are from 185 mm to 210 mm. The center of pressure in the left leg with no additional mass ranges from no additional mass from the x-axis from 80 mm to 180 mm and in the y-axis that are from 620 mm to 655 mm. We can see this in the comparison from Figs 18-22 with the additional mass and no mass.

Now the ranges with 10 kg of additional mass in the right leg, the range of movement of the Center of pressure (COP) one can see in Fig. 18 that the x-axis ranges from to 100 mm to 180 mm, and in the y-axis from 185 mm to 225 mm, and that the COP oscillates more in x-axis between from 100 mm to 160 mm, and in the y-axis from 195 mm to 220 mm. Fig. 19 shows that with 10 Kg additional mass the ranges are similar for the left leg. The x-axis oscillates between 100 mm to 160 mm and in the y-axis from 635 mm to 650 mm.

The right leg with 20 kg of additional mass, the range of motion of COP the ranges changes from the x-axis to 100 mm to 180 mm, and the y-axis from 205 mm to 220 mm, Fig. 20. For the left leg, the ranges are approximately the same. However, the COP is contained and thus is less than no additional weight as seen Fig. 21.

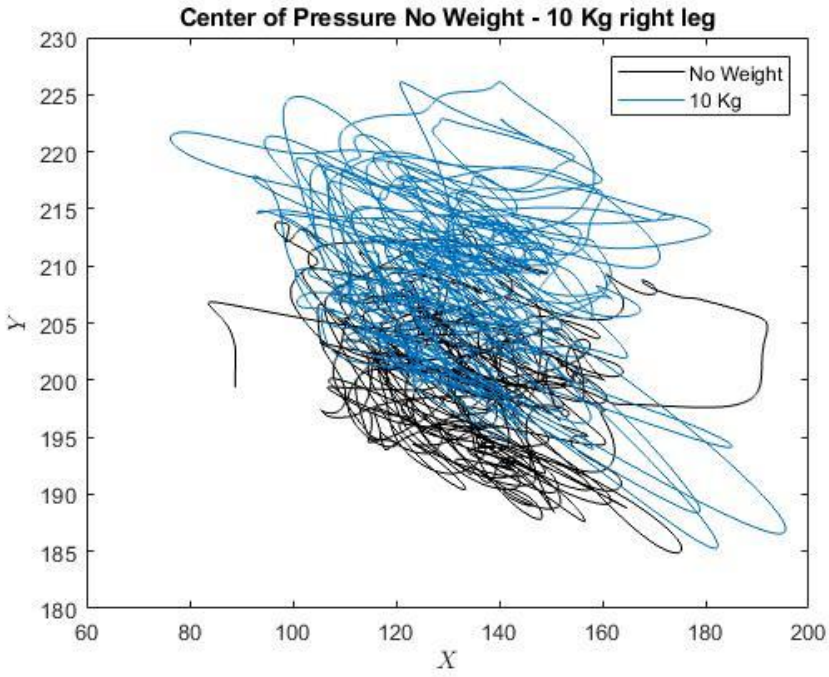

Figure 18 Position in millimeters of the Center of Pressure in the right leg with no weight and 10 Kg of added mass.

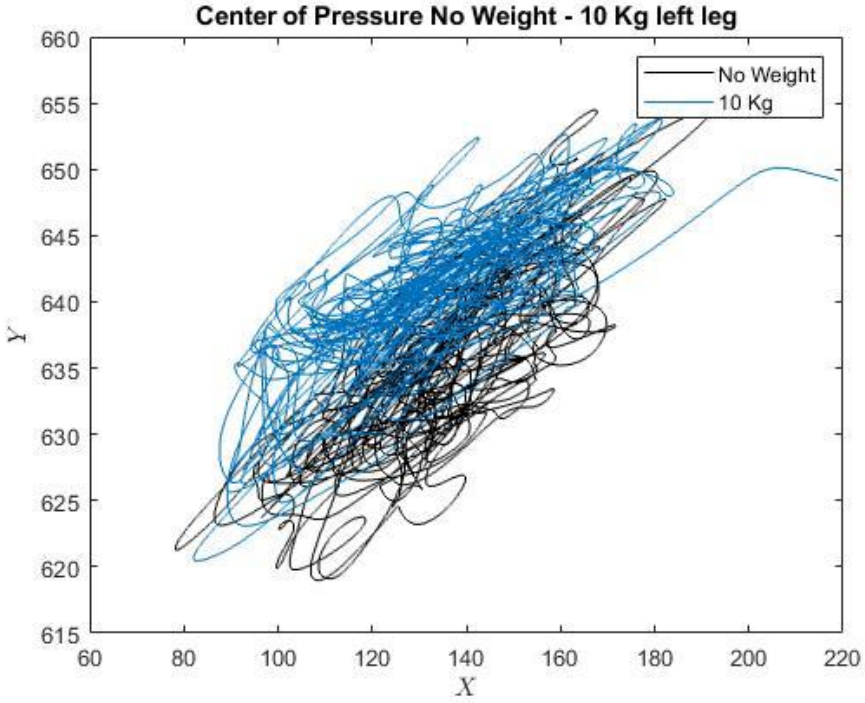

Figure 19 Position in millimeters of the Center of Pressure in the left leg with no weight and 10 Kg of added mass.

With the highest added weight of 32 Kg, one can see in fact that the COP ranged from the x-axis to 100 mm to 180 mm, and in the y-axis from 205 mm to 220 mm as it can be seen in Fig. 22. For the left leg the COP ranged from the x-axis to 80 mm to 180 mm, and in the y-axis from 625 mm to 660 mm as it can be seen in Fig. 23. The COP ranged more in the x-axis between 100 mm to 150 mm, and in the y-axis from 630 mm to 650 mm.

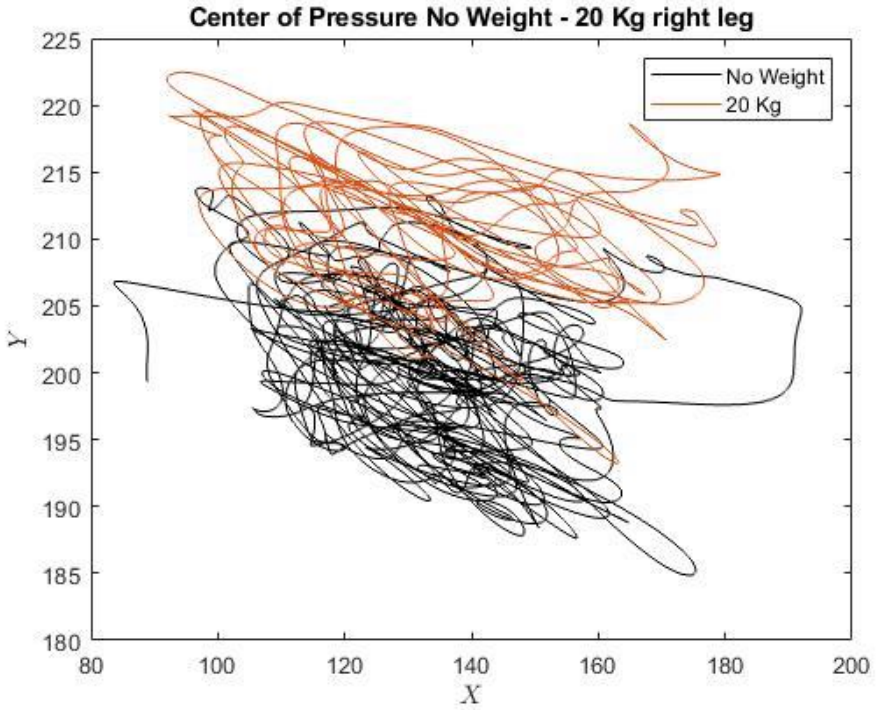

Figure 20 Position in millimeters of the Center of Pressure in the right leg with no weight and 20 Kg of added mass

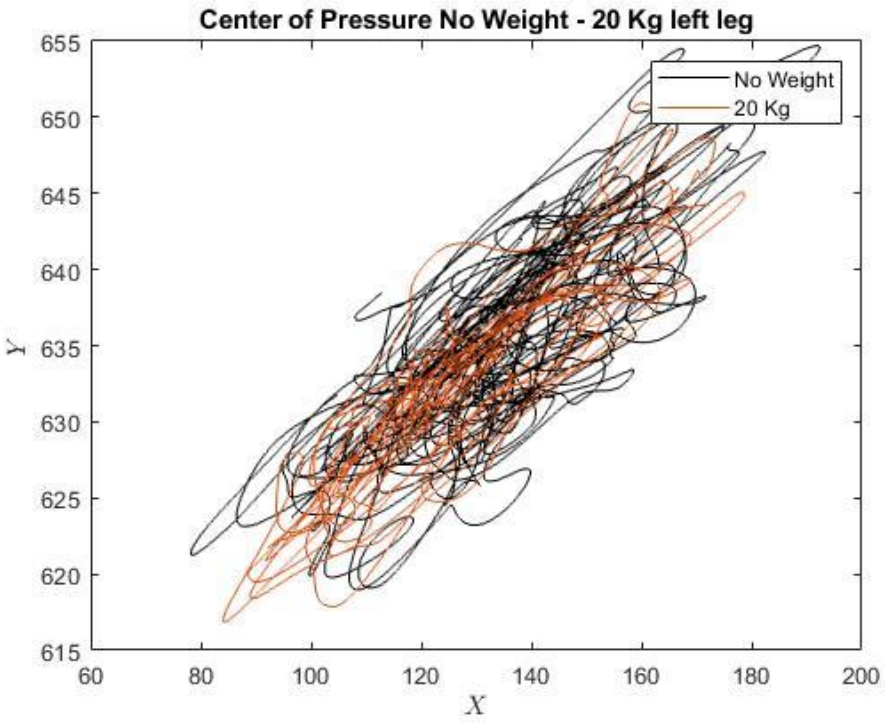

Figure 21 Position in millimeters of the Center of Pressure in the left leg with no weight and 20 Kg of added mass.

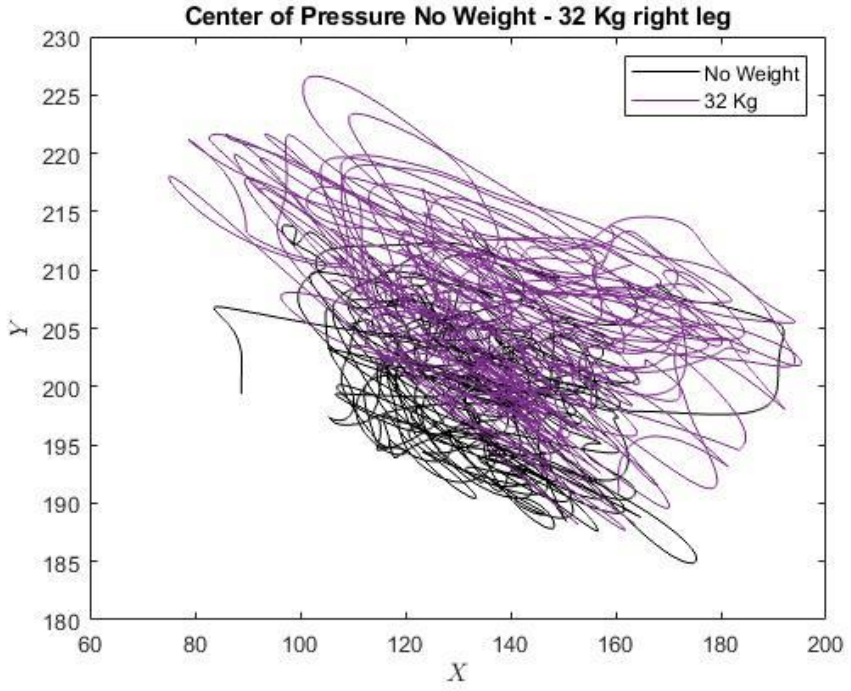

Figure 22 Position in millimeters of the Center of Pressure in the right leg with no weight and 32 Kg of added mass.

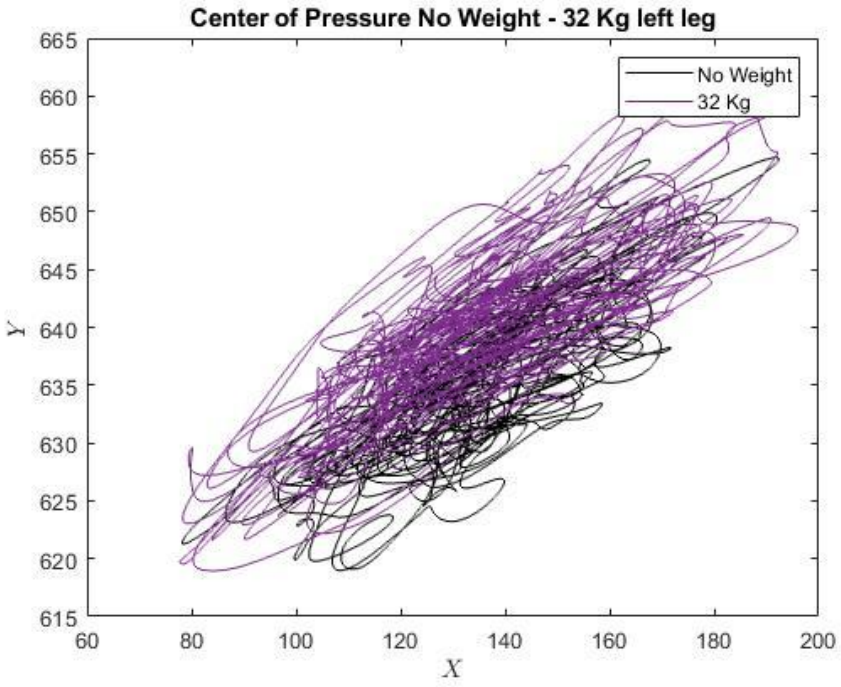

Figure 23 Position in millimeters of the Center of Pressure in the left leg with no weight and 32 Kg of added mass.

Stability of the Ground Reaction Forces and Center of Pressure

As recommended by Dingwell et al. [32], the Rosenstein method [18] is used to calculate the Lyapunov Exponents. First the Lyapunov exponents are calculated with with different time delays and orbital times to analyze how different the Lyapunov exponents are for the right leg ground reaction forces with no weight. The orbital time and time delay difference is negligible as seen in Fig. 24. The exponents for this analysis were calculated using Dingwell's et al. method of a fix interval using 150 time steps. Noticing that the time delay will not have a noticeable difference we proceeded on using a time delay of 3. Tenbroek et al. [33] mentioned that Rosenstein's method is more robust to calculate the values than Wolf's method. Look [21] reported values on a similar scale of our own.

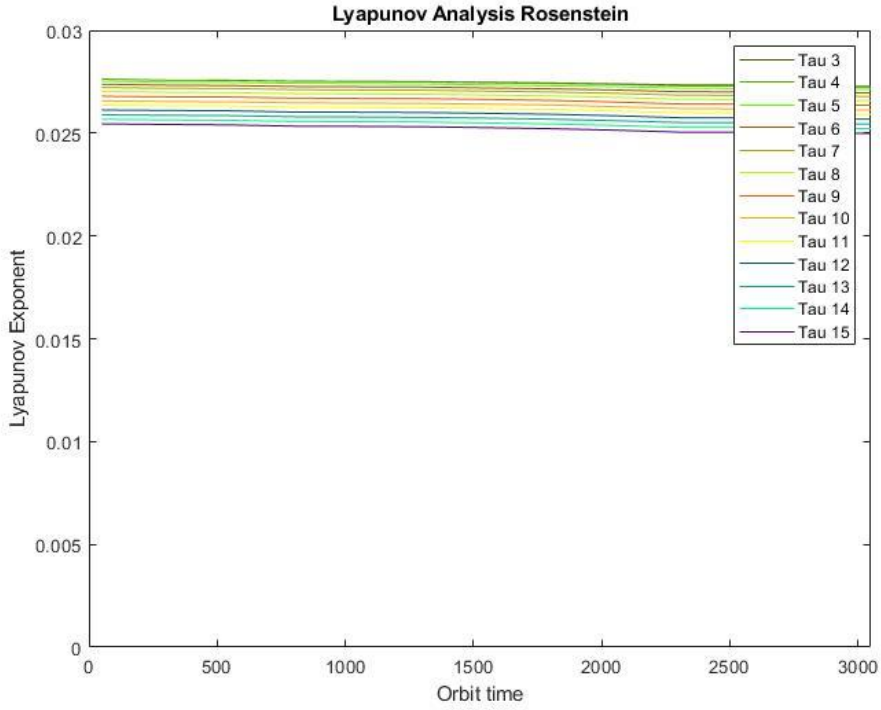

Figure 24 Lyapunov exponent values with Rosenstein method with different time delay reconstruction for the Ground Reaction Forces with no weight.

The results from the Lyapunov Exponents predict that the Ground Reaction Forces on both legs are more stable at 10 kg as seen in Fig. 25. Afterwards the Lyapunov exponents start increasing reaching its maximum at the 32 kg mark. The x coordinate of the Center of Pressure on the other hand behaves similarly for the right leg, but holding a constant and more stable value than no weight. However, the left leg gets unstable at 10 kg, being the maximum, and later being more stable with more weight.as seen in Fig. 26. The y coordinate, on the other hand, for the right leg starts to increase proportionally to the weight having its maximum at the 32 kg. The left leg then gets a maximum at 10 kg, being the maximum of all, then decreasing a 20 kg and increasing at 32 kg again achieving a similar value to the right leg as we can see in Fig. 27.

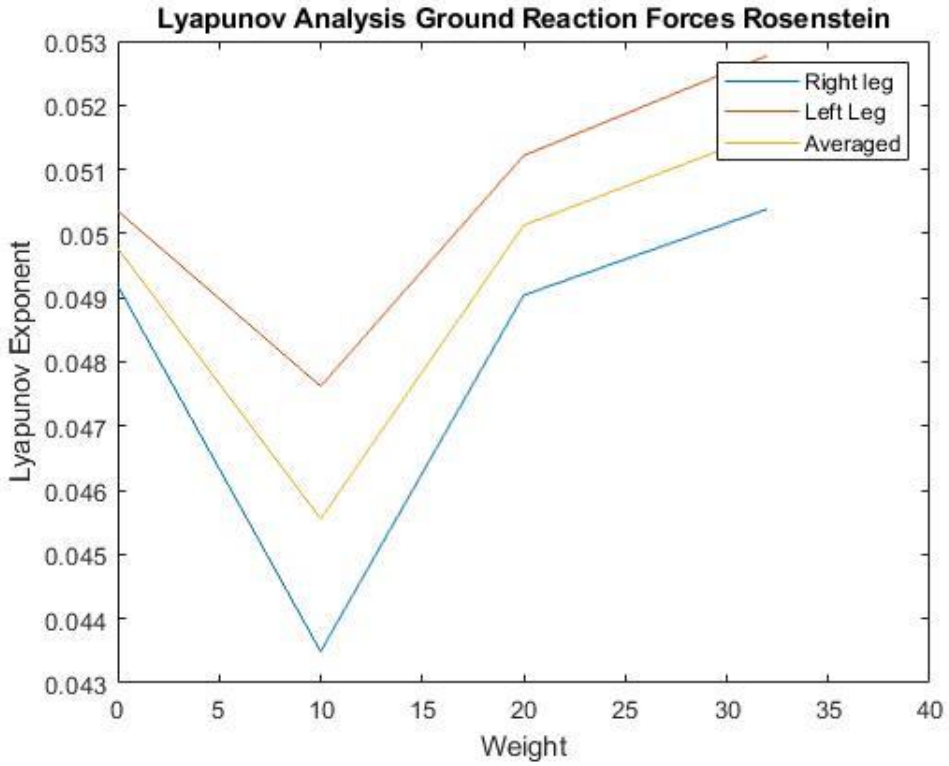

Figure 25 Lyapunov Analysis Ground Reaction Forces Rosenstein.

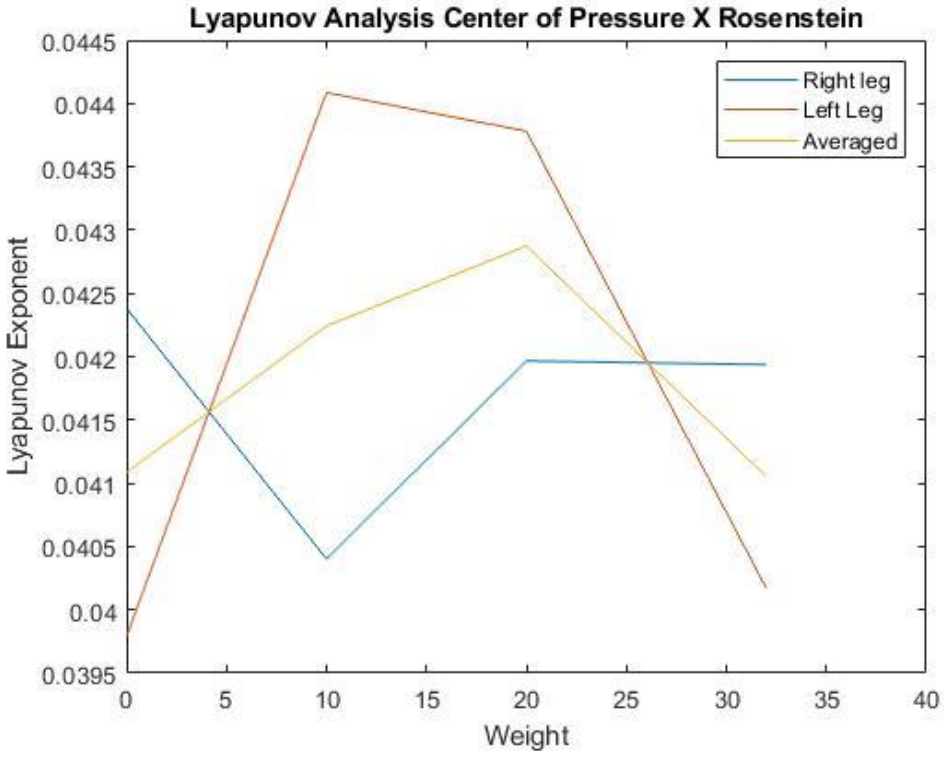

Figure 26 Lyapunov Analysis Center of Pressure of X Rosenstein.

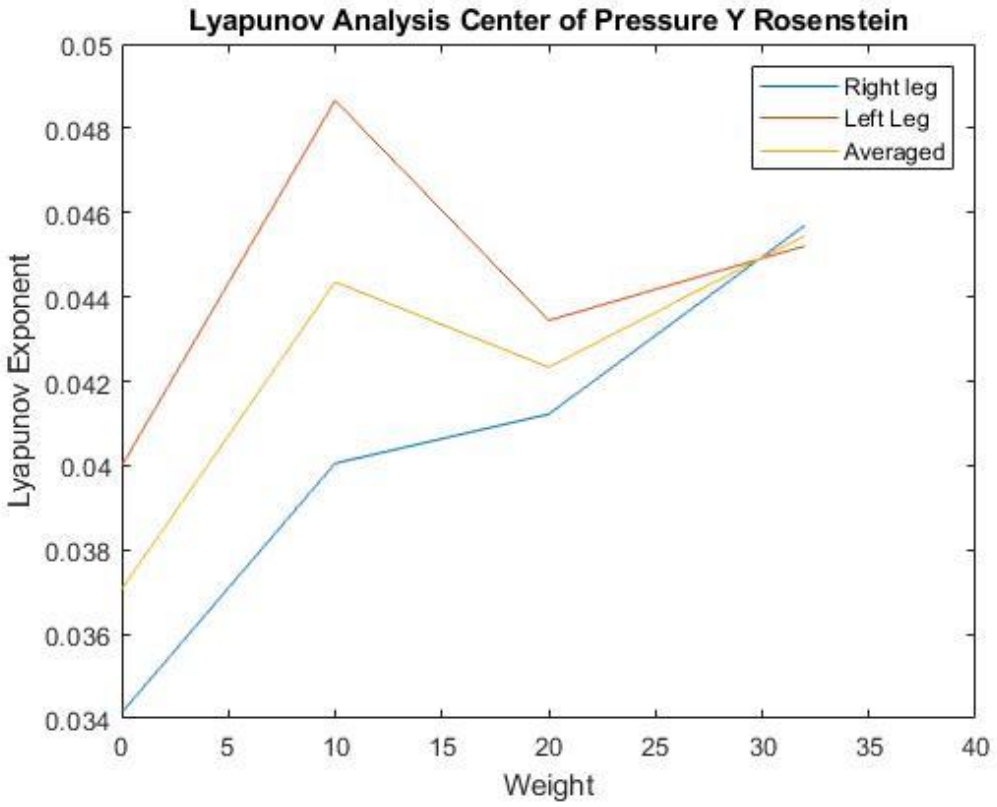

Figure 27 Lyapunov Analysis Center of Pressure of Y Rosenstein.

Knee Flexion Angle Stability Results

The Lyapunov Exponents of the right knee flexion angle was calculated using Rosenstein and Wolf's algorithm to check consistency. Using Wolf's algorithm [34], we calculated the Lyapunov Exponents with a range of different evolution time and different time delays for the state space reconstruction. This is done since the estimation varies depending to these values. One can see each case for 0 kg, 10 kg, 20 kg and 32 kg of added weight in Figs, 28-31, respectively. Having these curves, we averaged the value across the delay times at each evolution time to get an averaged curve as seen in Fig. 32. The overall behavior is that there is more stability at 10 kg, however we need to compare in more detail. The average of the averaged curve was taken to compare and the result is Fig. 33.

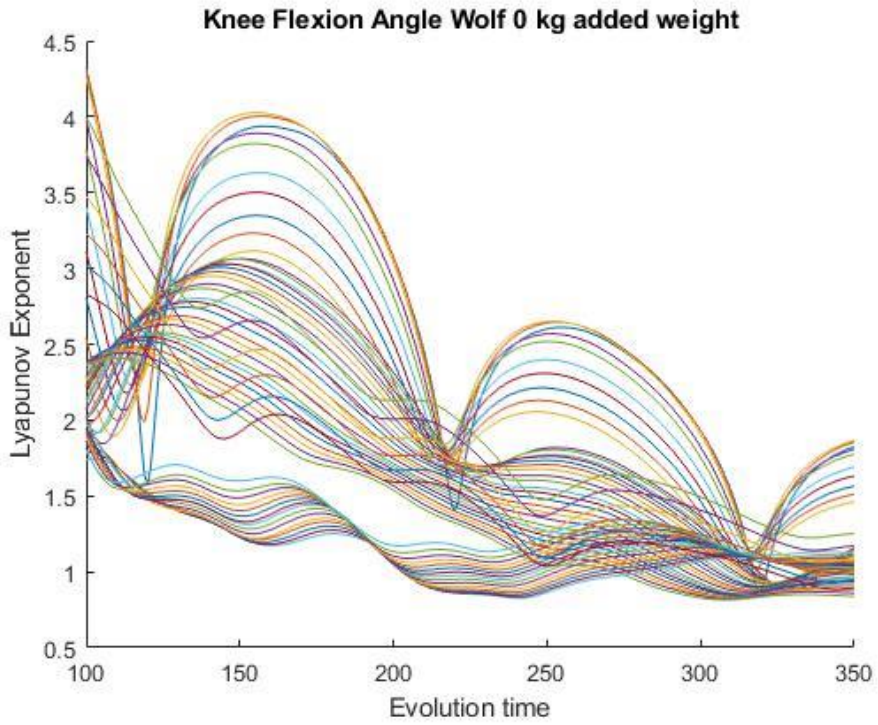

Figure 28 Lyapunov Exponent Curves for Right Knee Angle with 0 kg Added Weight with Wolf's Algorithm

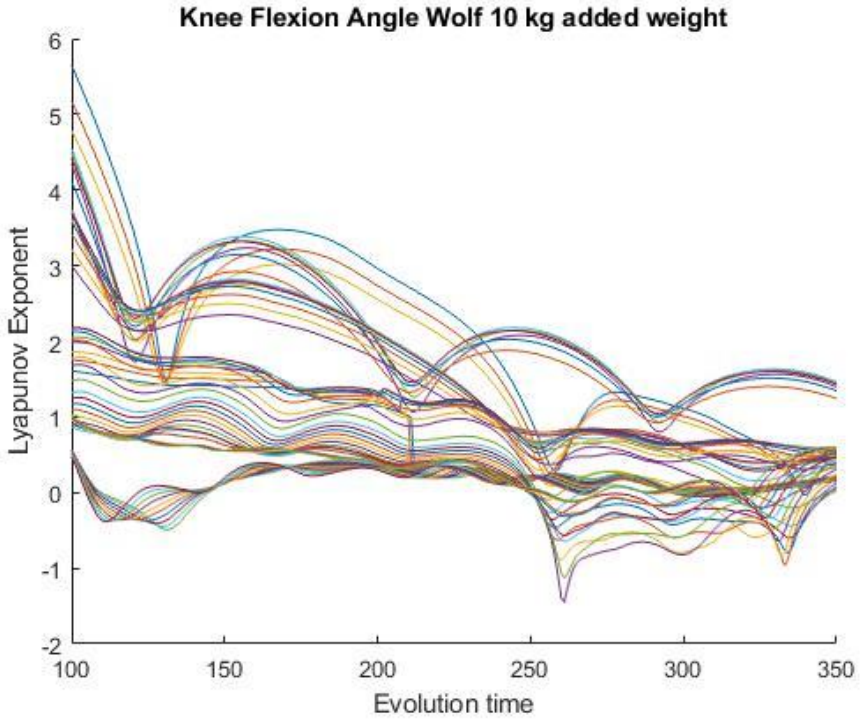

Figure 29 Lyapunov Exponent Curves for Right Knee Angle with 10 kg Added Weight with Wolf's Algorithm

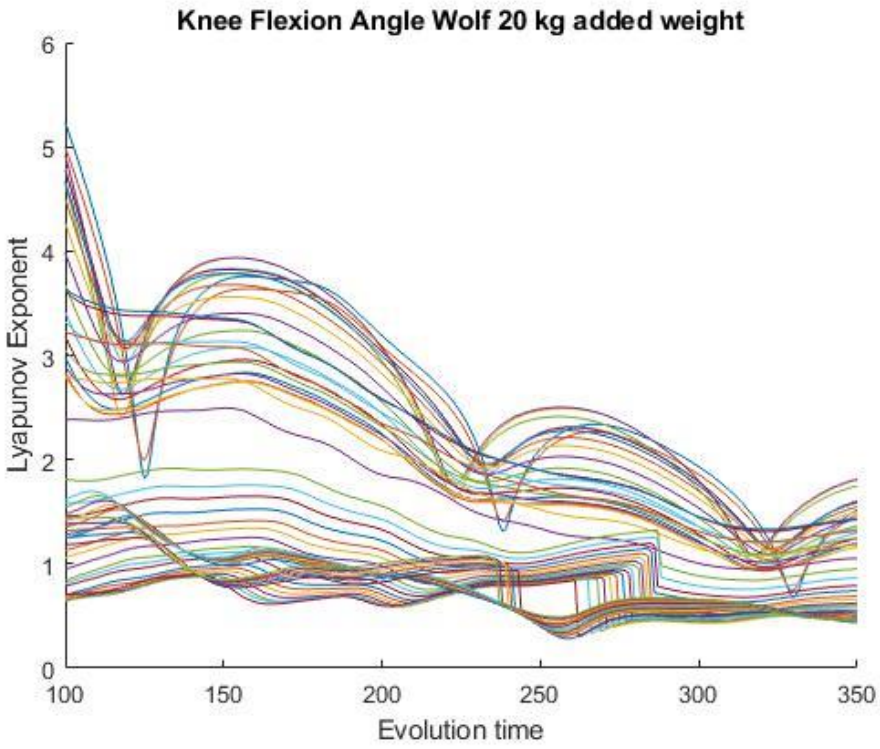

Figure 30 Lyapunov Exponent Curves for Right Knee Angle with 20 kg Added Weight with Wolf's Algorithm

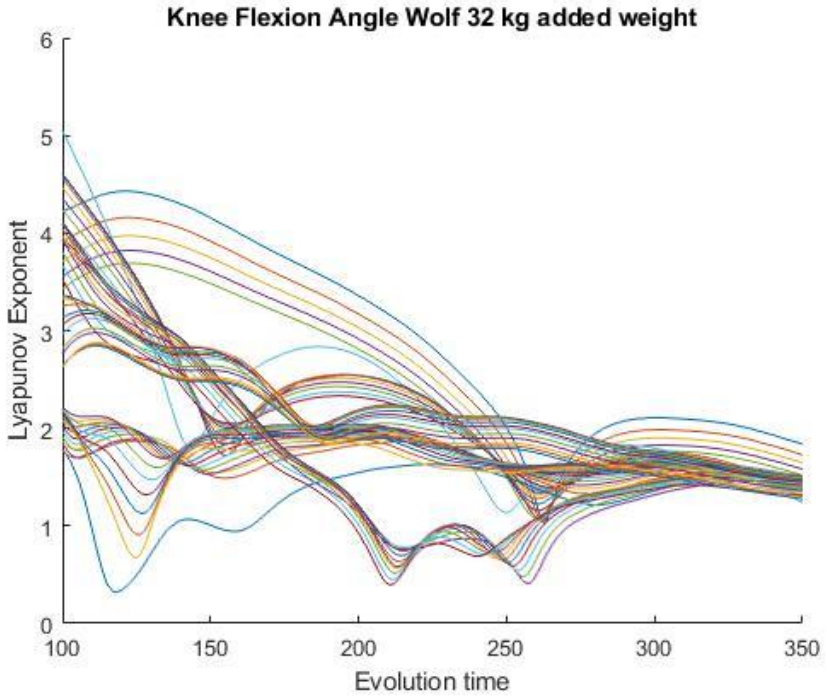

Figure 31 Lyapunov Exponent Curves for Right Knee Angle with 32 kg Added Weight with Wolf's Algorithm

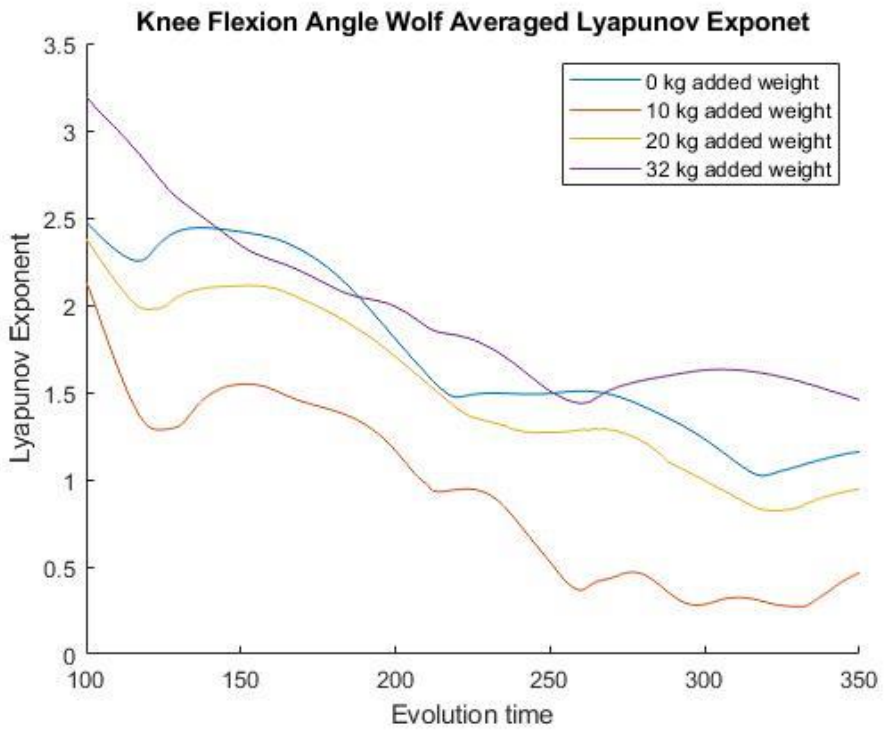

Figure 32 Lyapunov Exponent Averaged Curves for Right Knee Angle with Wolf's Algorithm

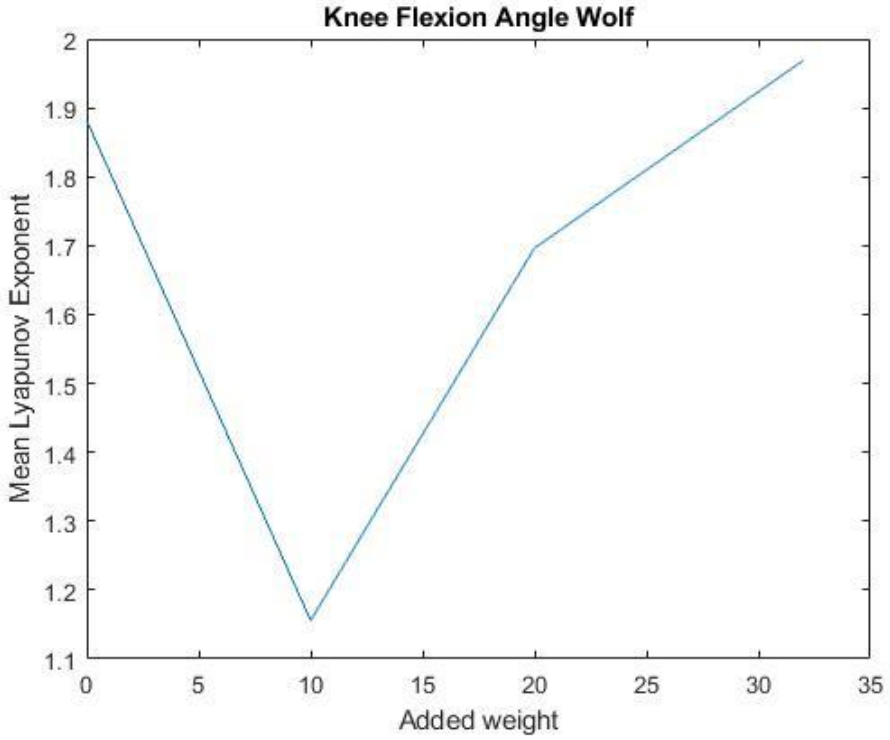

Figure 33 Mean Lyapunov Exponent from the Averaged Cures with Wolf's Algorithm

Using Rosenstein method, we proceed to calculate the Lyapunov exponents with the procedure of finding the least regression line with correlation of 0.9. We can see the results in Fig. 34 in which we can see that both algorithms agree in the results. The most stable case is 10 kg, where 0 kg and 20 kg of added weight are approximately the same. The most unstable case is the 32 kg of added weight.

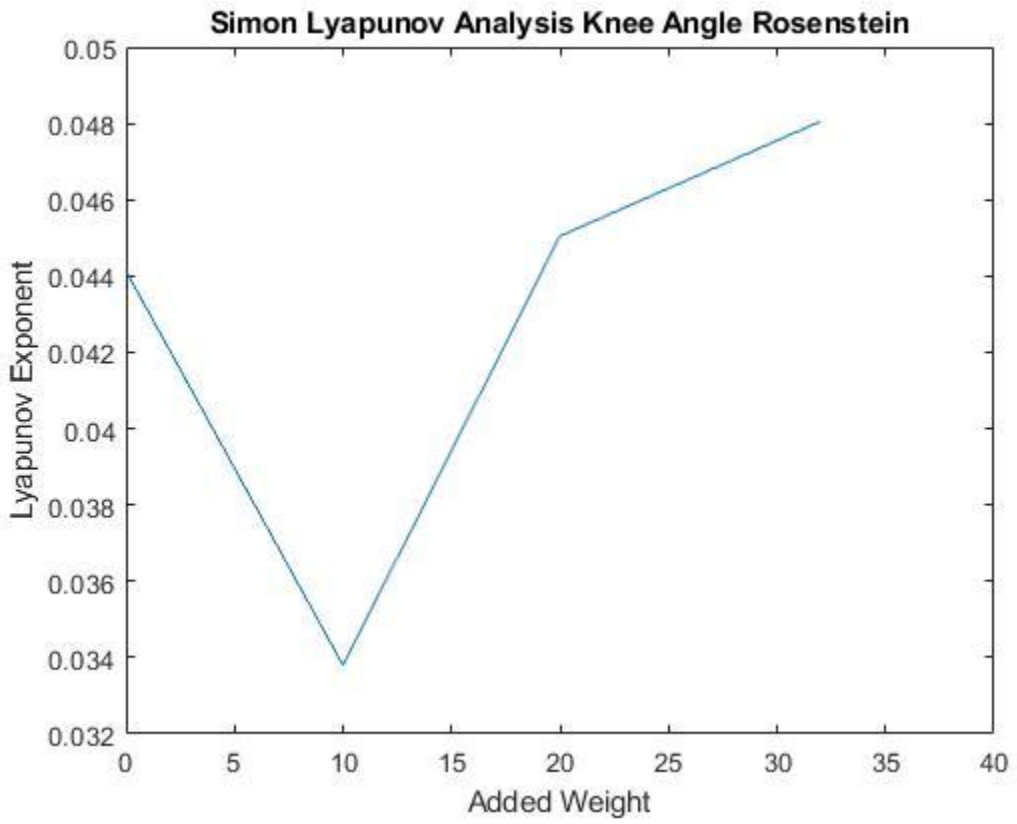

Figure 34 Lyapunov Exponent Right Knee Angle from a Regression line with 0.9 Correlation.

Moreover, there were two more subjects, Subject 2 which we will call Salvador, had a similar patter as we can see in Fig. 35. The 10 kg case is consistent with the previous subject in which is a stable point. However, he has a more stable point 32 kg. Also, a Third Subject, which we will call Chuy, has done the experiment and overall the results match the stability of the previous subject and in scale as seen in Fig. 35. Individual graphs for the Lyapunov Exponents of

Salvador and Chuy are in in the Appendix A as Figs. 165-166. Notice that Salvador's stability curve is actually overall more unstable comparing to the other two curves as seen in Fig. 35. However overall the trend is that at 10 kg is the movement is more stable.

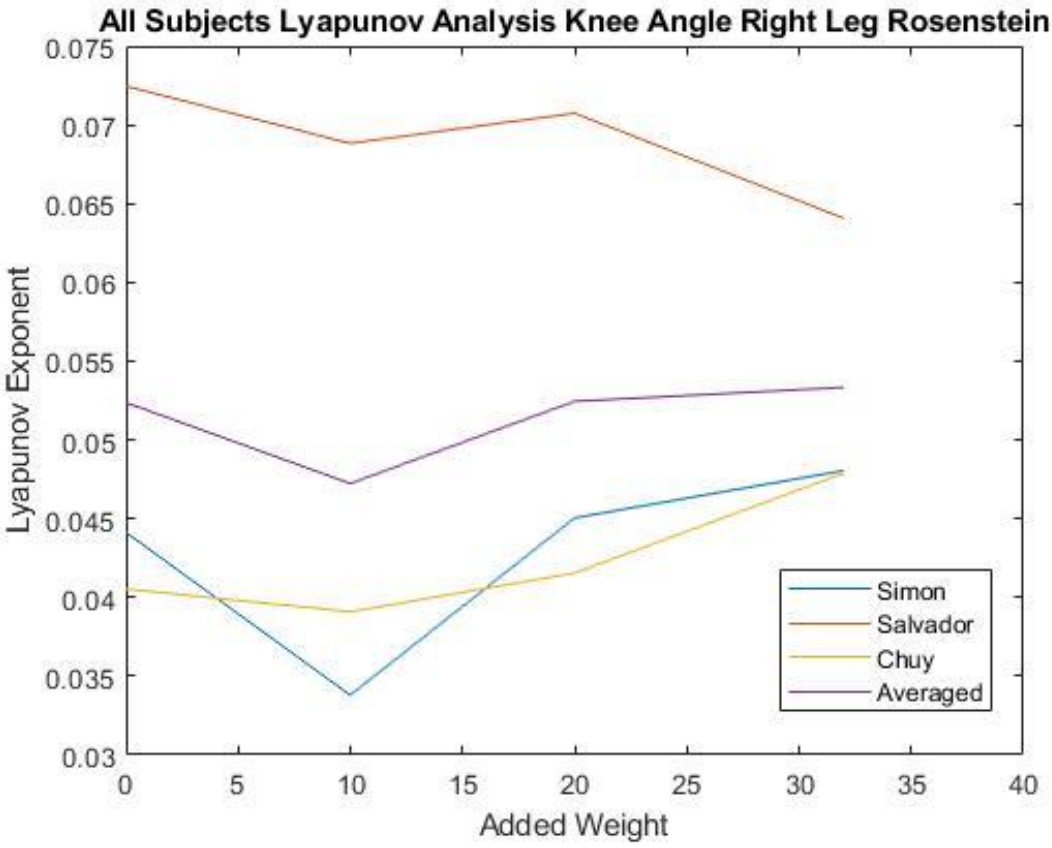

Figure 35 All subjects Lyapunov Exponent Values

CHAPTER V

DISCUSSION AND CONCLUSION

This research deals with the effect of additional weight on the stability of the center of pressure, ground reaction forces, and knee flexion angle of the squat exercise. The results show that additional weight increases knee flexion angle stability for 10 kg of additional weight. The stability decreases then with the increase of additional weight in the cases of 20 Kg and 32 Kg. The right leg is more stable as seen in Fig. 25 One can see the effect mentioned in the x and y coordinate in Figs 26-27, respectively.

Moreover, we see that the range of movement of the center of pressure coordinates is larger at 10 kg for the right leg than the left leg as seen in Figs. 18-19 Comparing the range of movement for added weight of 10 kg, one can see that larger range of movement means a more stable motion and lower Lyapunov Exponents when comparing the two legs. This is also true for 20 and 32 kg as seen in Figs. 20-23. The range of movement of the right leg is higher which gives a lower value for the Lyapunov exponent when comparing the two sides.

Now analyzing the leg by itself, the range of movement on the right leg seems to decrease in the y coordinate. The x coordinate has a major increase at 10 kg and the range is approximately the same with 20 kg and 32 kg. On the other hand for the left leg, we see that the range of movement of the y coordinate is constrained more with 10 kg, being approximately the same as 20 kg and 32 kg. The x coordinate has also the lowest range of movement at 10 Kg and

20 Kg. At 32 kg the range of movement is similar to the no weight case. This can be seen in Figs. 26-27. Stability Analysis with Lyapunov Exponent show that the highest values with 10 kg correlates with the low range of movement of the Center of Pressure of the left leg having a common range of movement in the orbits. It also correlates to the more stable ground reaction forces values and with the right leg Center of Pressure values for the x coordinate. One can conjecture that there is an adjustment from the subject to make the anterior-posterior direction (x coordinate) more stable. This will correlate for a more stable movement and the Lyapunov Exponents obtained. However, as the right leg makes adjustments for the x coordinate of the center of pressure, the left leg has difficulty adjusting. The left leg only achieves more stability until higher weights.

Similar studies [20-23] have the number subjects ranged from 6 to 30. Other studies simulate overweight subjects with additional weight [35-37]. Future work will involve more subjects, a larger range of additional weights. Also the procedure will be updated so we can do a random selection from a group of volunteers in order to minimize variability in male and female subjects, athletic to non-athletic subject, and left or right brain persons in order to generalize the result.

REFERENCES

[1] N. Stergiou and L. M. Decker, "Human movement variability, nonlinear dynamics, and pathology: is there a connection? " Human movement science, vol. 30, no. 5, p. 869 888., 2011.

[2] U. H. Buzzi, N. Stergiou, M. J. Kurz, P. A. Hageman and J. Heidel, "Nonlinear dynamics indicates aging affects variability during gait.," Clinical biomechanics, vol. 18, no. 5, pp. 435-443, 2003.Wind, W.M., Bergfeld, J.A., Parker, R.D., 2004. Evaluation and treatment of posterior cruciate ligament injuries. *The American Journal of Sport Medicine*, 32: 1765-1775.

[3] J. B. Dingwell and J. P. Cusumano, "Nonlinear time series analysis of normal and pathological human walking Chaos," An Interdisciplinary Journal of Nonlinear Science, vol. 10, no. 4, pp. 848-863, 2000.Most, E., Axe, J., Rubash, H., Li, G., 2004. Sensitivity of the knee joint kinematics calculation to selection of flexion axes. *Journal of Biomechanics*, 37: 1743-1748.

[4] R. E. van Emmerik and E. E. van Wegen, "On variability and stability in human movement," *Applied Biomechanics,* vol. 16, no. 4, pp. 394-406, 2000.

[5] J. T. Cavanaugh, K. M. Guskiewicz and N. Stergiou, "A non-linear dynamic approach for evaluating postural control," *Sports medicine,* vol. 35, no. 11, pp. 935-950, 2005

[6] Van Emmerik, R. E., Rosenstein, M. T., McDermott, W. J., and Hamill, J., 2004. “A nonlinear dynamics approach to human movement.” Journal of Applied Biomechanics, 20(4):396 420.

[7] J. Dingwell, J. Cusumano, P. Cavanagh and D. Sternad, "Local dynamic stability versus kinematic variability of continuous overground and treadmill walking.," *J. Biomech. Eng.,*

vol. 123, no. 1, pp. pp.27-32., 2001.

[8] Lockhart, T. E. and Liu, J. 2008. “Differentiating fall-prone and healthy adults using local dynamic stability” Ergonomics, 51(12):1860 1872.

[9] J. Dingwell, J. P. Cusumano, D. Sternad and P. R. Cavanagh, "Slower speeds in patients with diabetic neuropathy lead to improved local dynamic stability of continuous overground walking," *Journal of biomechanics,* vol. 33, no. 10, pp. 1269-1277, 2000.

[10] J. B. Dingwell and L. C. Marin, "Kinematic variability and local dynamic stability of upper body motions when walking at different speeds.," *Journal of biomechanics,* vol. 39, no. 3, pp. 444-452, 2006.

[11] A. J. Zink, W. C. Whiting, W. J. Vincent and A. J. Mclaine, "The effects of a weight belt on trunk and leg muscle activity and joint kinematics during the squat exercise," *The Journal of Strength & Conditioning Research,* vol. 15, no. 2, pp. 235-240, 2001.

[12] D. I. Caruntu, J. Galarza, S. Vasquez III, J. Ramos and M. Sander, "Effect of Obesity on Human Squat Exercise," in *ASME International Mechanical Engineering Congress and Exposition*, 2019.

[13] D. A. Winter, Biomechanics and motor control of human movement., New York, NY: Wiley, 1990.

[14] Y. Hurmuzlu and C. Basdogan , "On the measurement of dynamic stability of human locomotion," Journal of biomechanical engineering, vol. 116, no. 1, pp. 30-36, 1994.

[15] J. B. Dingwell and H. G. Kang, "Differences between local and orbital dynamic stability during human walking," Journal of biomechanical engineering, vol. 129, no. 4, pp. 586-593, 2007. Moreno, R., 2016, Knee joint internal forces during squat jump exercise. *ProQuest* 10191393.

[16] A. M. Fraser and H. L. Swinney, "Independent coordinates for strange attractors from mutual information," *Physical review,* vol. 33, no. 2, p. 1134, 1986. de Boor, Carl. *A Practical Guide to Splines*. Springer-Verlag, New York: 1978.

[17] M. B. Kennel, R. Brown and H. D. I. Abarbanel, "Determining embedding dimension for phase-space reconstruction using a geometrical construction," *Physical review A,* vol. 45, no. 6, p. 3403, 1992.

[18] M. T. Rosenstein, J. J. Collins and C. J. De Luca, "A practical method for calculating largest Lyapunov exponents from small data sets.," *Physica D: Nonlinear Phenomena,* Vols. 65(1-2), pp. 117-134, 1993.

[19] H. G. Kang and J. B. Dingwell, "Intra-session reliability of local dynamic stability of walking.," *Gait & posture,* vol. 24, no. 3, pp. 386-390, 2006.

[20] S. Brujin, J. H. van Dieën, O. Meijer and P. Beek, "Is slow walking more stable?," *Journal of biomechanics,* vol. 42, no. 10, pp. pp.1506-1512, 2009.

[21] N. Look, C. Arellano, A. Grabowski, W. McDermott, R. Kram and E. Bradley, "Dynamic stability of running: the effects of speed and leg amputations on the maximal Lyapunov exponent.," *Chaos: An Interdisciplinary Journal of Nonlinear Science,* vol. 23, no. 4, p. p.043131, 2013. Buff, H., Joines, L. C. and Hungerford, D. S., 1988. Experimental determination of forces transmitted through the patellofemoral joint," *Journal of Biomechanics*, 21: 17-22.

[22] R. B. Graham and S. H. Brown, "A direct comparison of spine rotational stiffness and dynamic spine stability during repetitive lifting tasks.," *Journal of biomechanics.,* vol. 45, no. 9, pp. 1593-1600., 2012.

[23] R. B. Graham, E. M. Sadler and J. M. Stevenson, "Local dynamic stability of trunk

movements during the repetitive lifting of loads.," *Human movement science.*, vol. 31, no. 3, pp. 592-603, 2012.

[24] J. Lee and M. A. Nussbaum, "Experienced workers may sacrifice peak torso kinematics/kinetics for enhanced balance/stability during repetitive lifting.," *Journal of biomechanics*, vol. 46, no. 6, pp. 1211-1215, 2013.

[25] G. Box, "Signal-to-noise ratios, performance criteria, and transformations.," *Technometrics*, vol. 30, no. 1, pp. pp.1-17., 1988.

[26] R. M. Haralick, H. Joo, C. N. Lee, X. Zhuang, V. G. Vaidya and M. B. Kim, "Pose estimation from corresponding point data. ," *IEEE Transactions on Systems, Man, and Cybernetics.*, Vols. 19, no. 2, pp. pp.1426-1446., 1989

[27] M. E. Alexander, R. Baumgartner, A. R. Summers, C. Windischberger, M. Klarhoefer, E. Moser and R. L. Somorjai, "A wavelet-based method for improving signal-to-noise ratio and contrast in MR images.," *Magnetic Resonance Imaging.*, vol. 18, no. 2, pp. pp.169-180., 2000.

[28] M. Ducros, M. Laubscher, B. Karamata, S. Bourquin, T. Lasser and R. P. Salathe, "Parallel optical coherence tomography in scattering samples using a two-dimensional smart-pixel detector array.," *Optics Communications*, Vols. 202(1-3), pp. pp. 29-35., 2002.

[29] A. J. Onwuegbuzie and L. G. Daniel, "Uses and misuses of the correlation coefficient.," 1999

[30] P. Schober, C. Boer and L. Schwarte, "Correlation coefficients: appropriate use and interpretation.," *Anesthesia & Analgesia*, vol. 126(5), pp. pp.1763-1768., 2018.

[31] M. Mckean and B. Burket, "Knee Behaviour in Squatting," *National Strength & Conditioning Association Journal*, 2012.

[32] J. B. Dingwell, "Lyapunov exponents," in *Encyclopedia of biomedical engineering.*, Wiley, 2006.

[33] T. Tenbroek, C. Van Emmerik and J. Hasson, "Lyapunov exponent estimation for human gait acceleration signals. InProc. In.," in *Int. Soc. of Biomechanics XXI Congress*, Taipei, Taiwan, 1–5 July 2007., 2007.

[34] A. Wolf, J. B. Swift, H. L. Swinney and J. A. Vastano, "Determining Lyapunov exponents from a time series.," *Physica D: Nonlinear Phenomena*, vol. 16, no. 3, pp. 285-317, 1985.

[35] N. Teasdale, M. Simoneau, P. Corbeil, G. Handrigan, A. Tremblay and O. Hue, "Obesity alters balance and movement control.," *Current Obesity Reports*, vol. 2, no. 3, pp. 235-240, 2013.

[36] X. Li and A. S. Aruin, "The effect of short-term changes in the body mass on anticipatory postural adjustments.," *Experimental brain research*, vol. 181, no. 2, pp. 333-346, 2007.

[37] K. E. Costello, S. L. Matrangola and M. L. Madigan, "Independent effects of adding weight and inertia on balance during quiet standing.," *Biomedical engineering online*, vol. 11, no. 1, p. 20, 2012.

APPENDIX

APPENDIX

The following is a list of graphs that were done as part of the study, main subject was subject 1 for testing purposes of the MATLAB code:

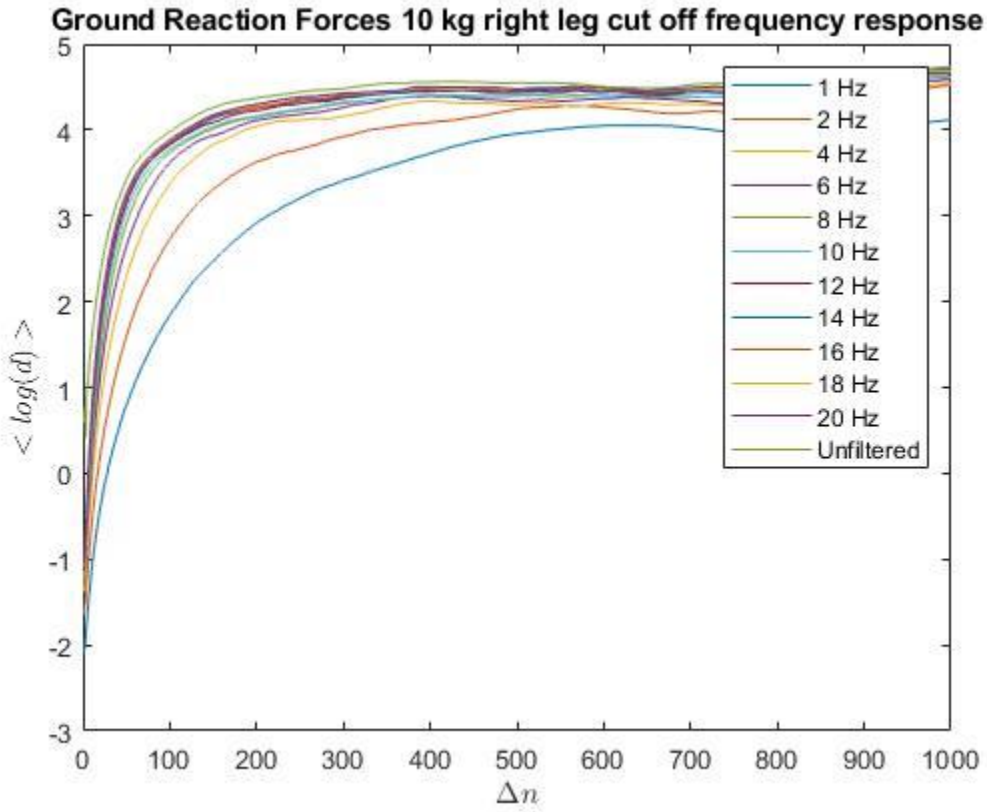

Figure 36 Ground Reaction Forces 10 kg right leg log divergence curve per cut off frequency (1-20 Hz).

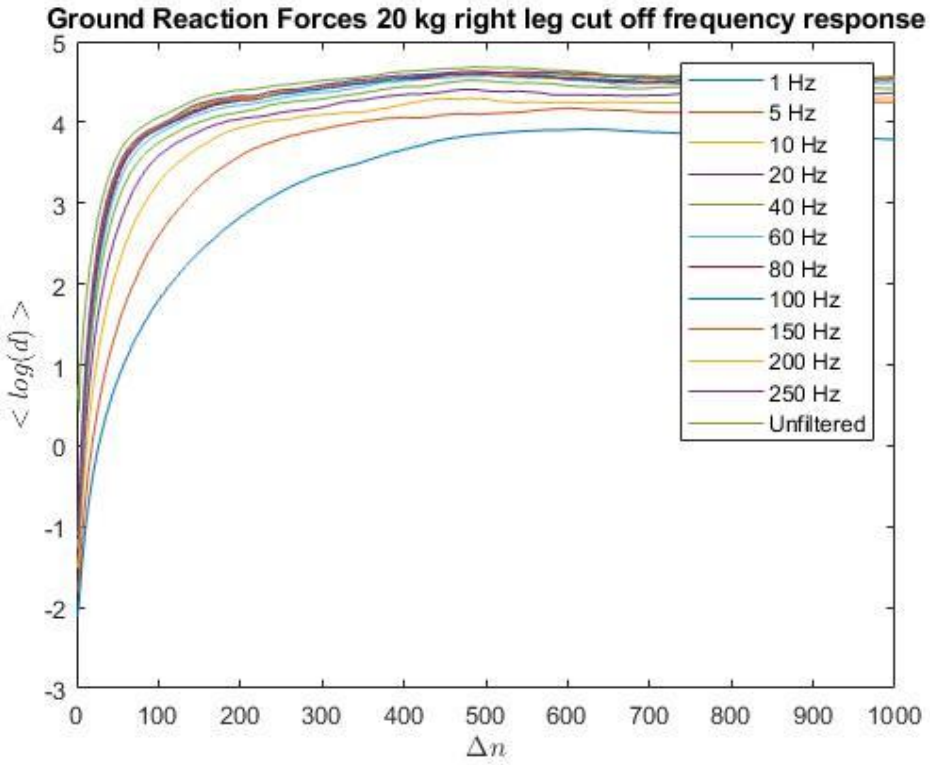

Figure 37 Ground Reaction Forces 20 kg right leg log divergence curve per cut off frequency (1-20 Hz).

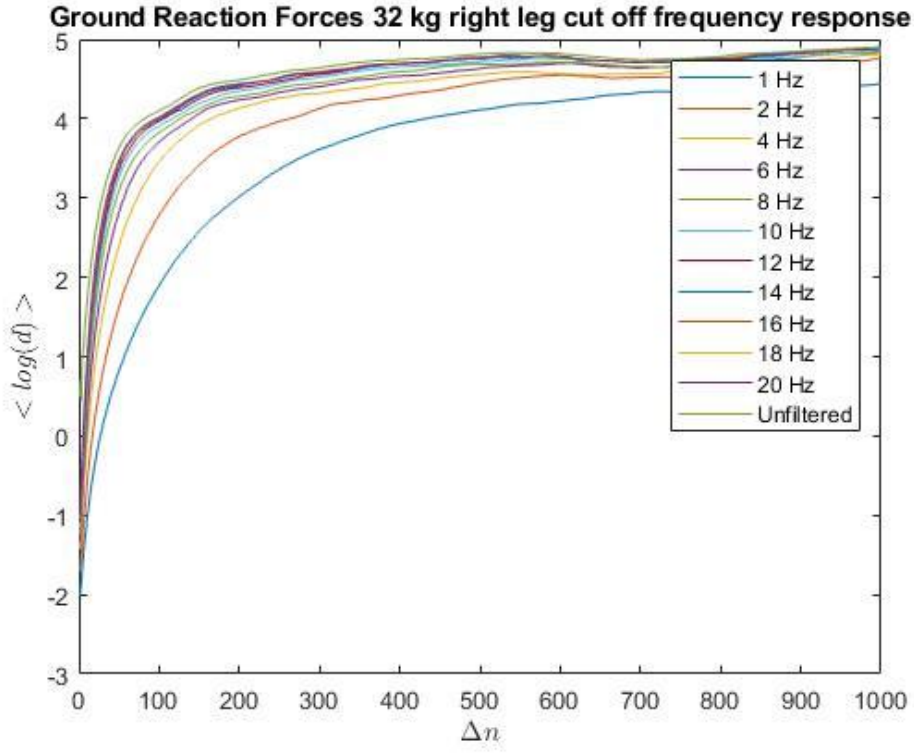

Figure 38 Ground Reaction Forces 32 kg right leg log divergence curve per cut off frequency (1-20 Hz).

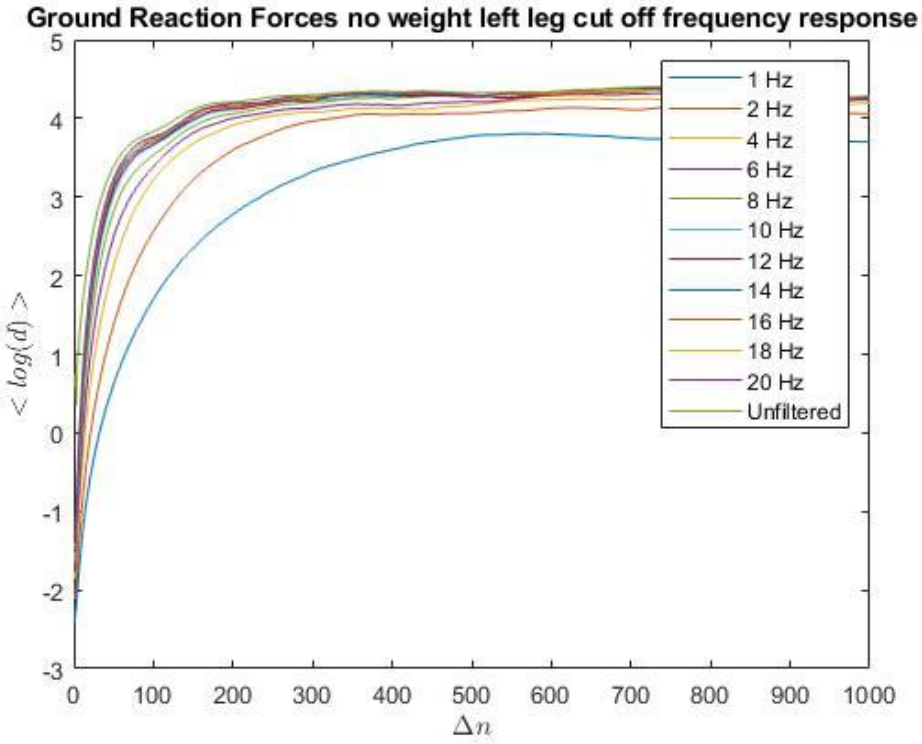

Figure 39 Ground Reaction Forces no weight left leg log divergence curve per cut off frequency (1-20 Hz).

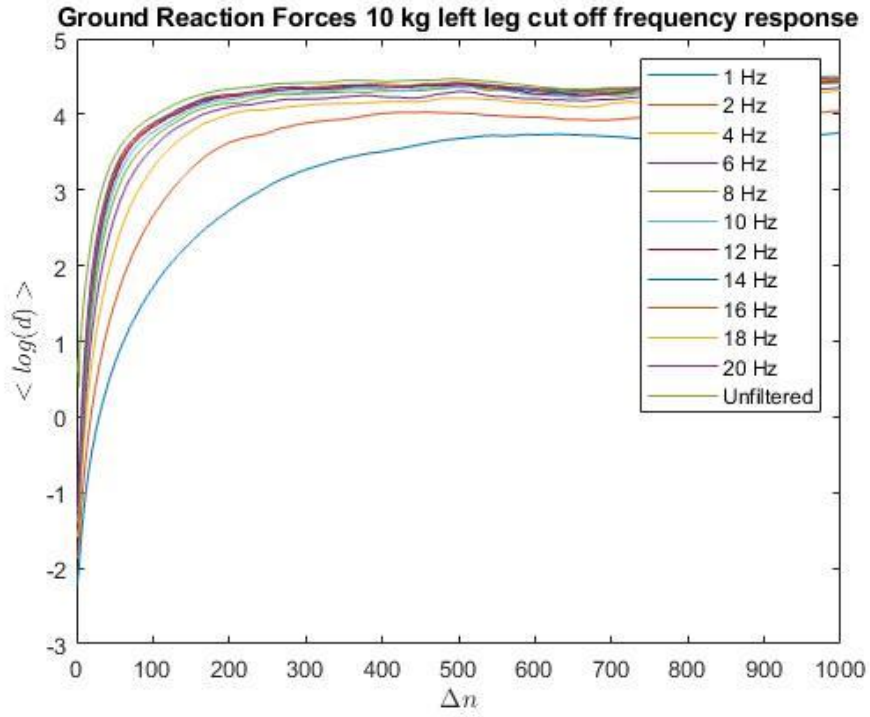

Figure 40 Ground Reaction Forces 10 kg left leg log divergence curve per cut off frequency (1-20 Hz).

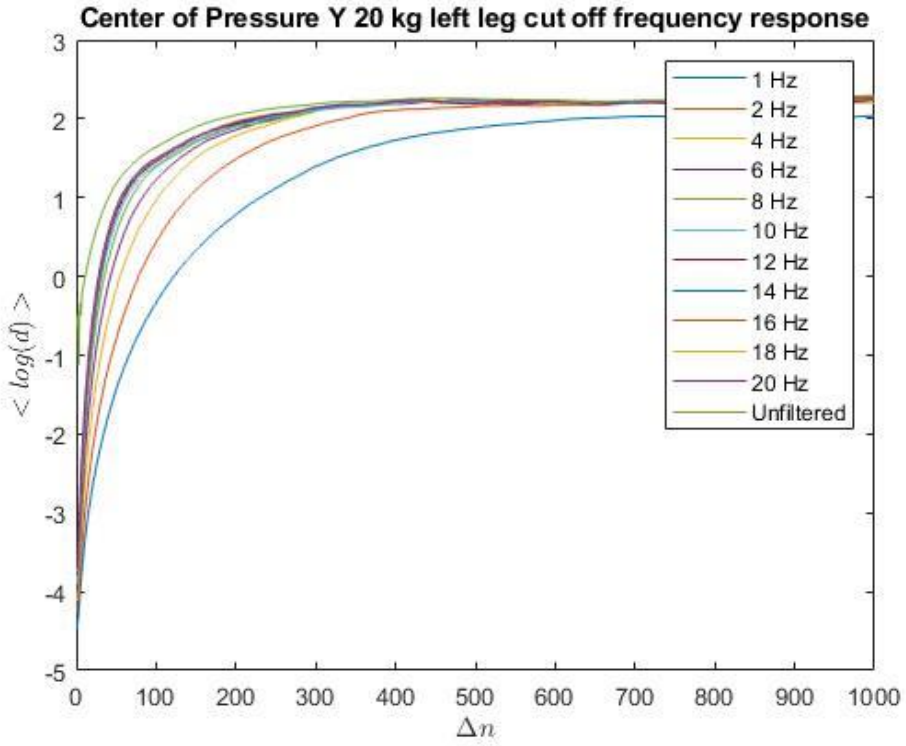

Figure 41 Ground Reaction Forces 20 kg left leg log divergence curve per cut off frequency (1-20 Hz).

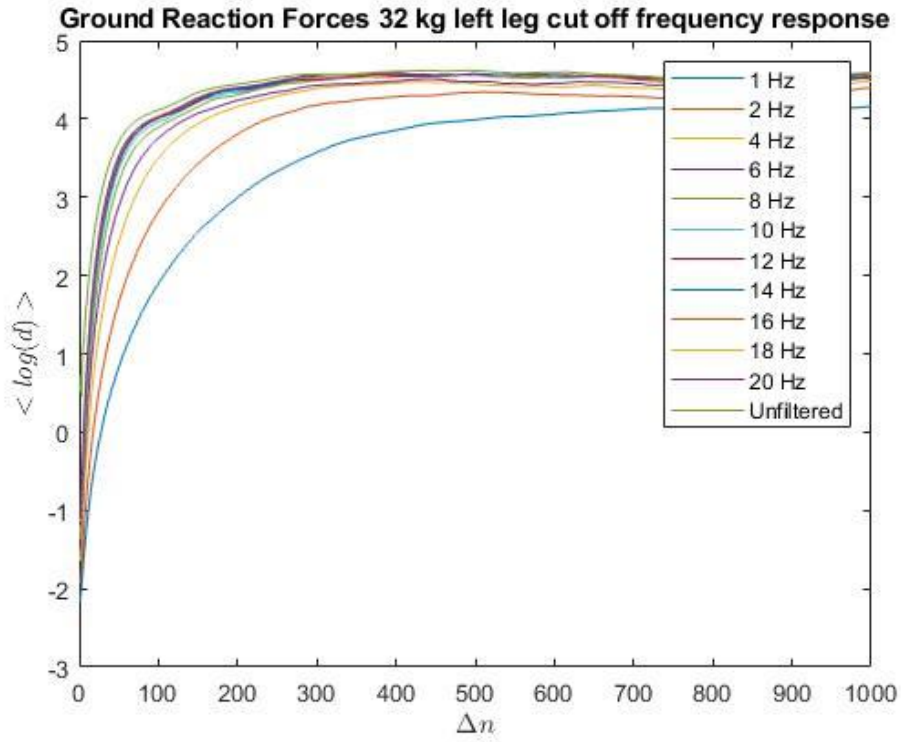

Figure 42 Ground Reaction Forces 32 kg left leg log divergence curve per cut off frequency (1-20 Hz).

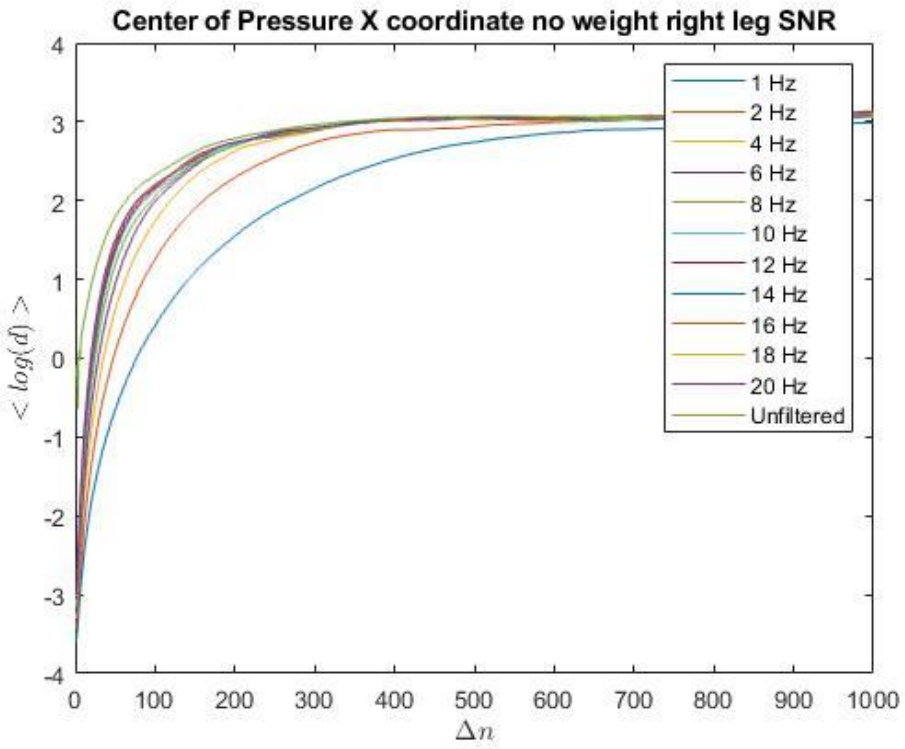

Figure 43 Center of Pressure X coordinate no weight right leg left leg log divergence curve per cut off frequency (1-20 Hz).

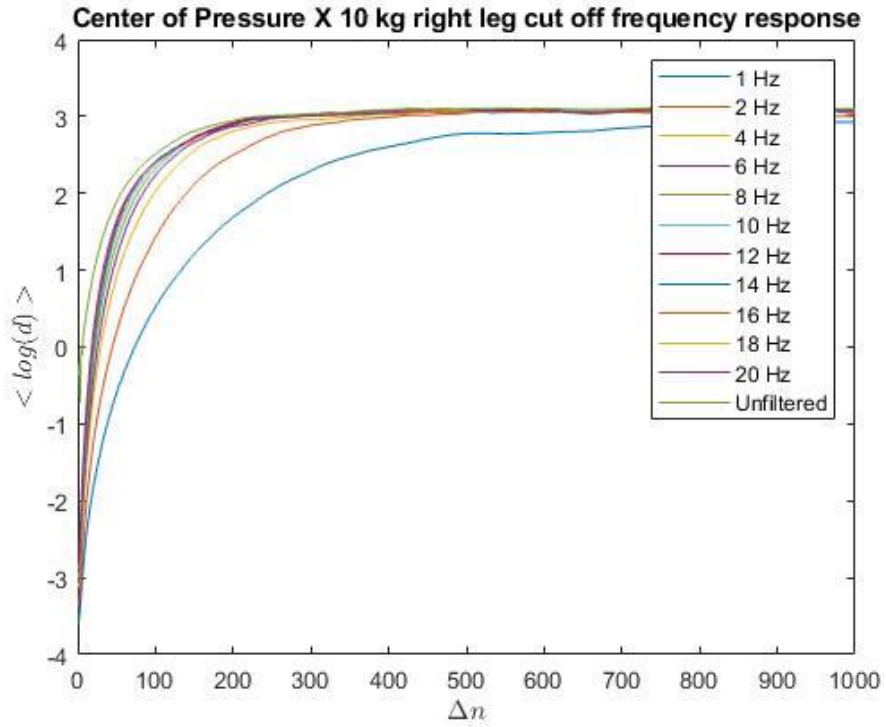

Figure 44 Center of Pressure X coordinate 10 kg right leg left leg log divergence curve per cut off frequency (1-20 Hz).

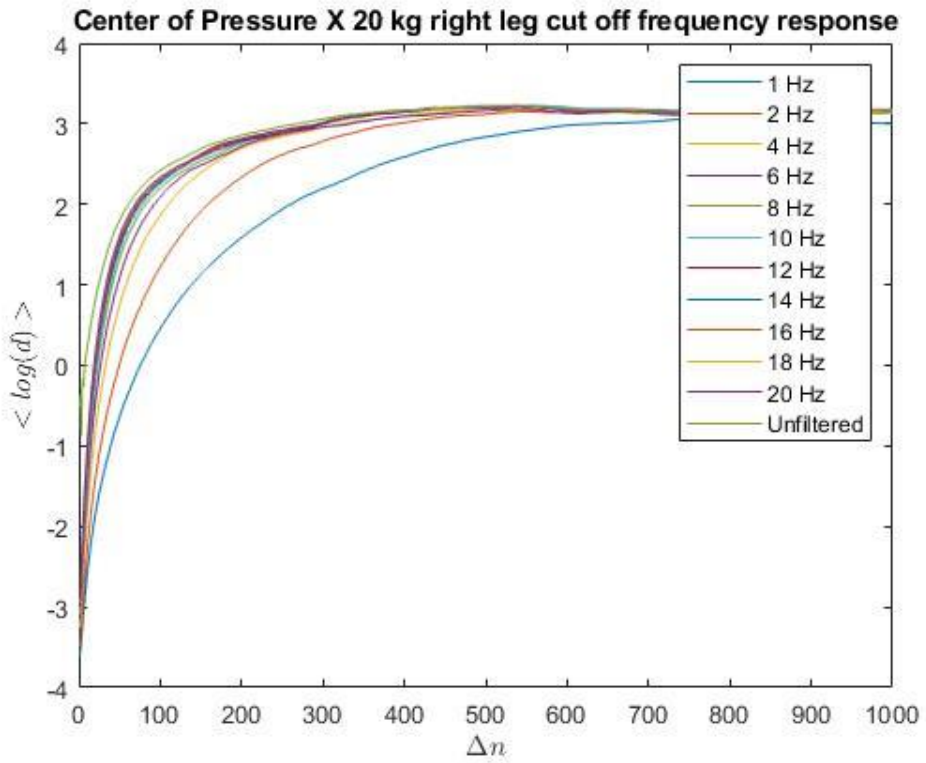

Figure 45 Center of Pressure X coordinate 20 kg right leg left leg log divergence curve per cut off frequency (1-20 Hz).

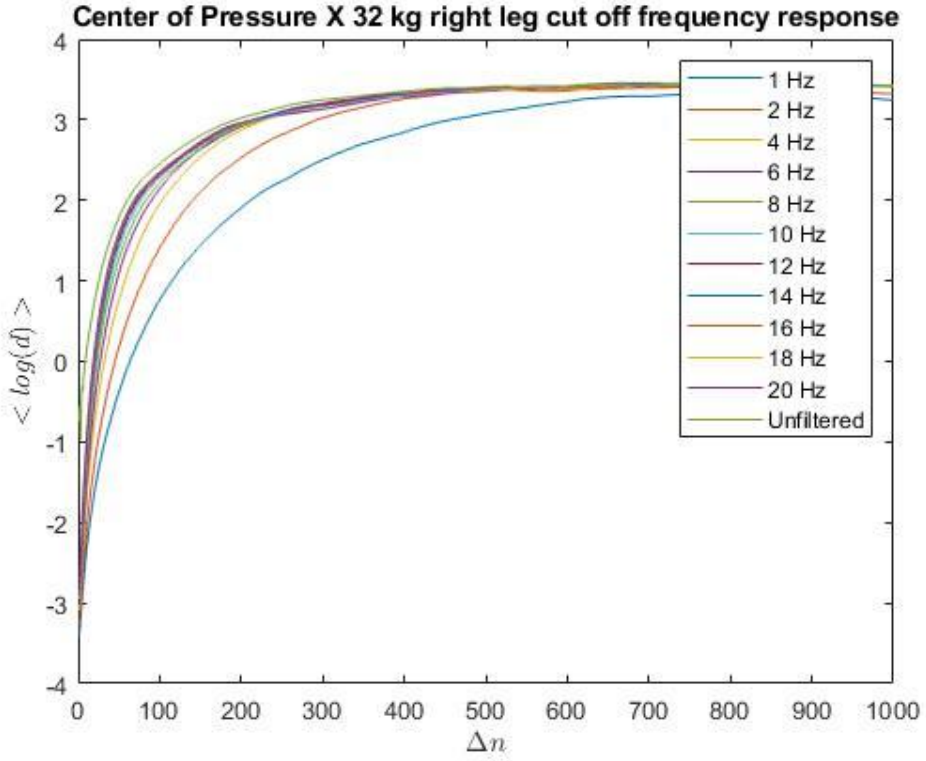

Figure 46 Center of Pressure X coordinate 32 kg right leg left leg log divergence curve per cut off frequency (1-20 Hz).

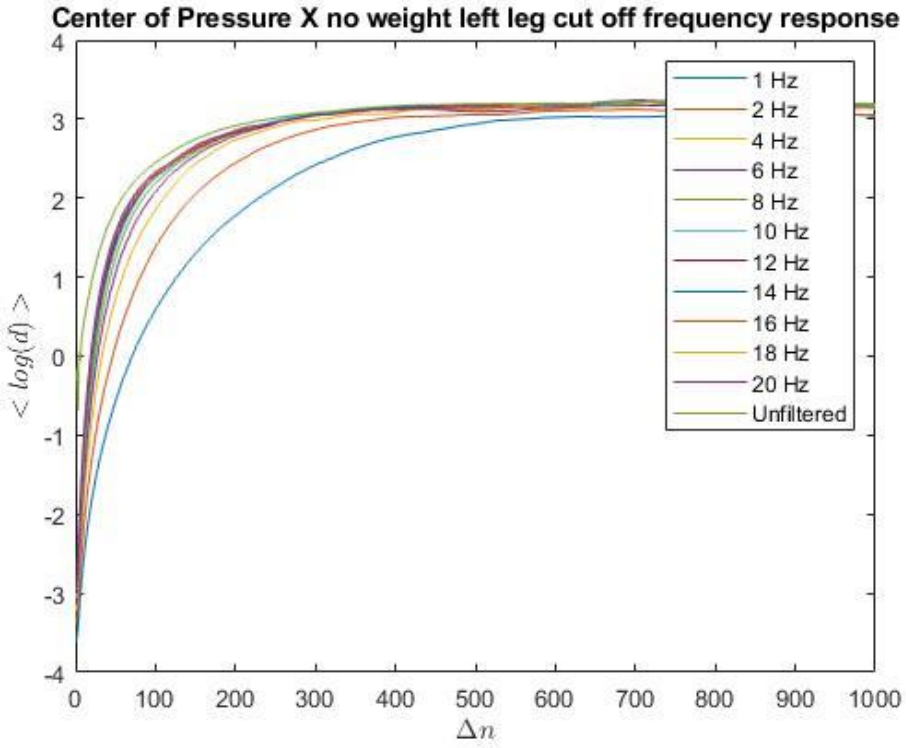

Figure 47 Center of Pressure X coordinate no weight left leg left leg log divergence curve per cut off frequency (1-20 Hz).

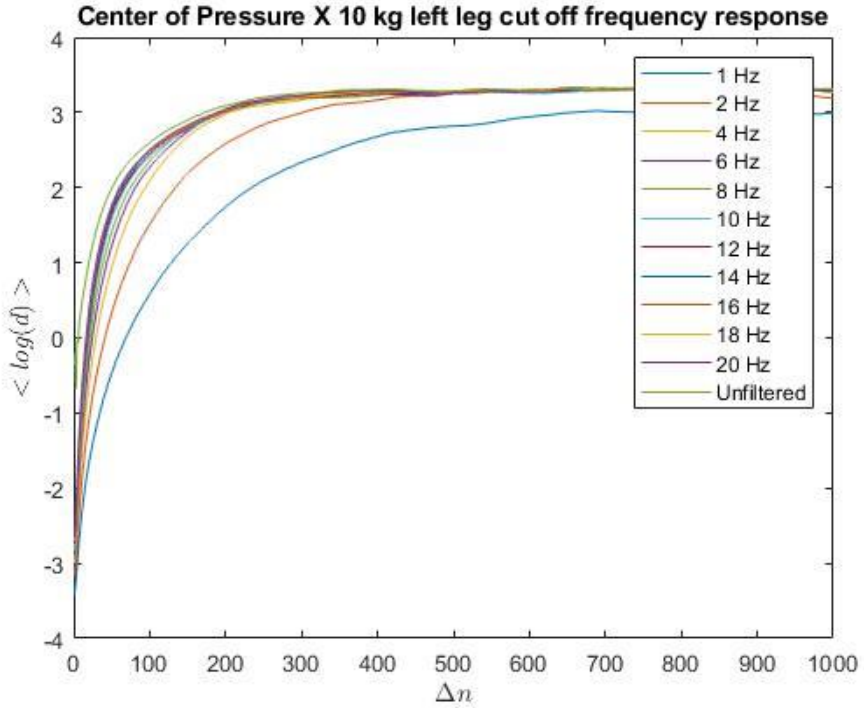

Figure 48 Center of Pressure X coordinate 10 kg left leg left leg log divergence curve per cut off frequency (1-20 Hz).

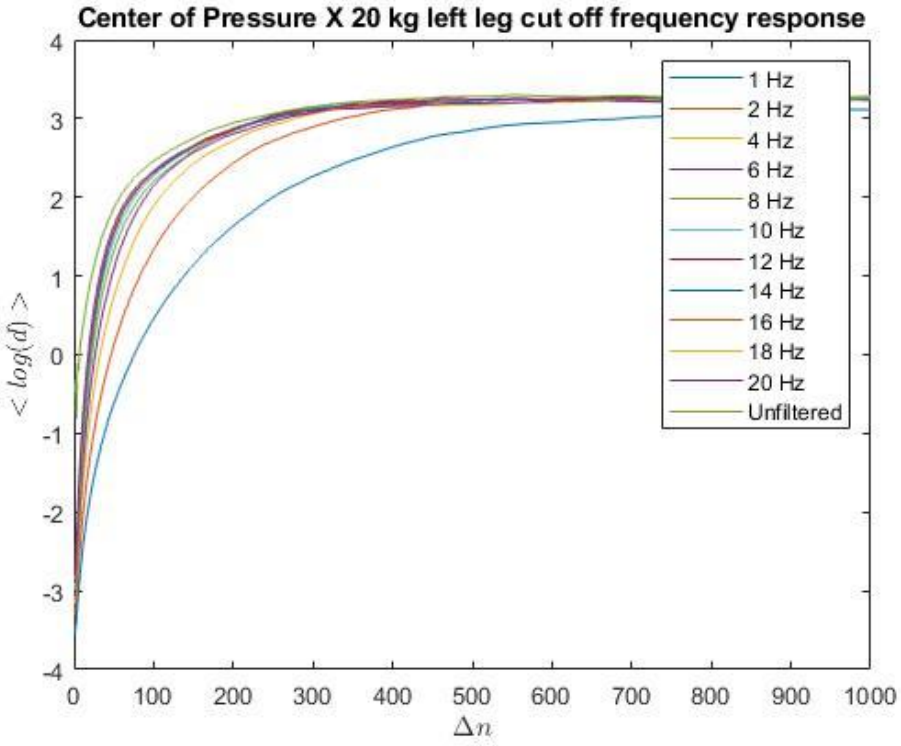

Figure 49 Center of Pressure X coordinate 20 kg left leg left leg log divergence curve per cut off frequency (1-20 Hz).

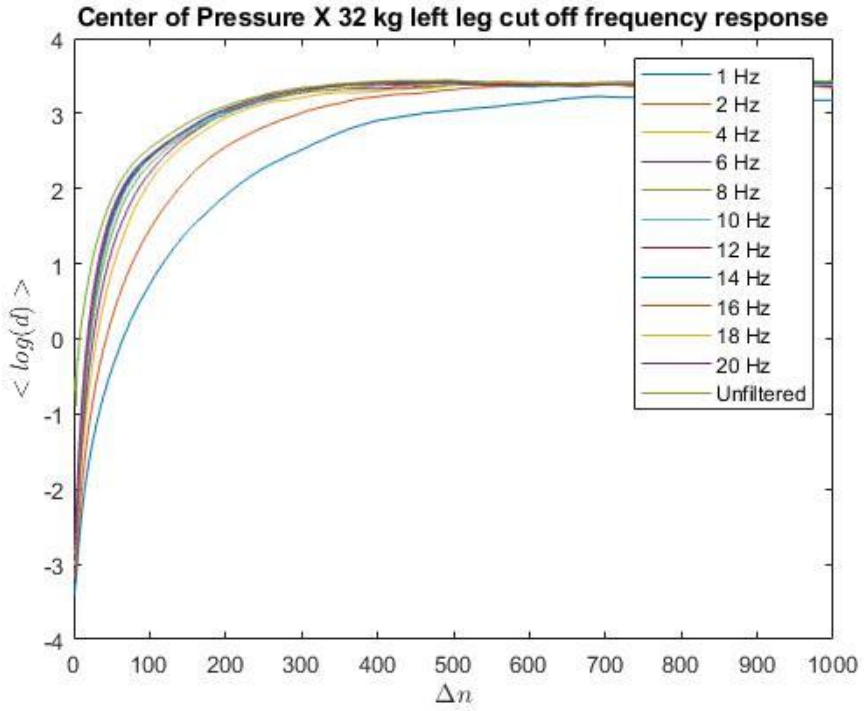

Figure 50 Center of Pressure X coordinate 32 kg left leg left leg log divergence curve per cut off frequency (1-20 Hz).

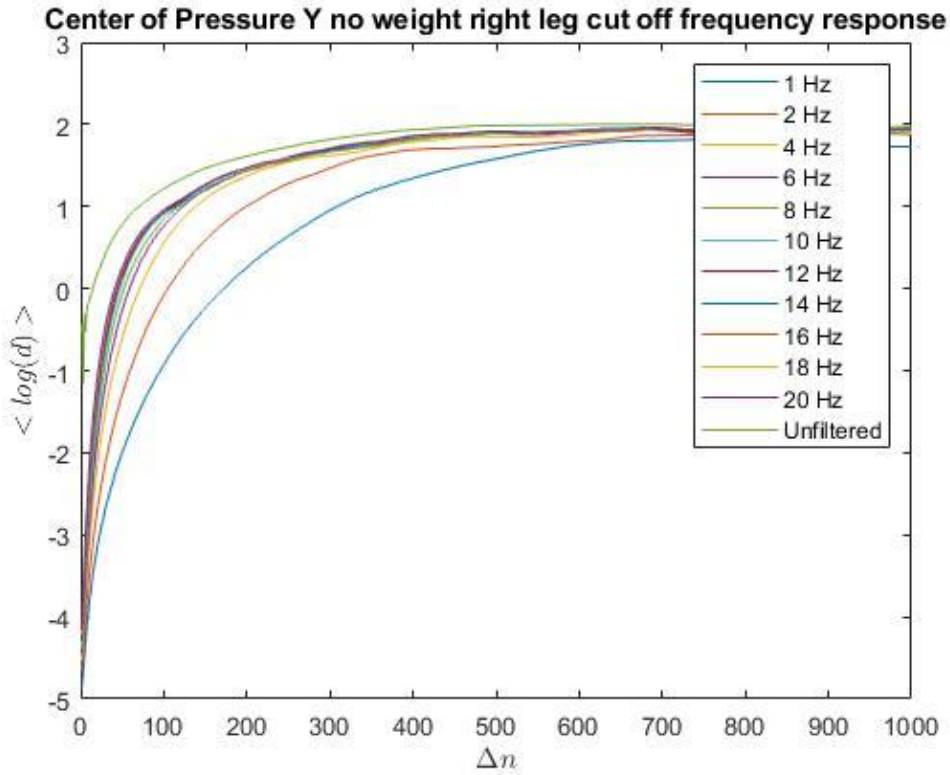

Figure 51 Center of Pressure Y coordinate no weight right leg left leg log divergence curve per cut off frequency (1-20 Hz).

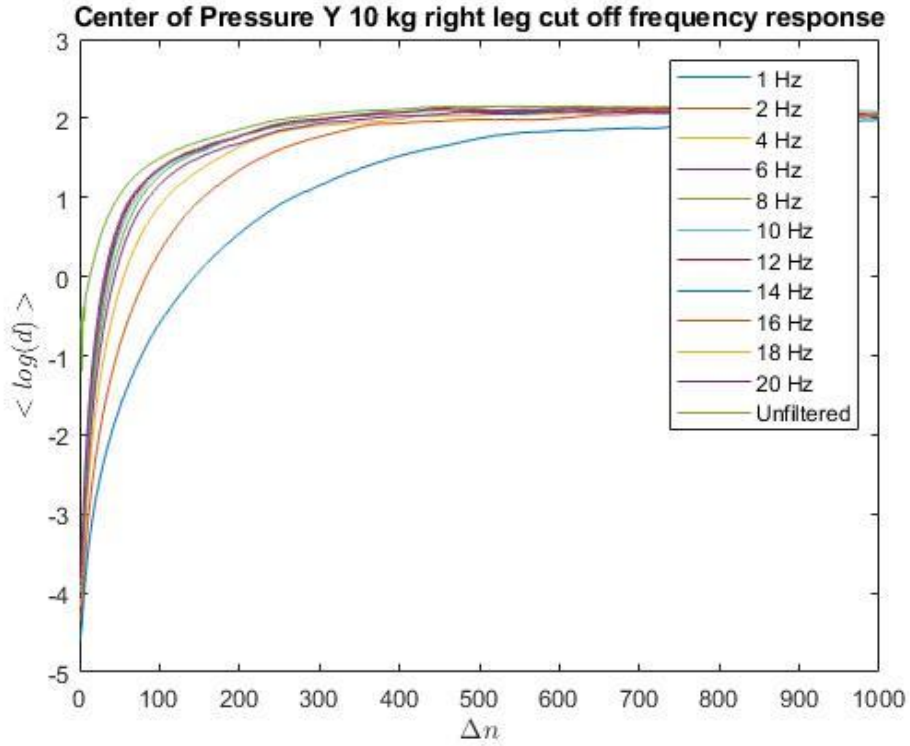

Figure 52 Center of Pressure Y coordinate 10 kg right leg left leg log divergence curve per cut off frequency (1-20 Hz).

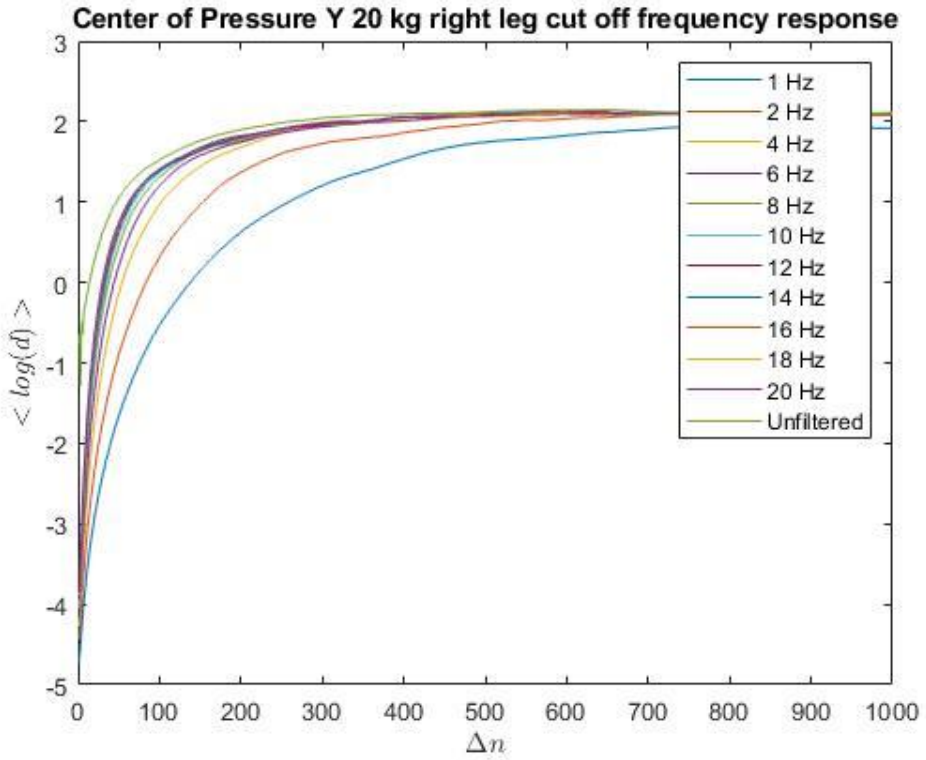

Figure 53 Center of Pressure Y coordinate 20 kg right leg left leg log divergence curve per cut off frequency (1-20 Hz).

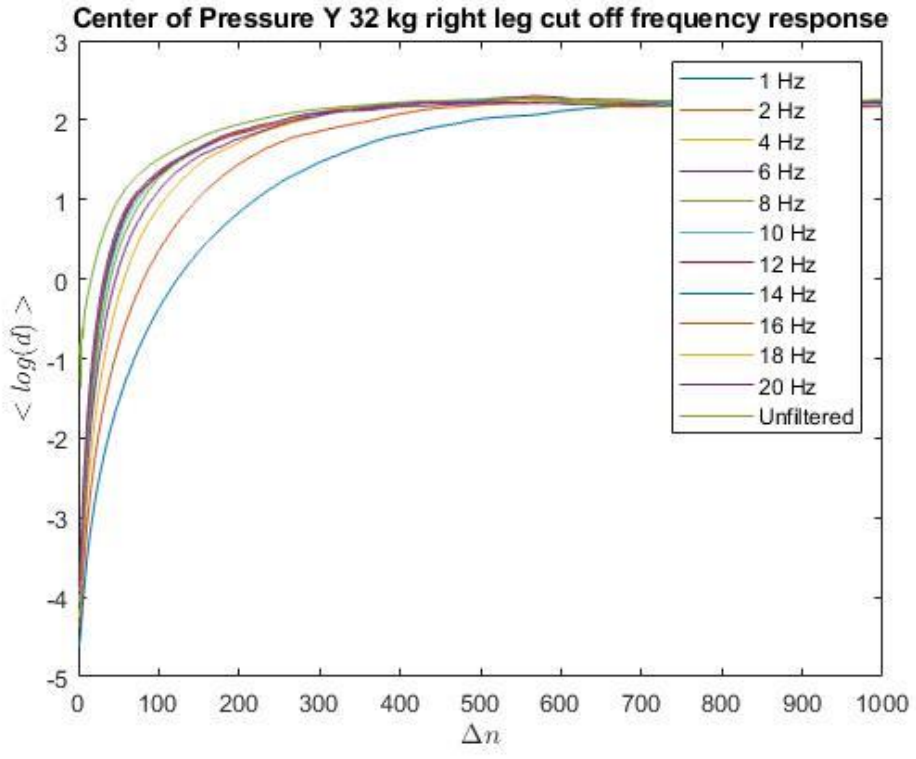

Figure 54 Center of Pressure Y coordinate 32 kg right leg left leg log divergence curve per cut off frequency (1-20 Hz).

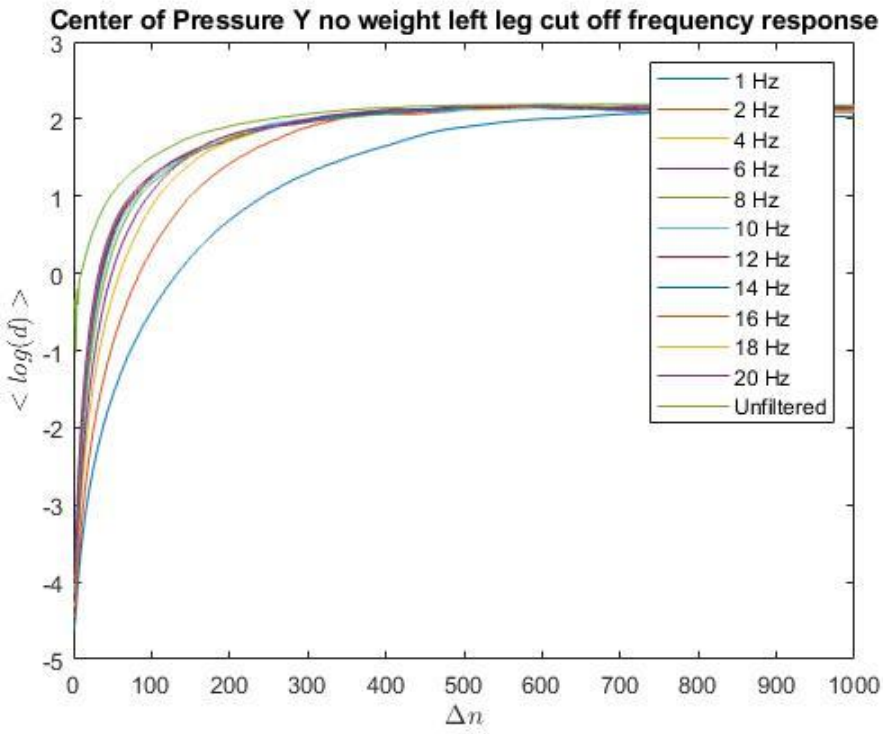

Figure 55 Center of Pressure Y coordinate no weight left leg left leg log divergence curve per cut off frequency (1-20 Hz).

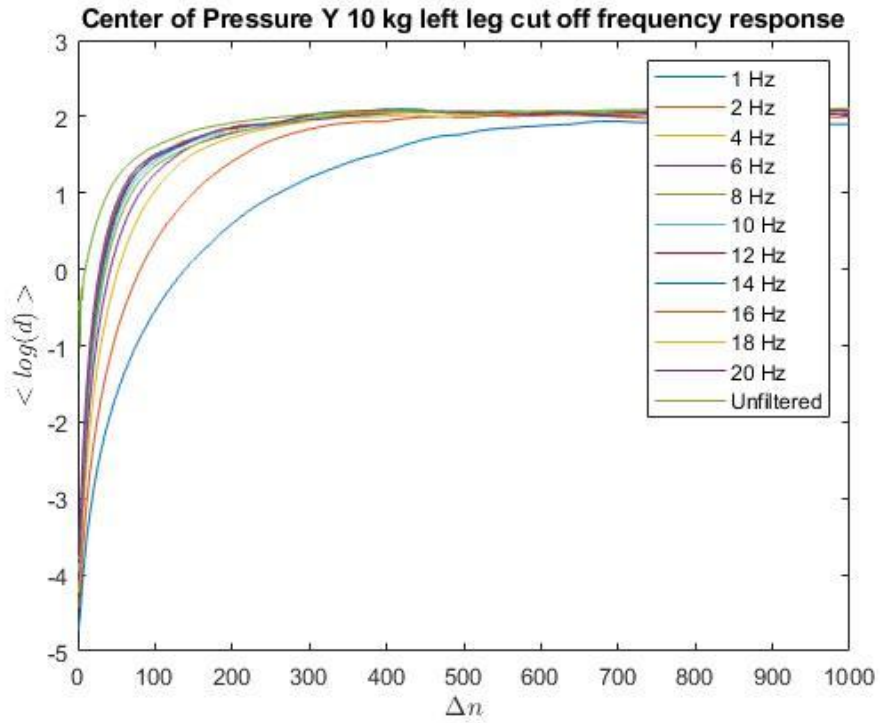

Figure 56 Center of Pressure Y coordinate 10 kg left leg left leg log divergence curve per cut off frequency (1-20 Hz).

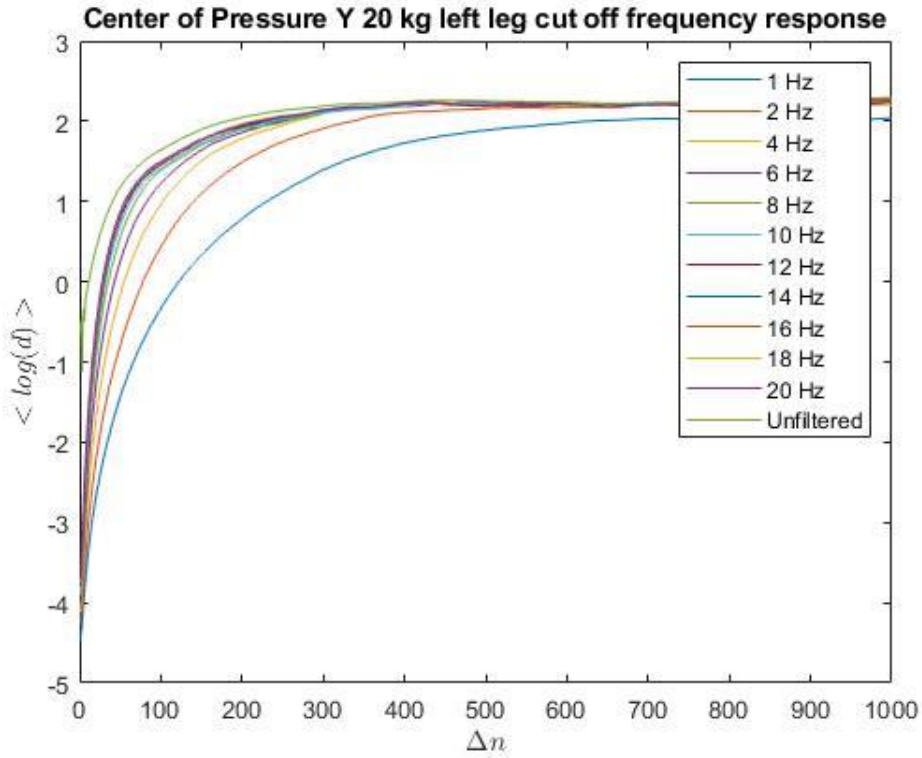

Figure 57 Center of Pressure Y coordinate 20 kg left leg left leg log divergence curve per cut off frequency (1-20 Hz).

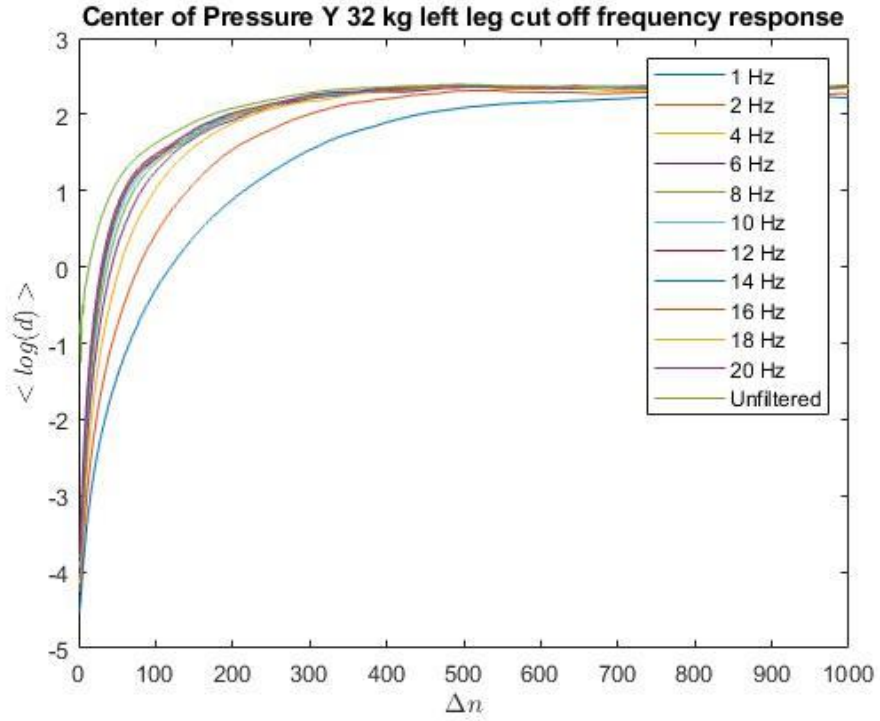

Figure 58 Center of Pressure Y coordinate 32 kg left leg left leg log divergence curve per cut off frequency (1-20 Hz).

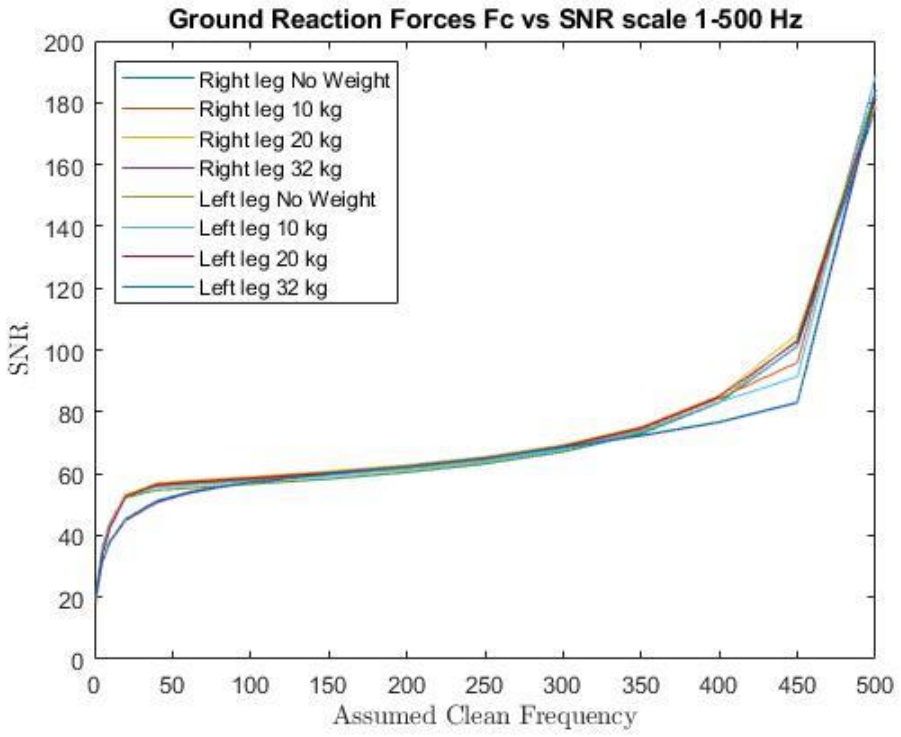

Figure 59 Ground Reaction Forces High Frequency SNR.

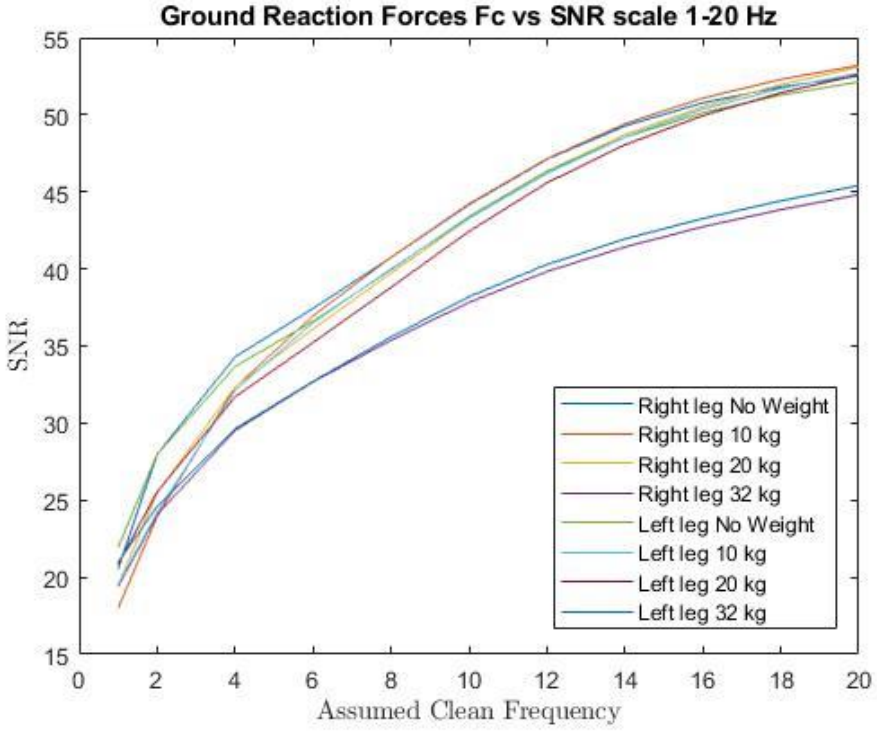

Figure 60 Ground Reaction Forces SNR.

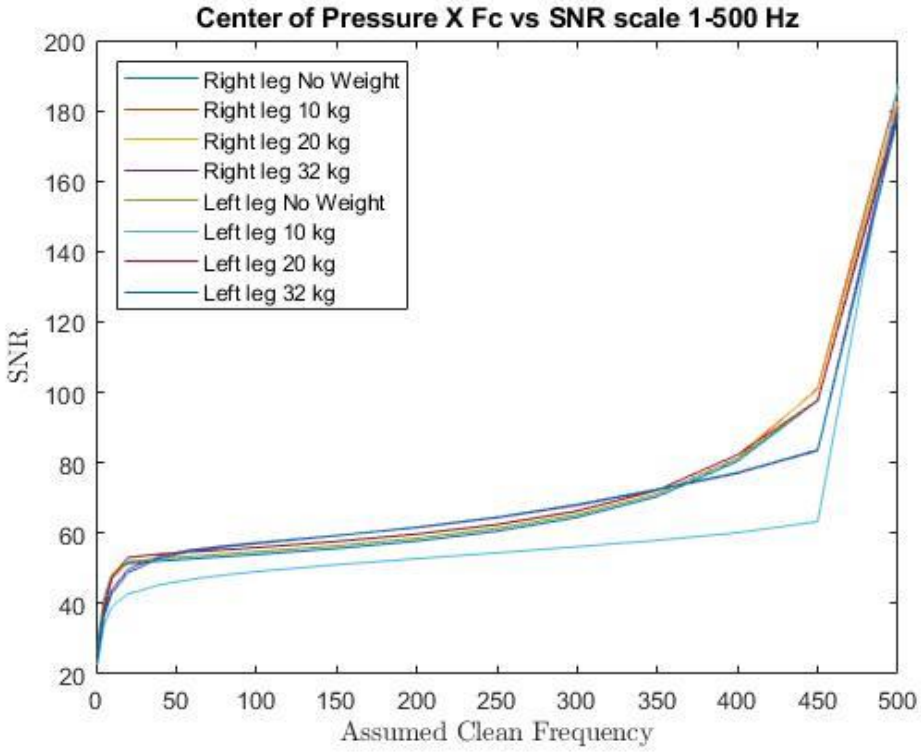

Figure 61 Center of Pressure X High Frequency SNR.

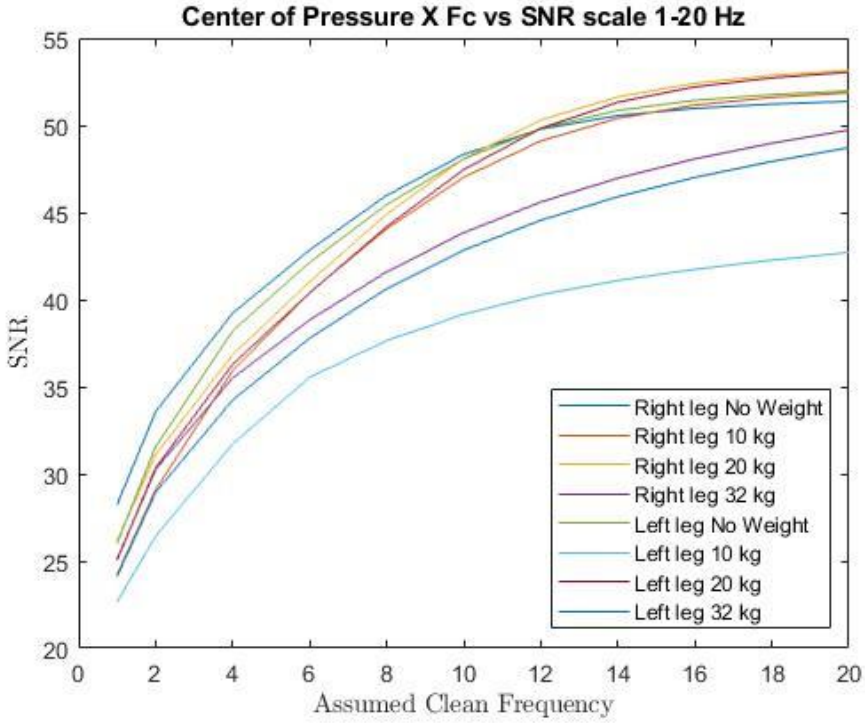

Figure 62 Center of Pressure X SNR.

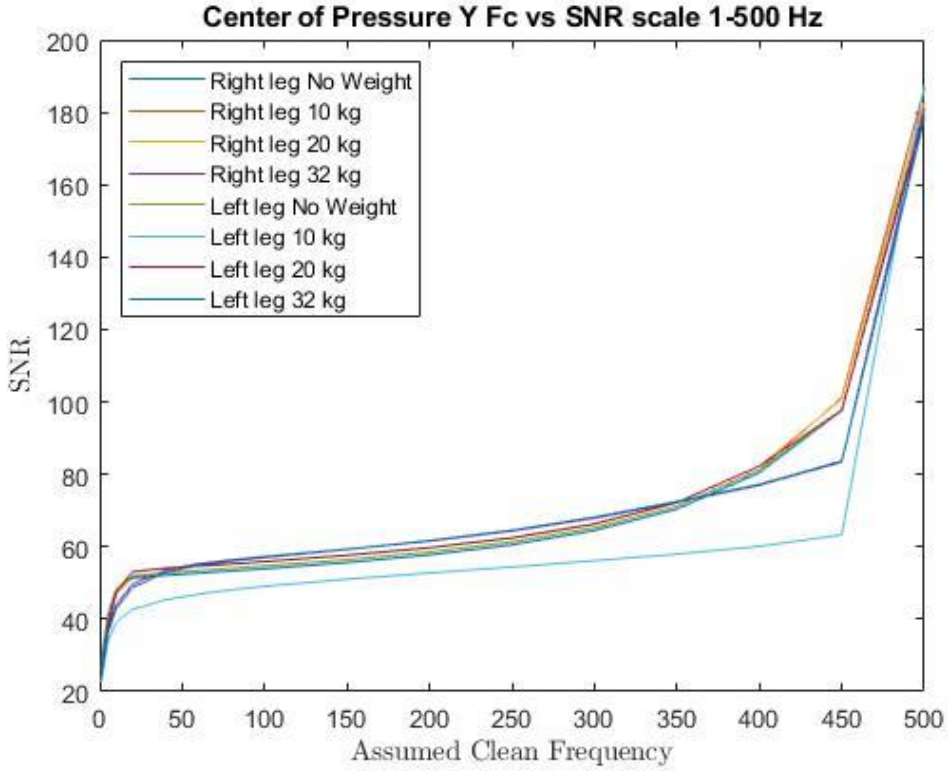

Figure 63 Center of Pressure Y High Frequency SNR.

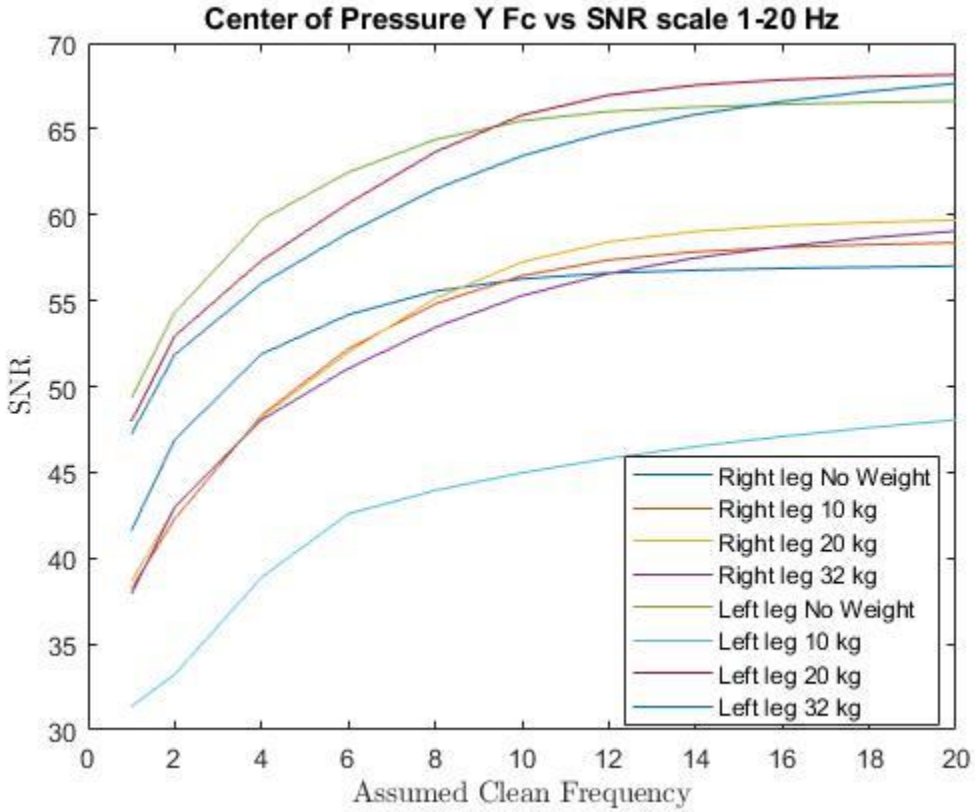

Figure 64 Center of Pressure Y SNR.

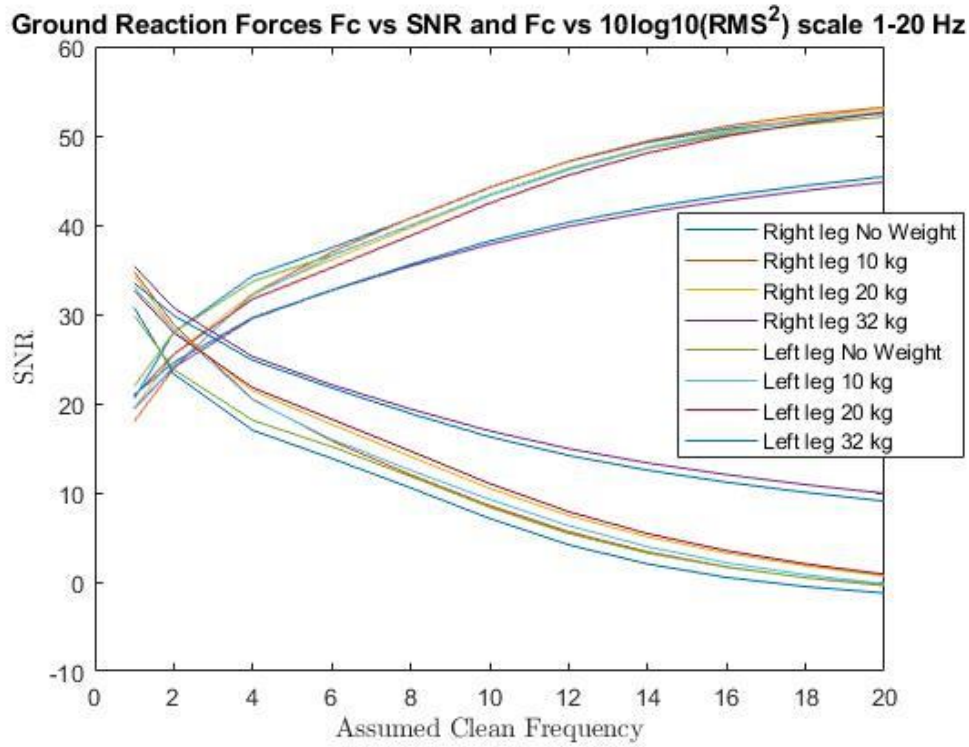

Figure 65 Ground Reaction Forces Fc vs SNR and Fc vs $10Log_{10}(RMS^2)$ for Ground Reaction Force.

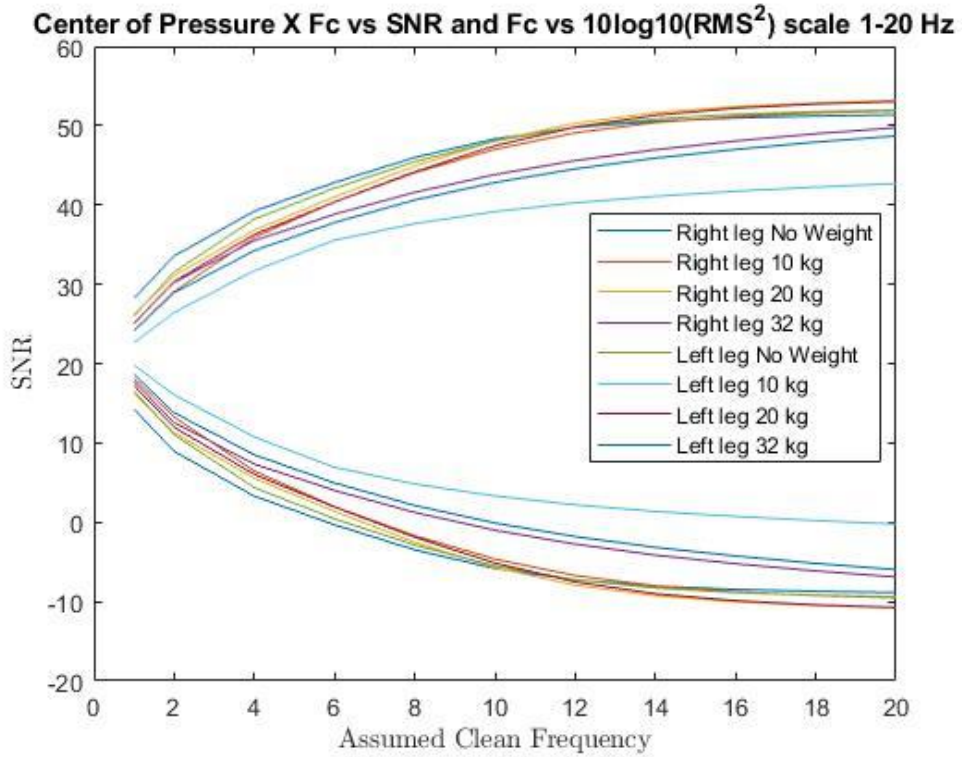

Figure 66 Center of Pressure X Fc vs SNR and Fc vs $10Log_{10}(RMS^2)$ for Center of Pressure X.

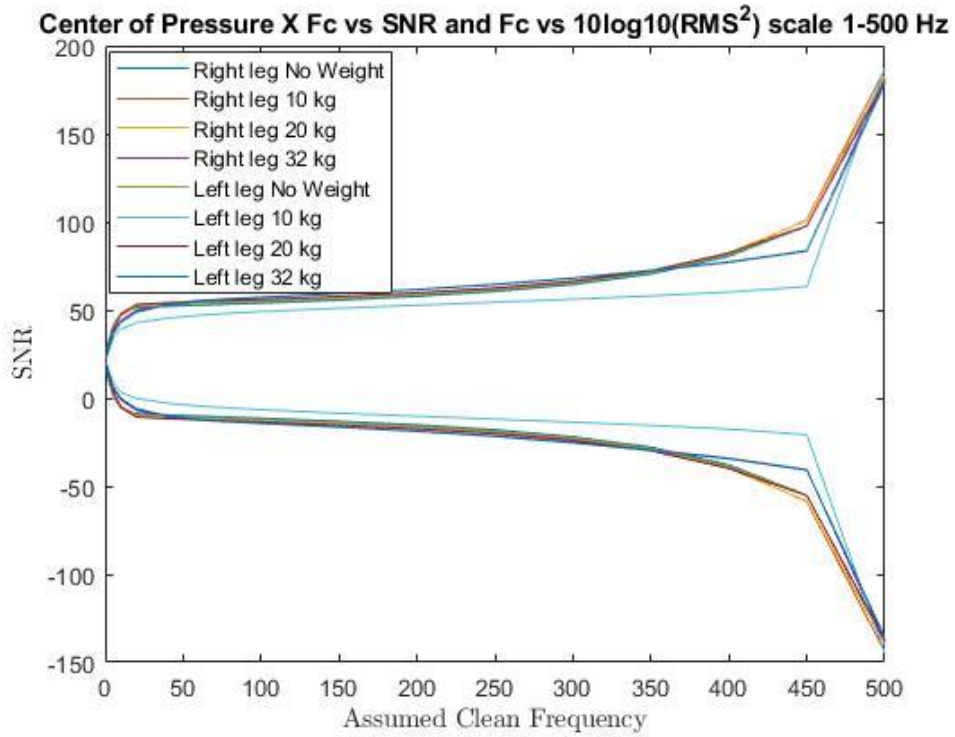

Figure 67 Center of Pressure X Fc vs SNR and Fc vs $10Log_{10}(RMS^2)$ for Center of Pressure X High Frequency.

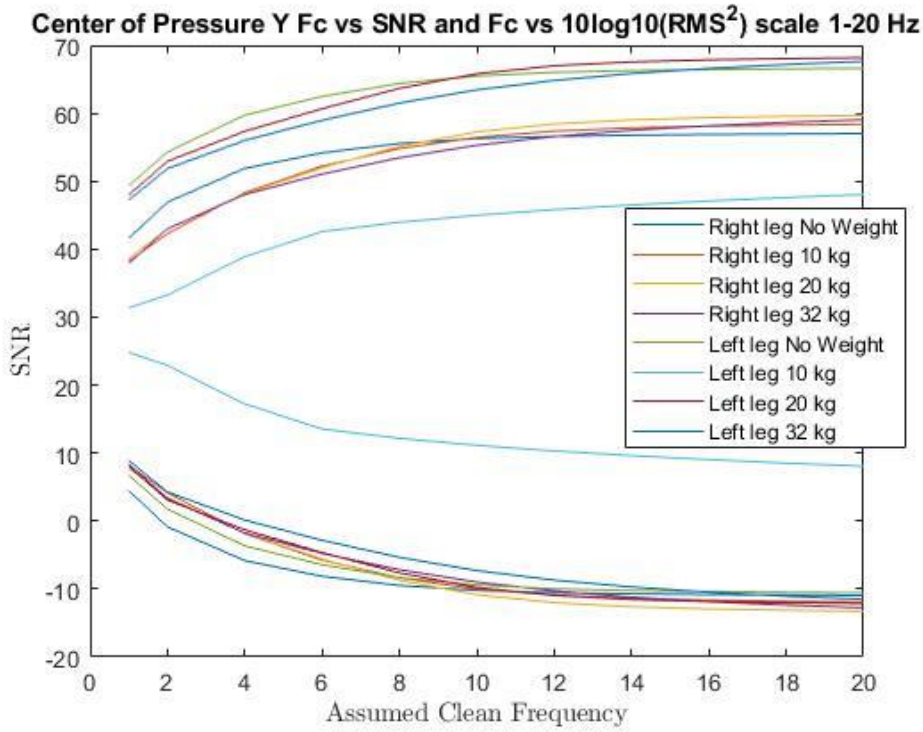

Figure 68 Center of Pressure Y Fc vs SNR and Fc vs $10Log_{10}(RMS^2)$ for Center of Pressure Y.

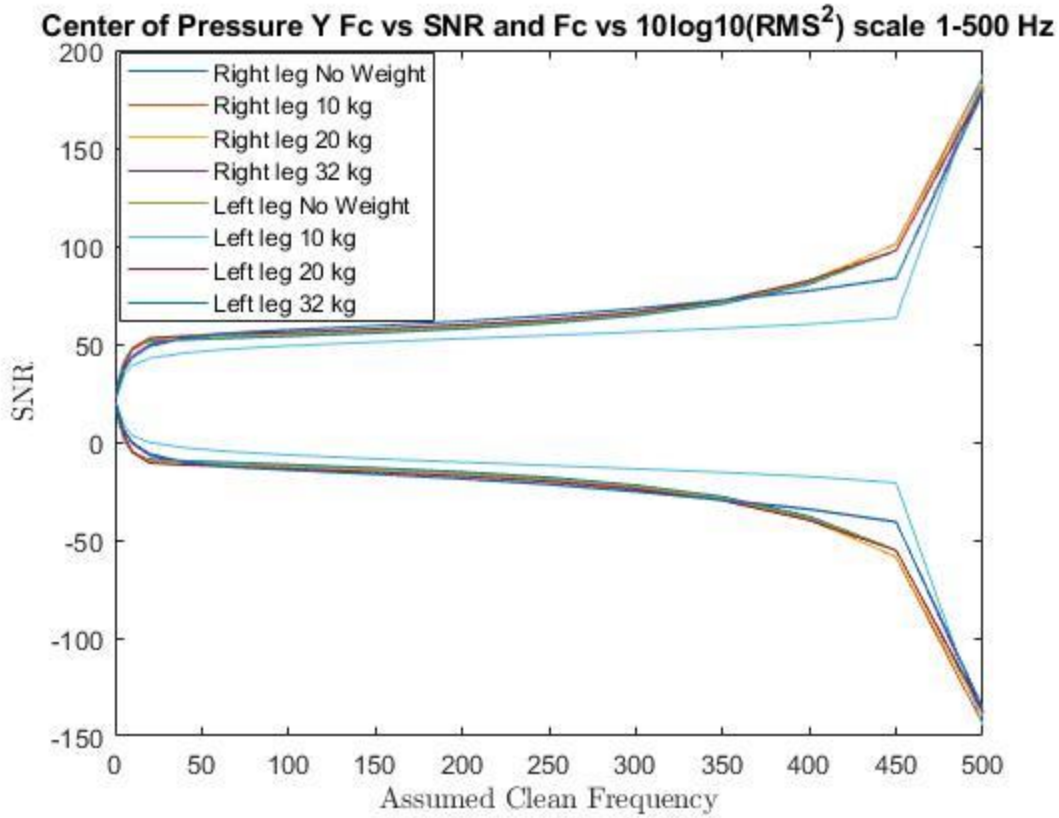

Figure 69 Center of Pressure Y Fc vs SNR and Fc vs $10Log_{10}(RMS^2)$ for Center of Pressure Y High Frequency.

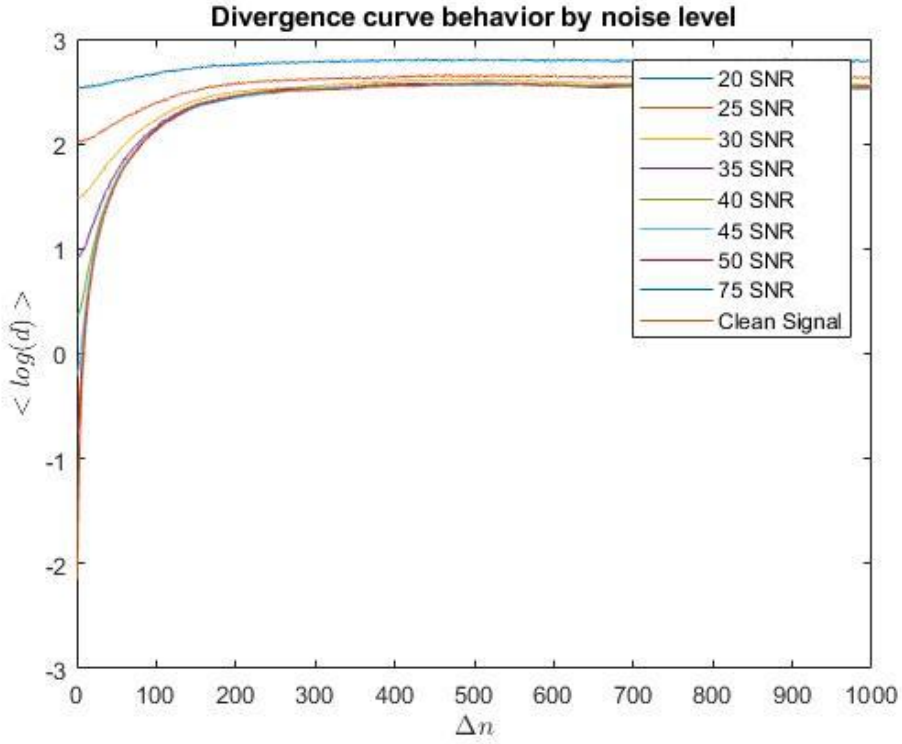

Figure 70 Divergence curve behavior by noise level.

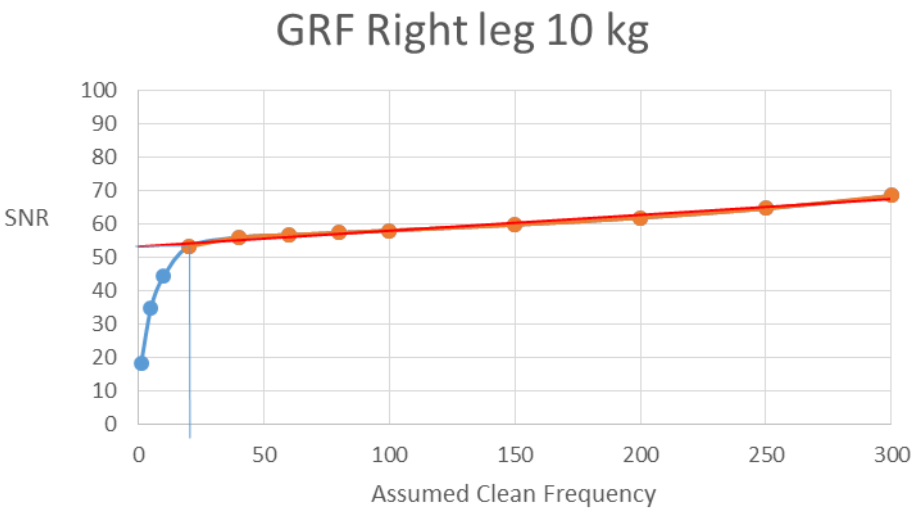

Figure 71 SNR vs Assumed Clean Frequency Ground Reaction Forces of right leg with 10 kg of additional weight.

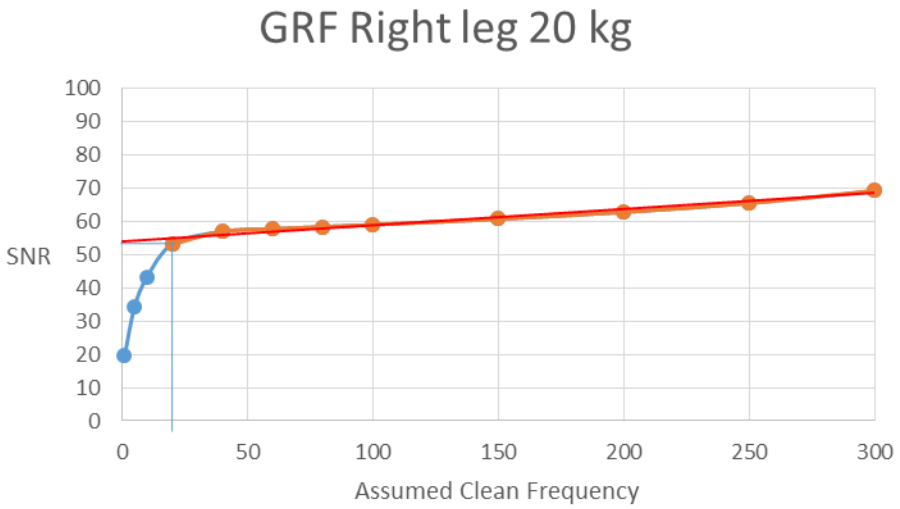

Figure 72 SNR vs Assumed Clean Frequency Ground Reaction Forces of right leg with 20 kg of additional weight.

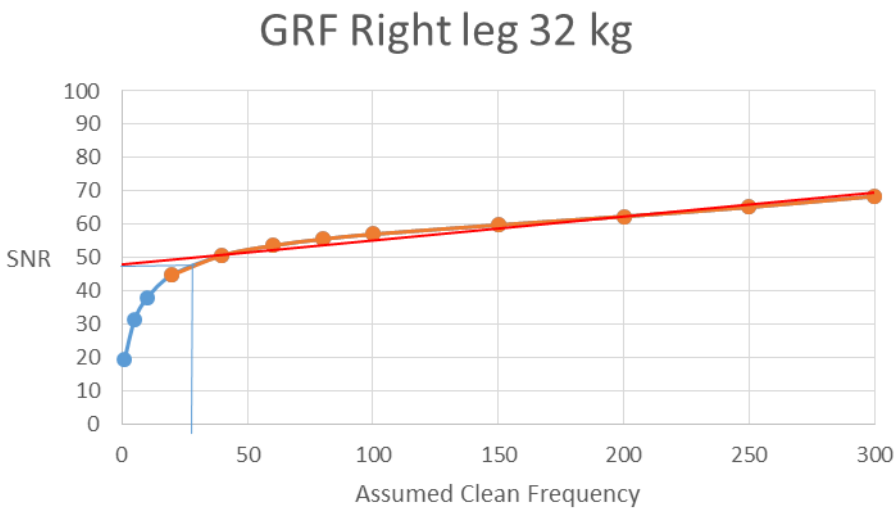

Figure 73 SNR vs Assumed Clean Frequency Ground Reaction Forces of right leg with 32 kg of additional weight.

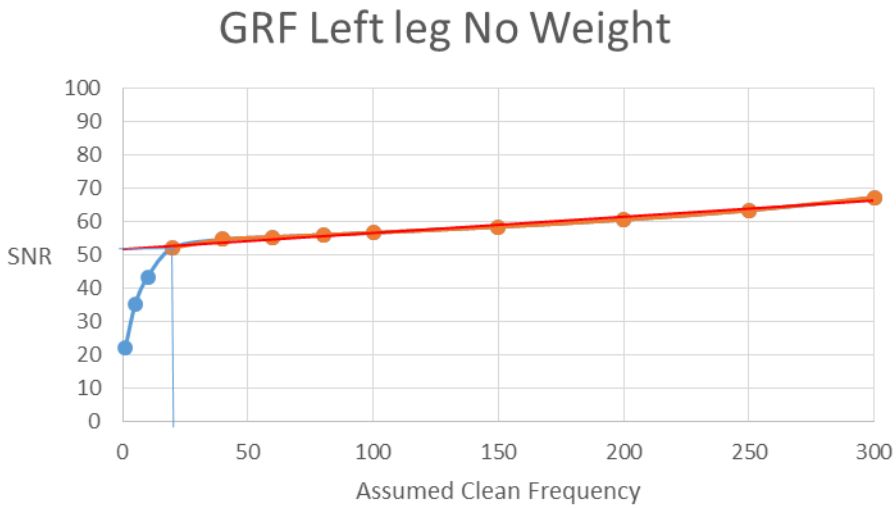

Figure 74 SNR vs Assumed Clean Frequency Ground Reaction Forces of left leg with no additional weight.

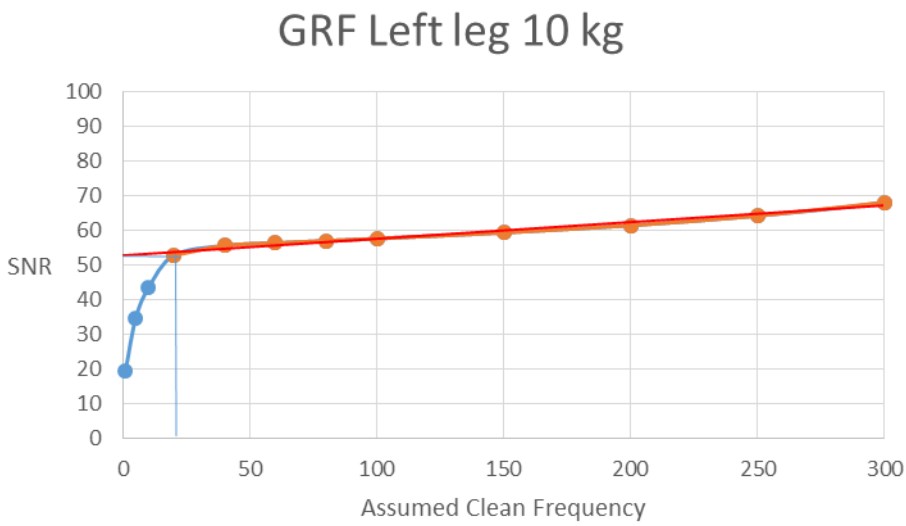

Figure 75 SNR vs Assumed Clean Frequency Ground Reaction Forces of left leg with 10 kg of additional weight.

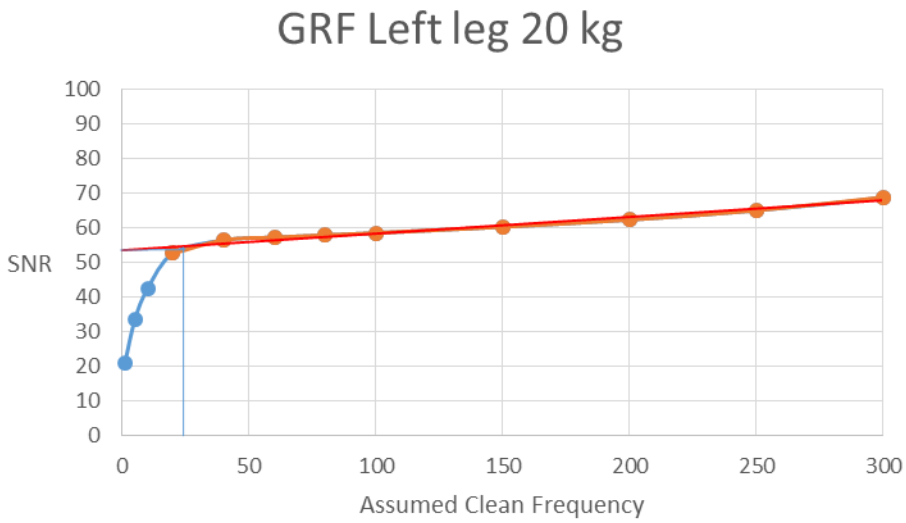

Figure 76 SNR vs Assumed Clean Frequency Ground Reaction Forces of left leg with 20 kg of additional weight.

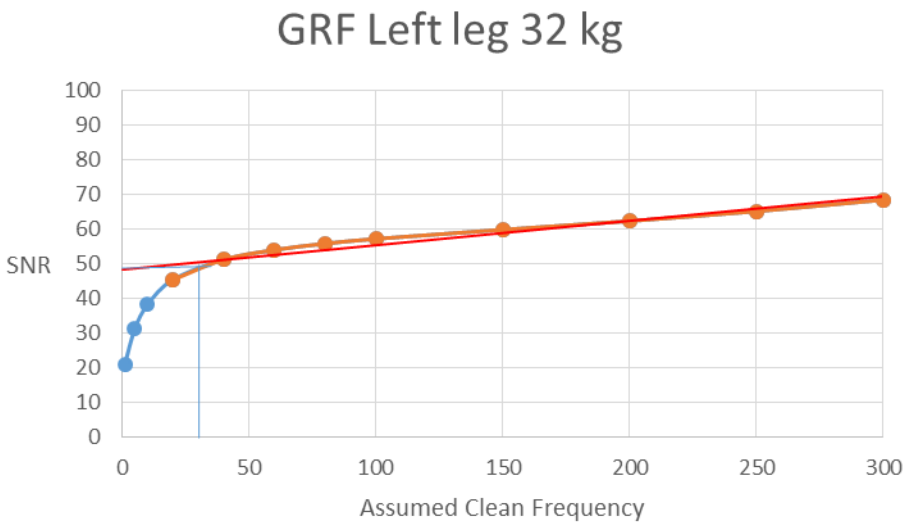

Figure 77 SNR vs Assumed Clean Frequency Ground Reaction Forces of left leg with 32 kg of additional weight.

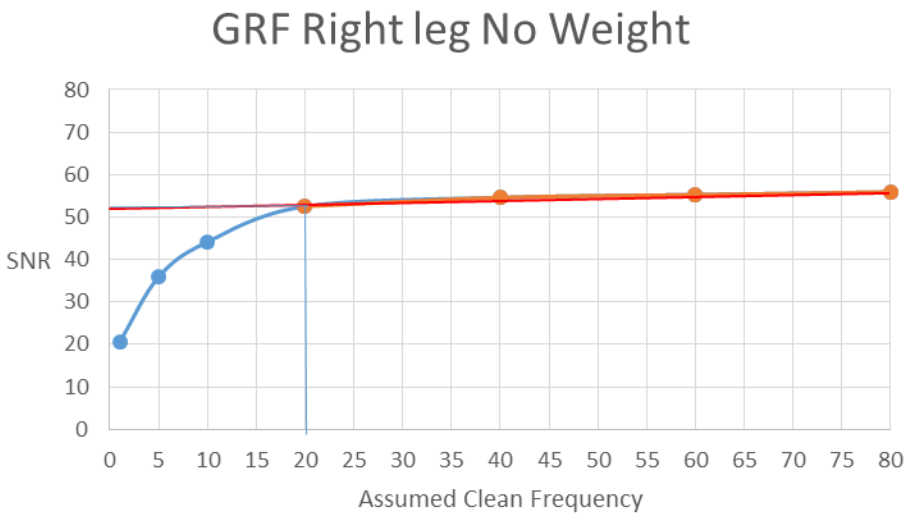

Figure 78 Zoomed in initial section of the SNR vs Assumed Clean Frequency Ground Reaction Forces of right leg with no additional weight.

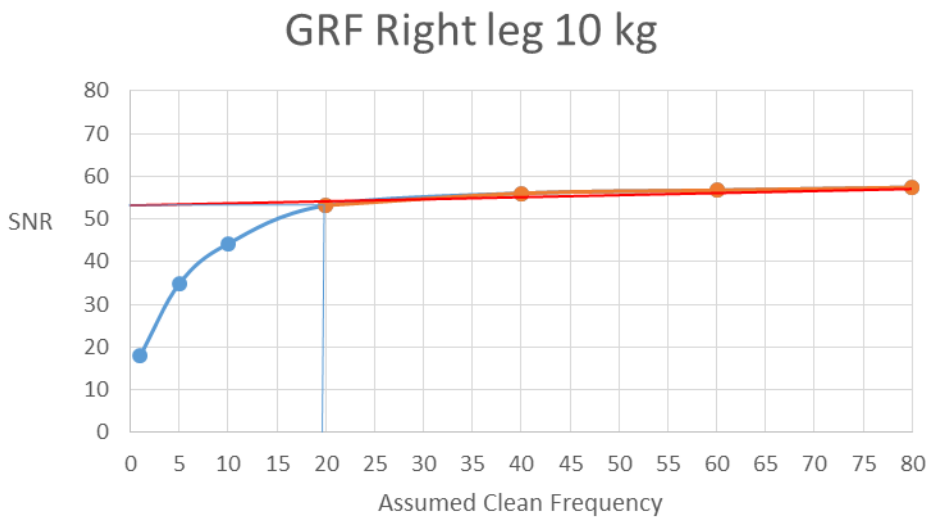

Figure 79 Zoomed in initial section of the SNR vs Assumed Clean Frequency Ground Reaction Forces of right leg with 10 kg of additional weight.

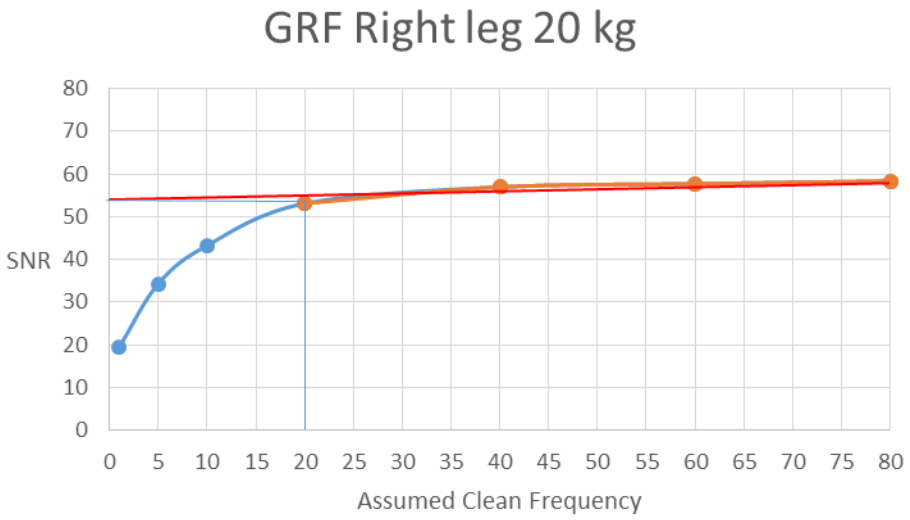

Figure 80 Zoomed in initial section of the SNR vs Assumed Clean Frequency Ground Reaction Forces of right leg with 20 kg of additional weight.

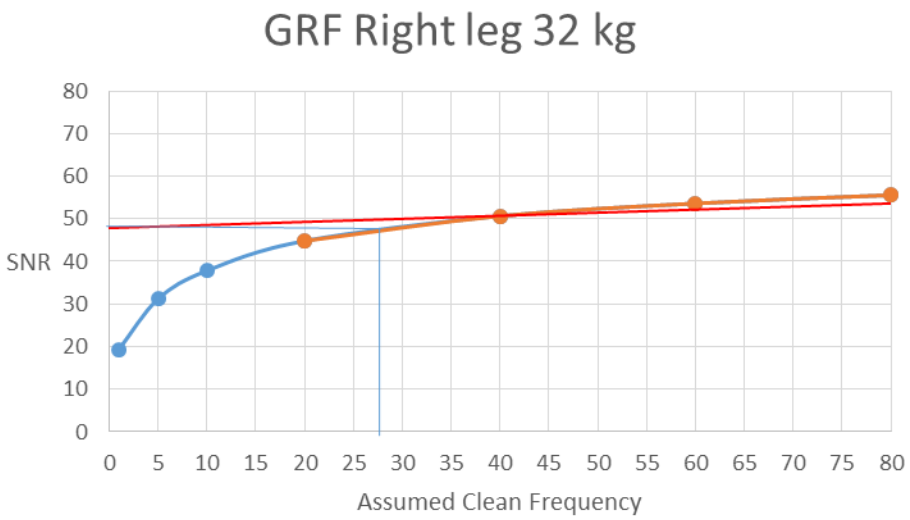

Figure 81 Zoomed in initial section of the SNR vs Assumed Clean Frequency Ground Reaction Forces of right leg with 32 kg of additional weight.

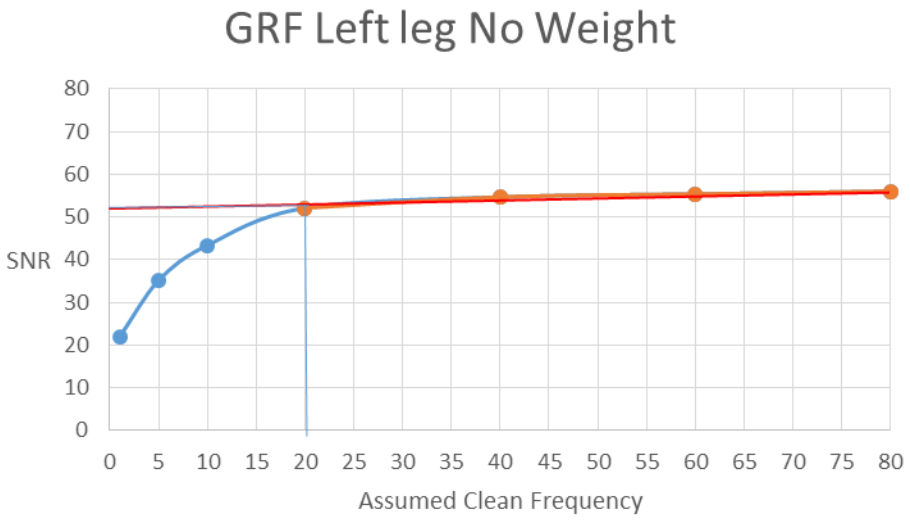

Figure 82 Zoomed in initial section of the SNR vs Assumed Clean Frequency Ground Reaction Forces of left leg with no additional weight.

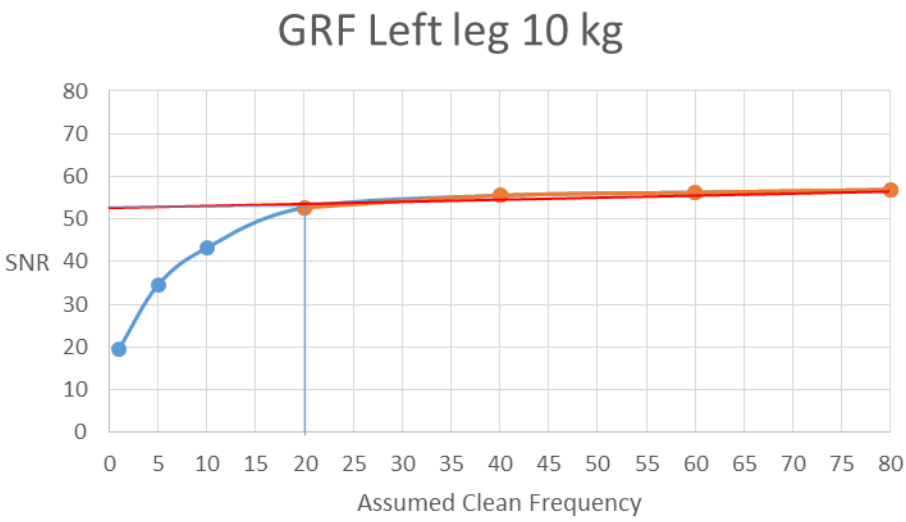

Figure 83 Zoomed in initial section of the SNR vs Assumed Clean Frequency Ground Reaction Forces of left leg with 10 kg of additional weight.

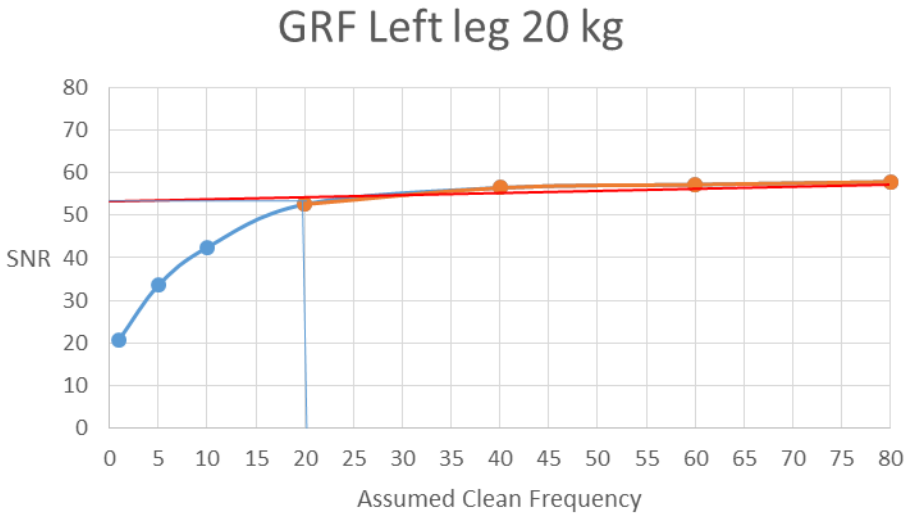

Figure 84 Zoomed in initial section of the SNR vs Assumed Clean Frequency Ground Reaction Forces of left leg with 20 kg of additional weight.

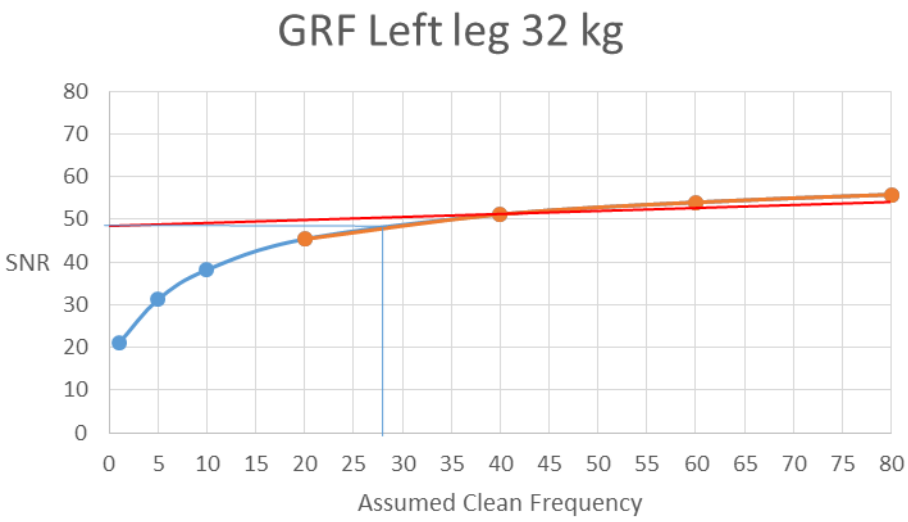

Figure 85 Zoomed in initial section of the SNR vs Assumed Clean Frequency Ground Reaction Forces of left leg with 32 kg of additional weight.

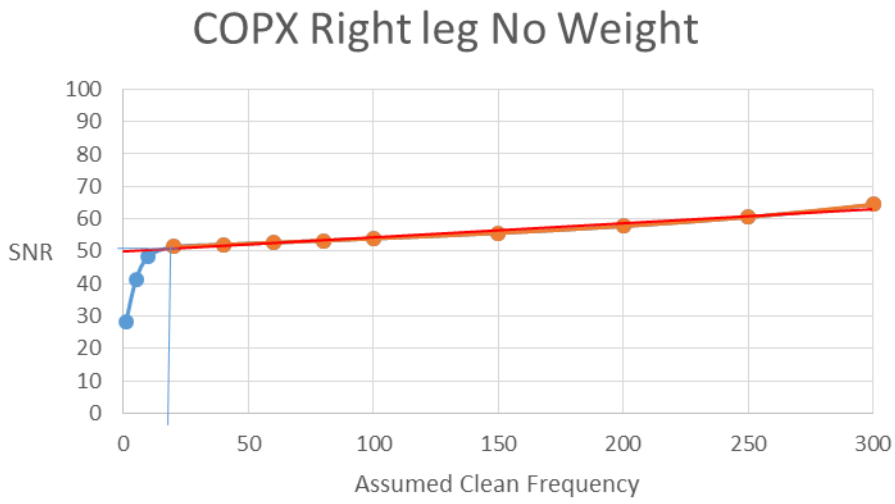

Figure 86 SNR vs Assumed Clean Frequency Center of Pressure X of right leg with no additional weight.

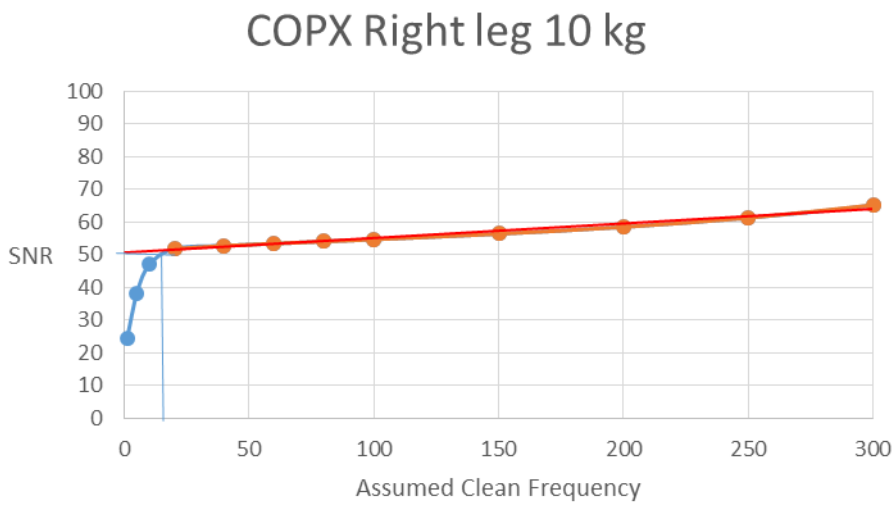

Figure 87 SNR vs Assumed Clean Frequency Center of Pressure X of right leg with 10 kg additional weight.

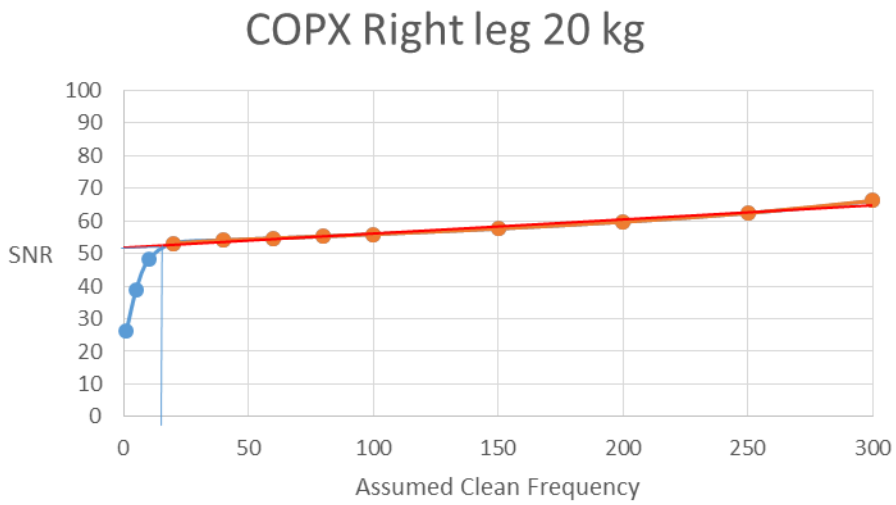

Figure 88 SNR vs Assumed Clean Frequency Center of Pressure X of right leg with 20 kg additional weight.

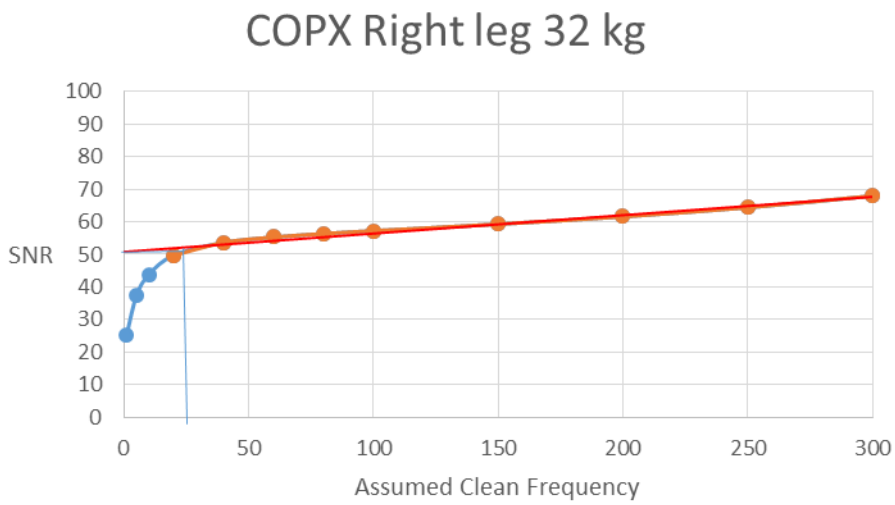

Figure 89 SNR vs Assumed Clean Frequency Center of Pressure X of right leg with 32 kg additional weight.

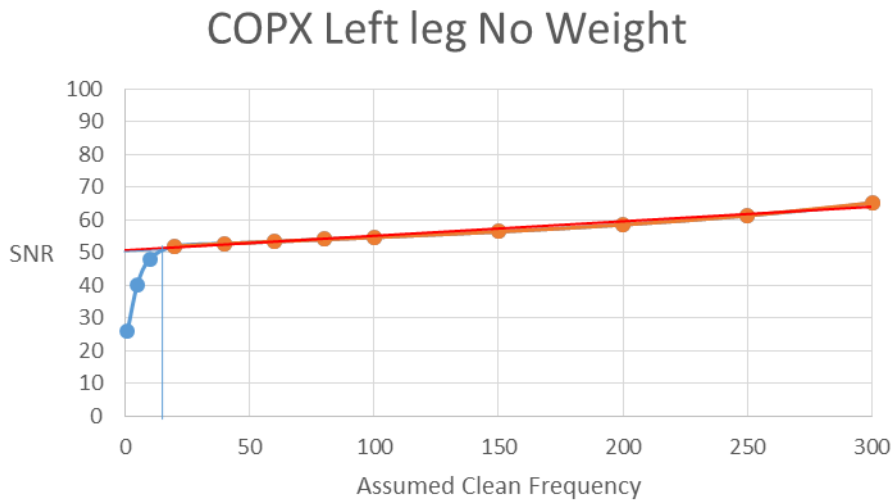

Figure 90 SNR vs Assumed Clean Frequency Center of Pressure X of left leg with no additional weight.

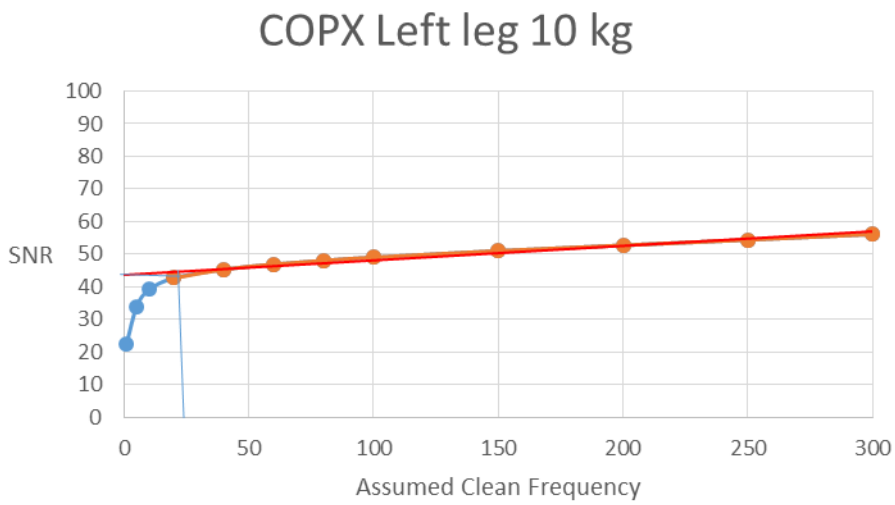

Figure 91 SNR vs Assumed Clean Frequency Center of Pressure X of left leg with 10 kg additional weight.

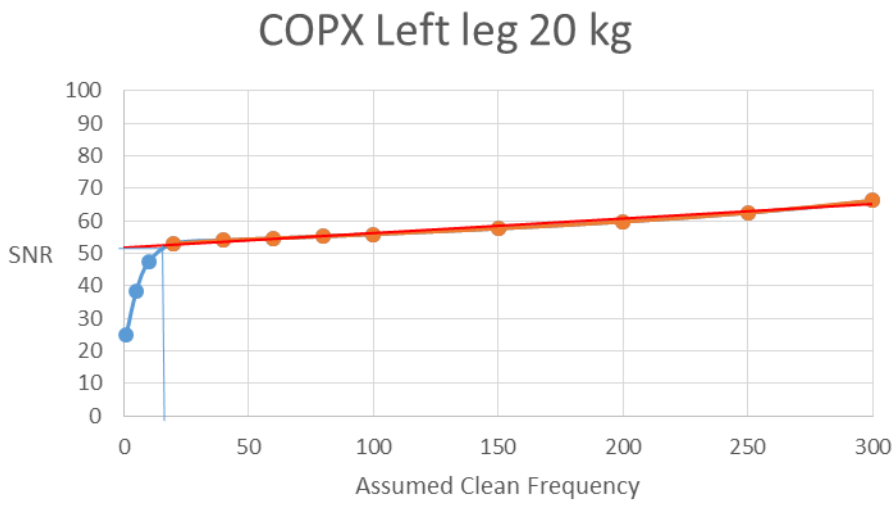

Figure 92 SNR vs Assumed Clean Frequency Center of Pressure X of left leg with 20 kg additional weight.

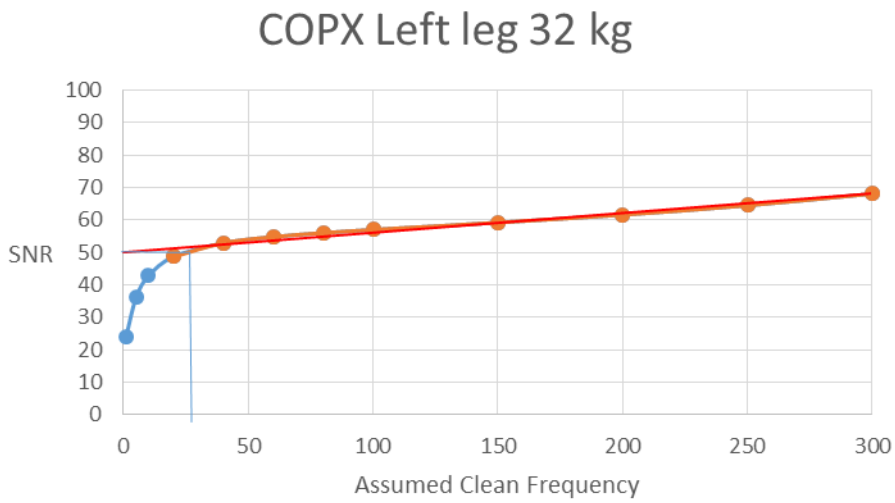

Figure 93 SNR vs Assumed Clean Frequency Center of Pressure X of left leg with 32 kg additional weight.

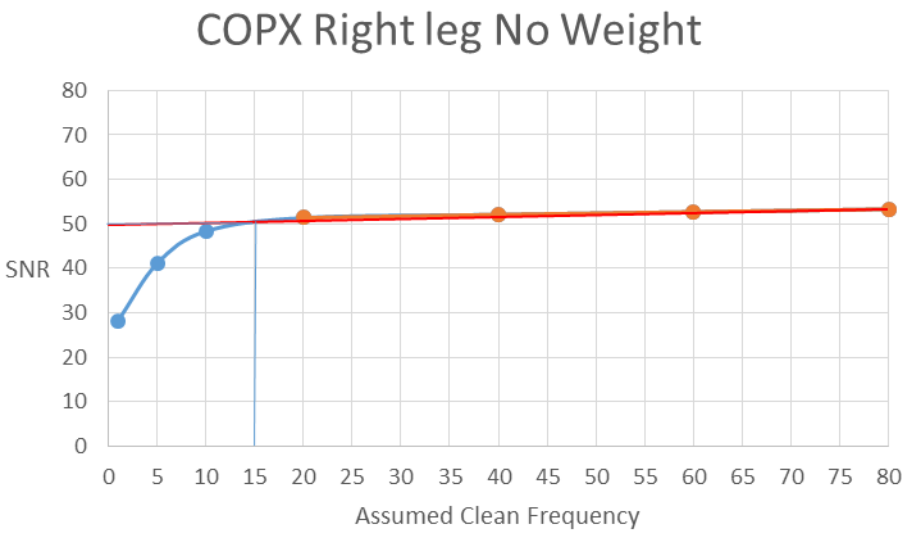

Figure 94 Zoomed in initial section of the SNR vs Assumed Clean Frequency Center of Pressure X of right leg with no additional weight.

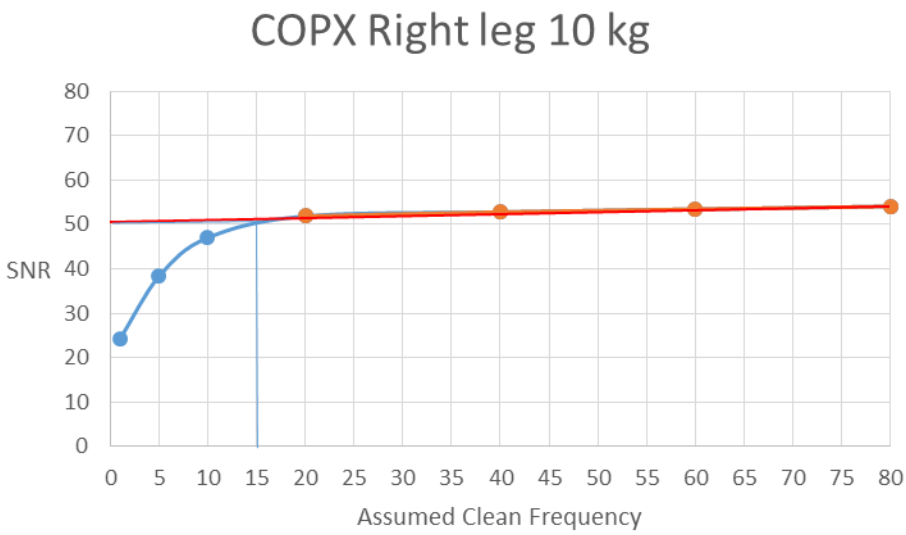

Figure 95 Zoomed in initial section of the SNR vs Assumed Clean Frequency Center of Pressure X of right leg with 10 kg additional weight.

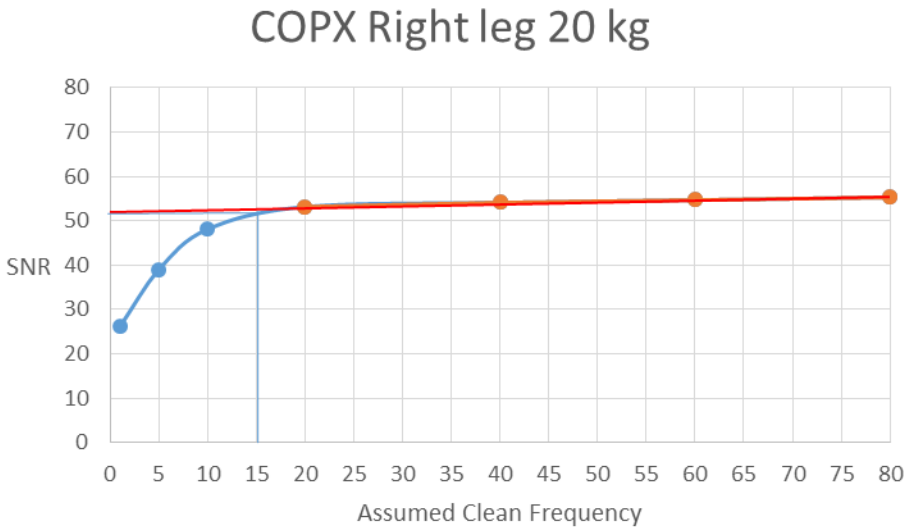

Figure 96 Zoomed in initial section of the SNR vs Assumed Clean Frequency Center of Pressure X of right leg with 20 kg additional weight.

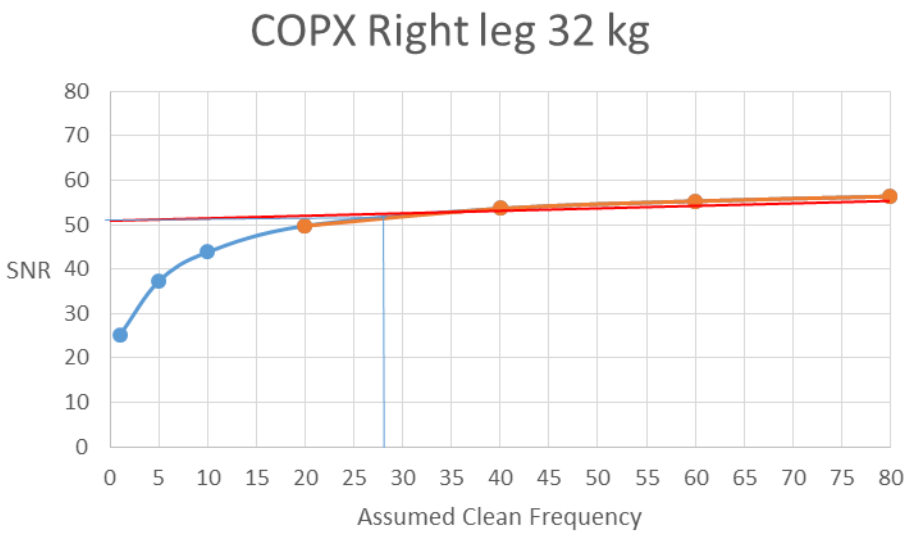

Figure 97 Zoomed in initial section of the SNR vs Assumed Clean Frequency Center of Pressure X of right leg with 32 kg additional weight.

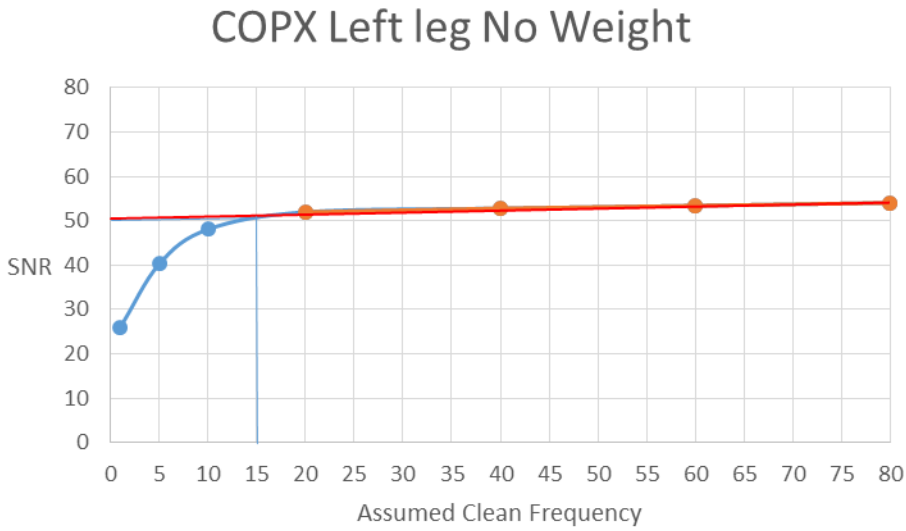

Figure 98 Zoomed in initial section of the SNR vs Assumed Clean Frequency Center of Pressure X of left leg with no additional weight.

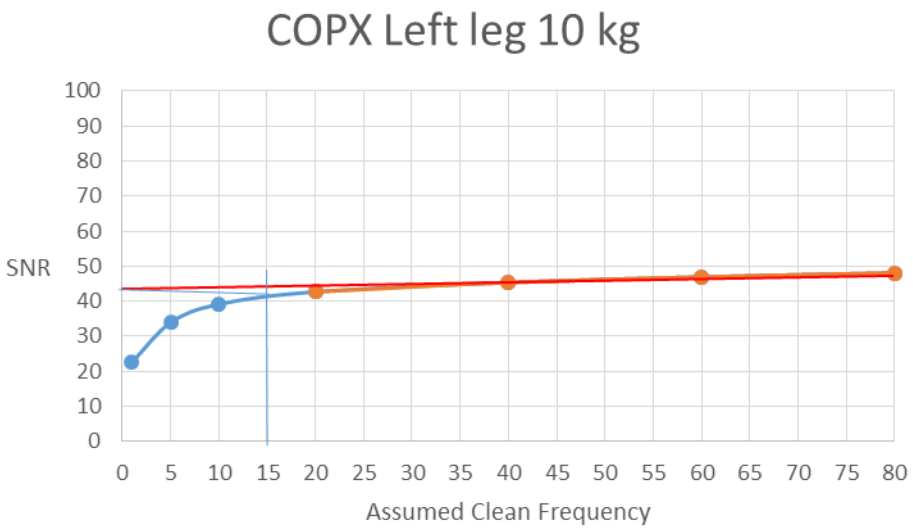

Figure 99 Zoomed in initial section of the SNR vs Assumed Clean Frequency Center of Pressure X of left leg with 10 kg additional weight.

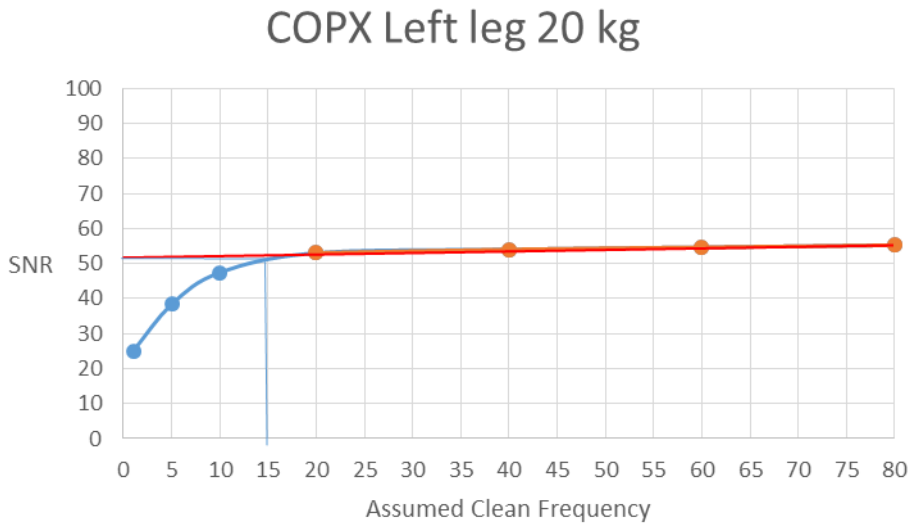

Figure 100 Zoomed in initial section of the SNR vs Assumed Clean Frequency Center of Pressure X of left leg with 20 kg additional weight.

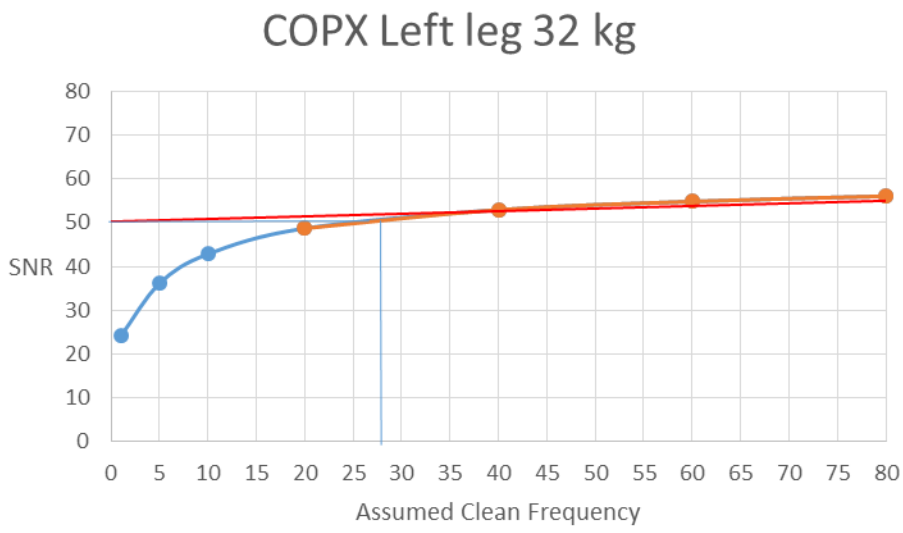

Figure 101 Zoomed in initial section of the SNR vs Assumed Clean Frequency Center of Pressure X of left leg with 32 kg additional weight.

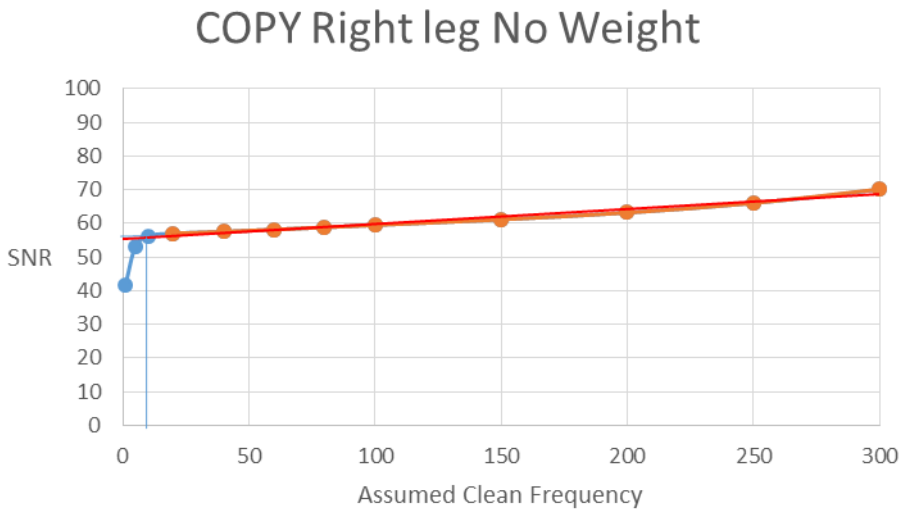

Figure 102 SNR vs Assumed Clean Frequency Center of Pressure Y of right leg with no additional weight.

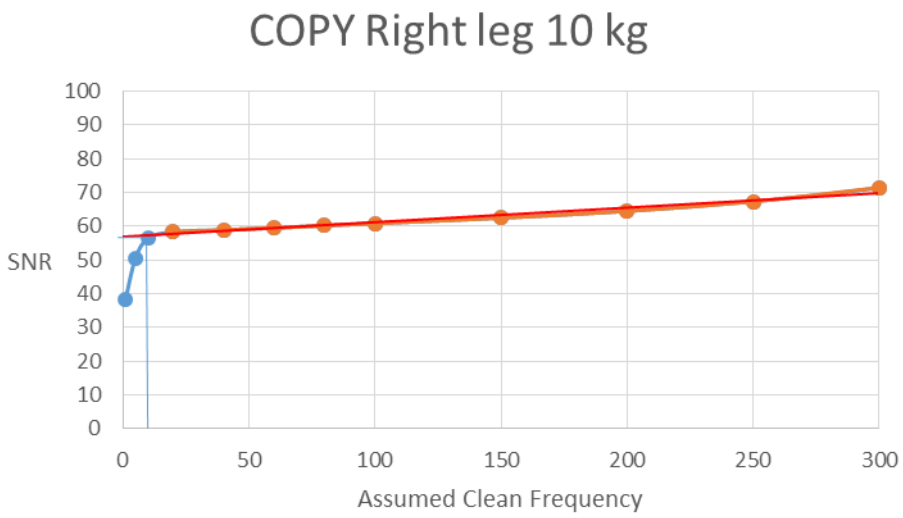

Figure 103 SNR vs Assumed Clean Frequency Center of Pressure Y of right leg with 10 kg additional weight.

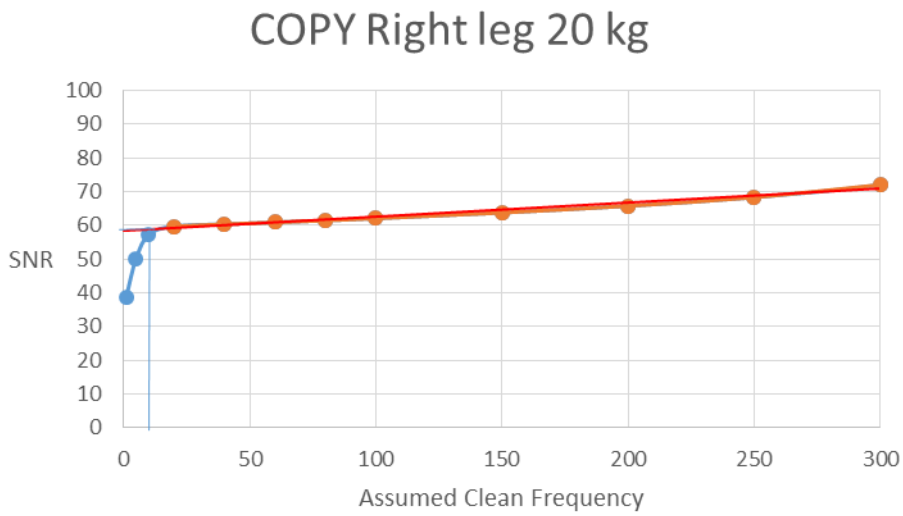

Figure 104 SNR vs Assumed Clean Frequency Center of Pressure Y of right leg with 20 kg additional weight.

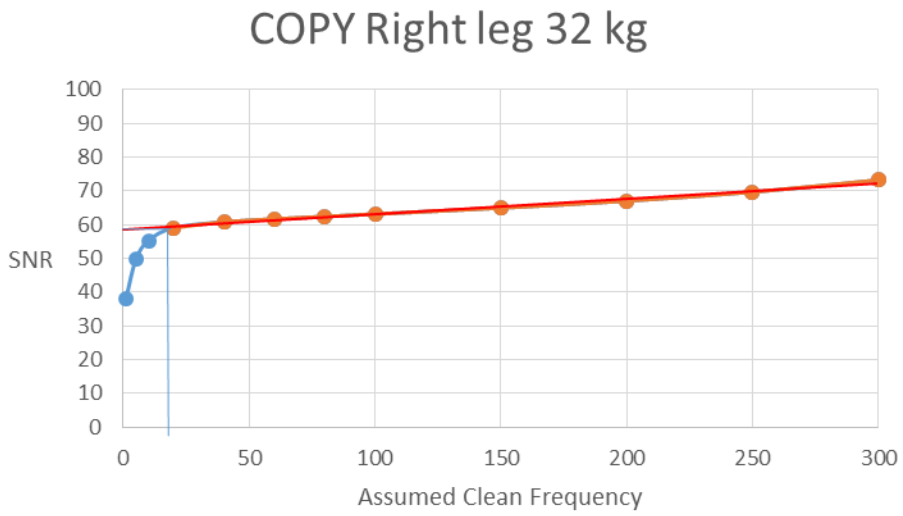

Figure 105 SNR vs Assumed Clean Frequency Center of Pressure Y of right leg with 32 kg additional weight.

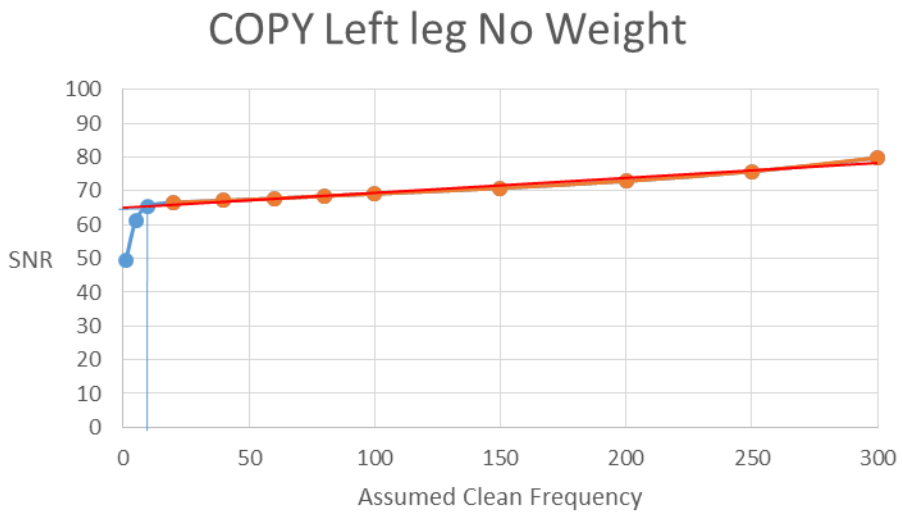

Figure 106 SNR vs Assumed Clean Frequency Center of Pressure Y of left leg with no additional weight.

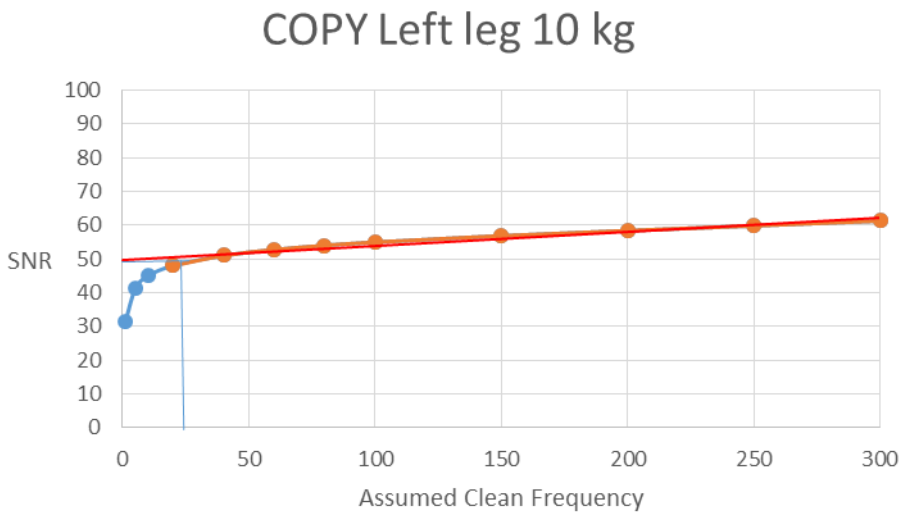

Figure 107 SNR vs Assumed Clean Frequency Center of Pressure Y of left leg with 10 additional weight.

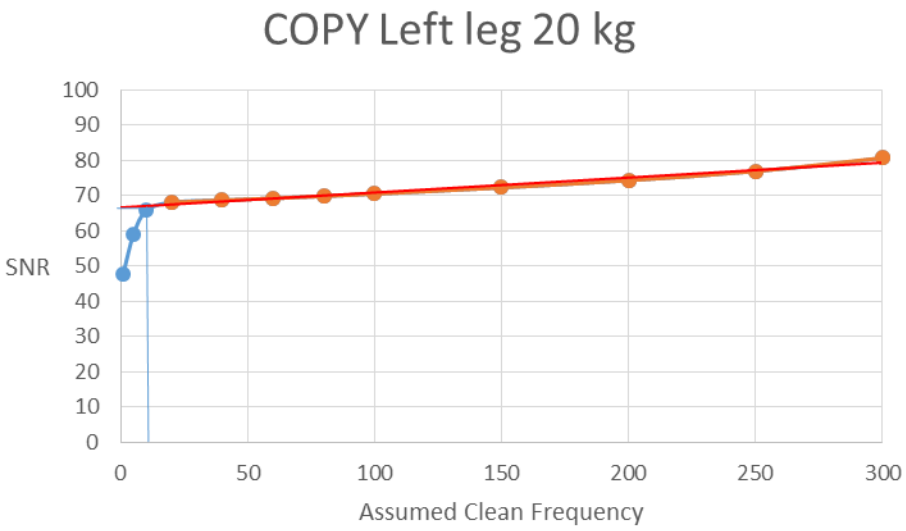

Figure 108 SNR vs Assumed Clean Frequency Center of Pressure Y of left leg with 20 additional weight.

Figure 109 SNR vs Assumed Clean Frequency Center of Pressure Y of left leg with 32 additional weight.

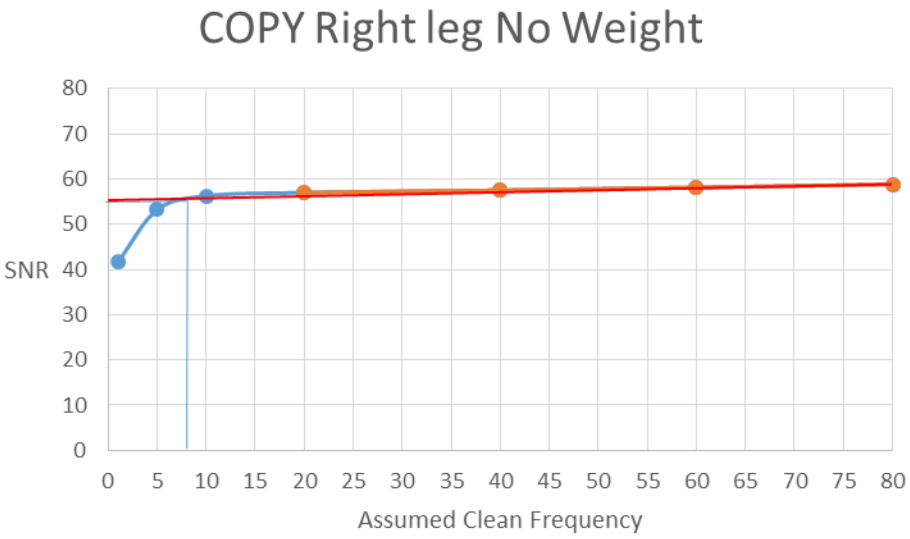

Figure 110 Zoomed in initial section of the SNR vs Assumed Clean Frequency Center of Pressure Y of right leg with no additional weight.

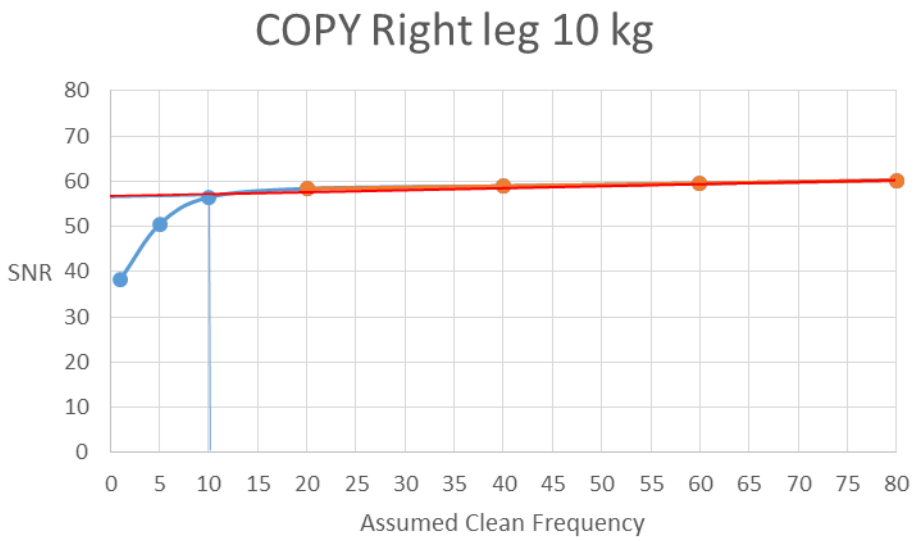

Figure 111 Zoomed in initial section of the SNR vs Assumed Clean Frequency Center of Pressure Y of right leg with 10 kg additional weight.

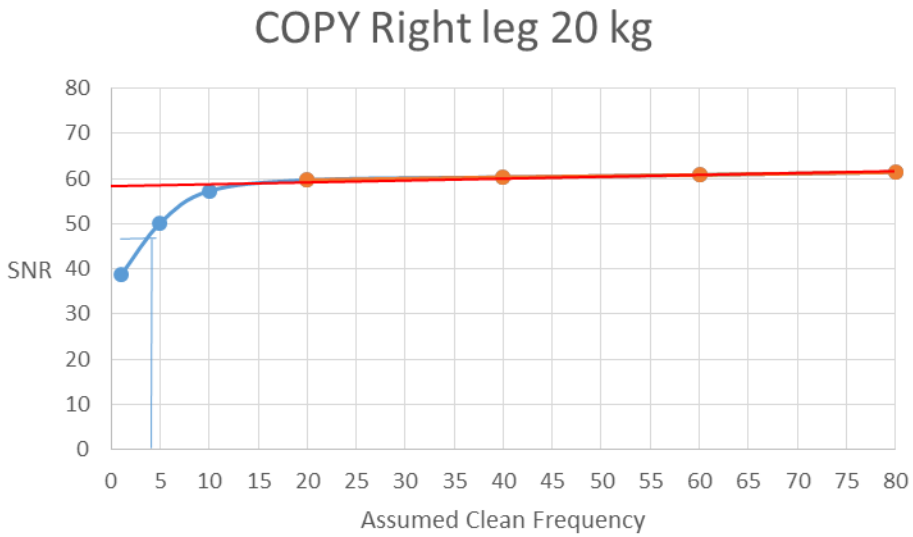

Figure 112 Zoomed in initial section of the SNR vs Assumed Clean Frequency Center of Pressure Y of right leg with 20 kg additional weight.

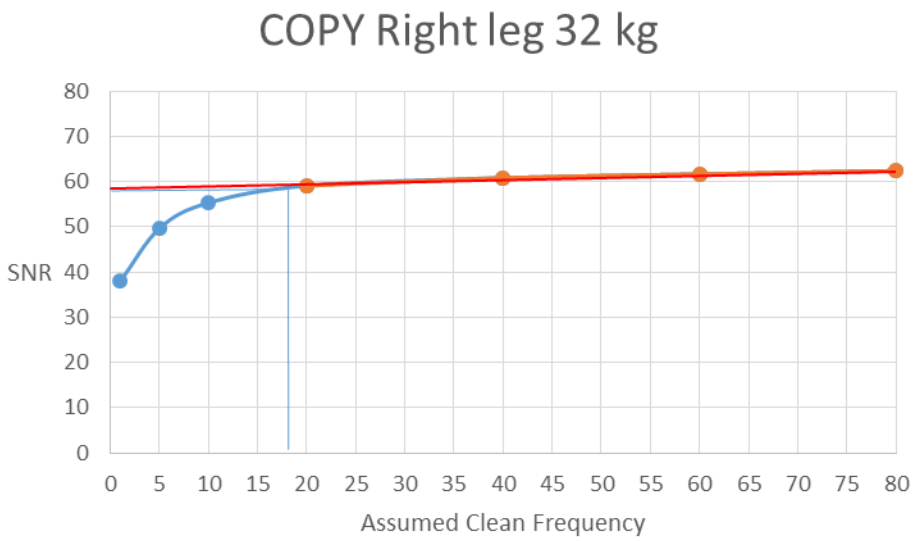

Figure 113 Zoomed in initial section of the SNR vs Assumed Clean Frequency Center of Pressure Y of right leg with 32 kg additional weight.

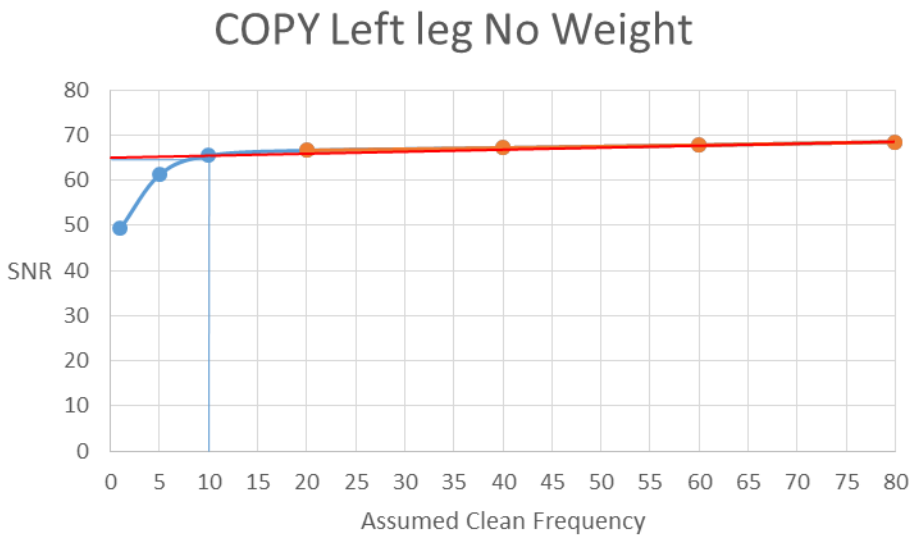

Figure 114 Zoomed in initial section of the SNR vs Assumed Clean Frequency Center of Pressure Y of left leg with no additional weight.

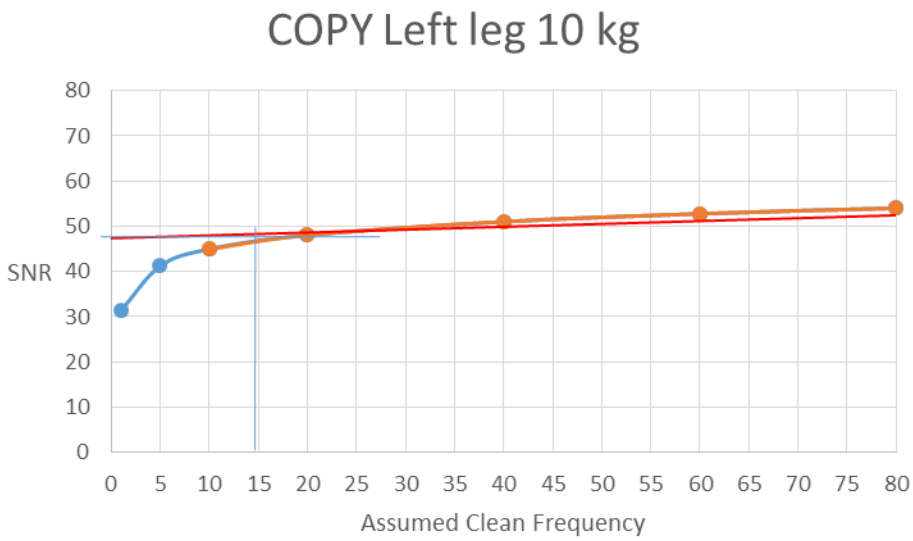

Figure 115 Zoomed in initial section of the SNR vs Assumed Clean Frequency Center of Pressure Y of left leg with 10 additional weight.

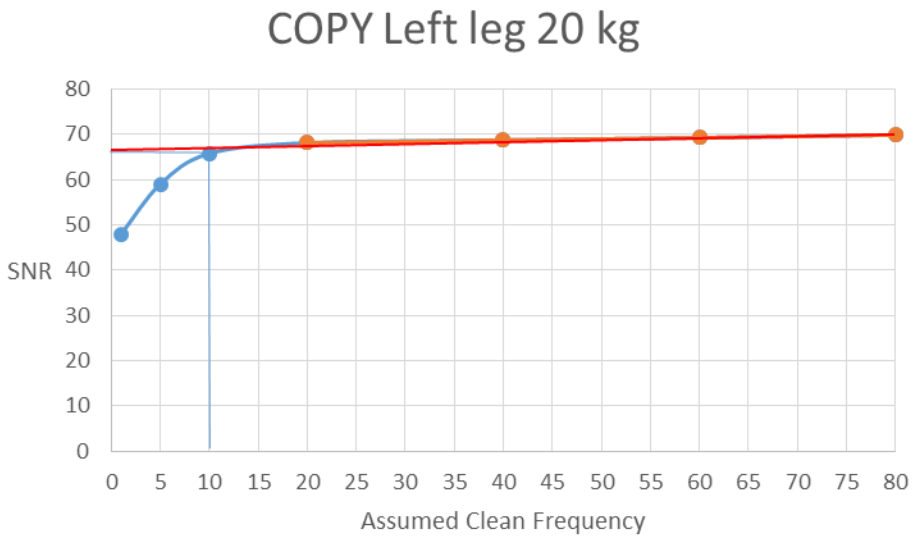

Figure 116 Zoomed in initial section of the SNR vs Assumed Clean Frequency Center of Pressure Y of left leg with 20 additional weight.

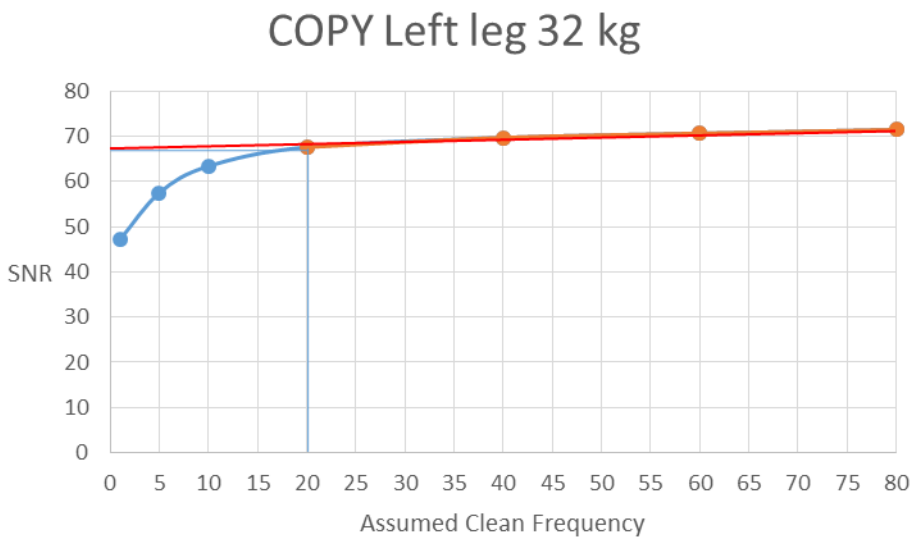

Figure 117 Zoomed in initial section of the SNR vs Assumed Clean Frequency Center of Pressure Y of left leg with 32 additional weight.

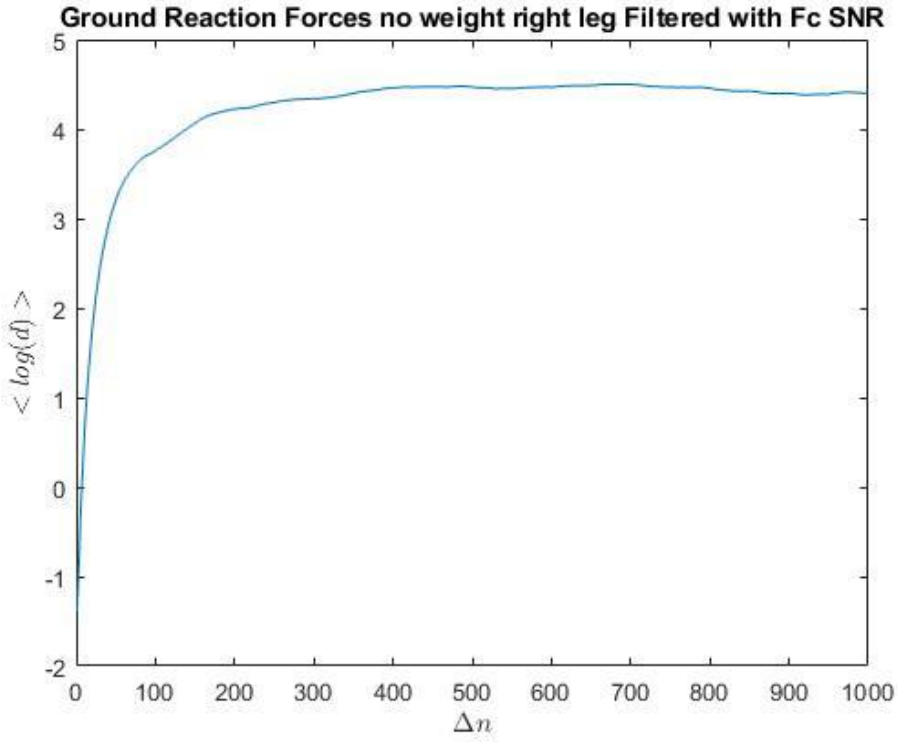

Figure 118 Divergence Curve of Ground Reaction Forces no weight right leg Filtered with cut off Frequency using SNR Analysis.

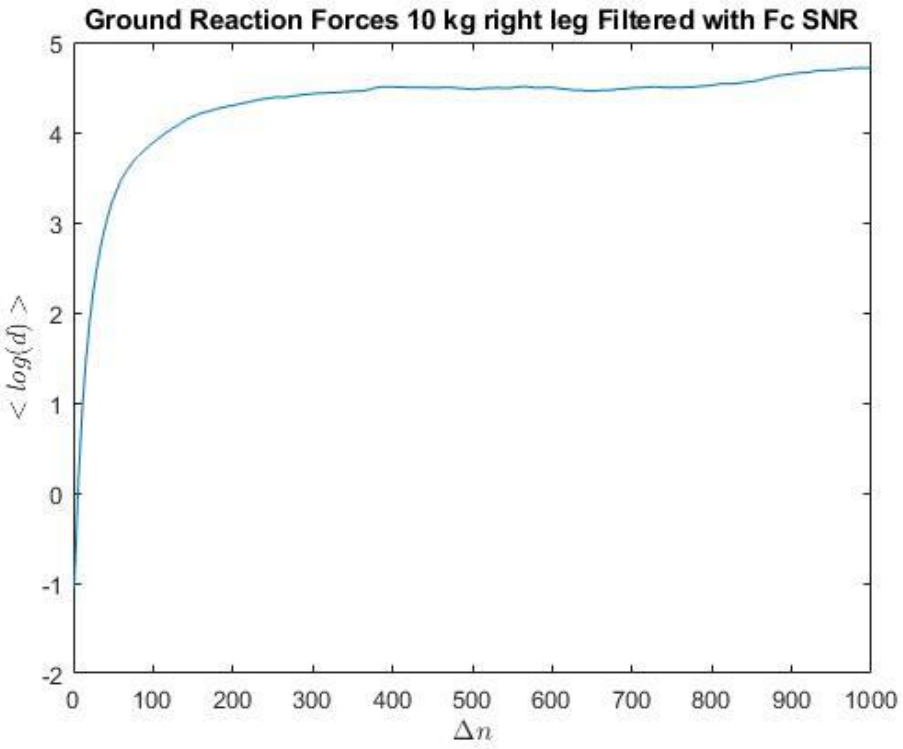

Figure 119 Divergence Curve of Ground Reaction Forces 10 kg right leg Filtered with Filtered with cut off Frequency using SNR Analysis.

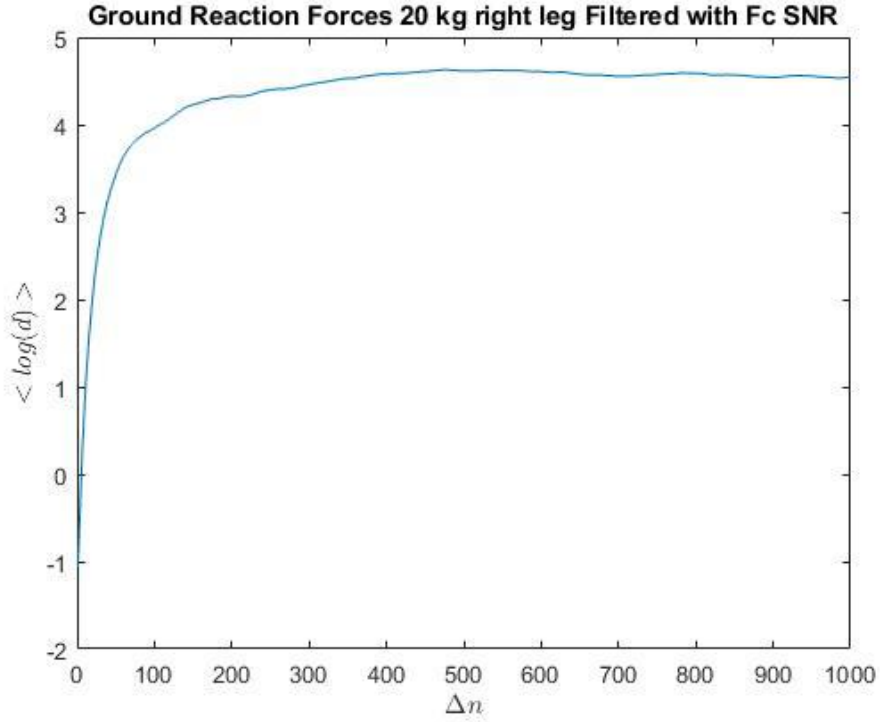

Figure 120 Divergence Curve of Ground Reaction Forces 20 kg right leg Filtered with cut off Frequency using SNR Analysis.

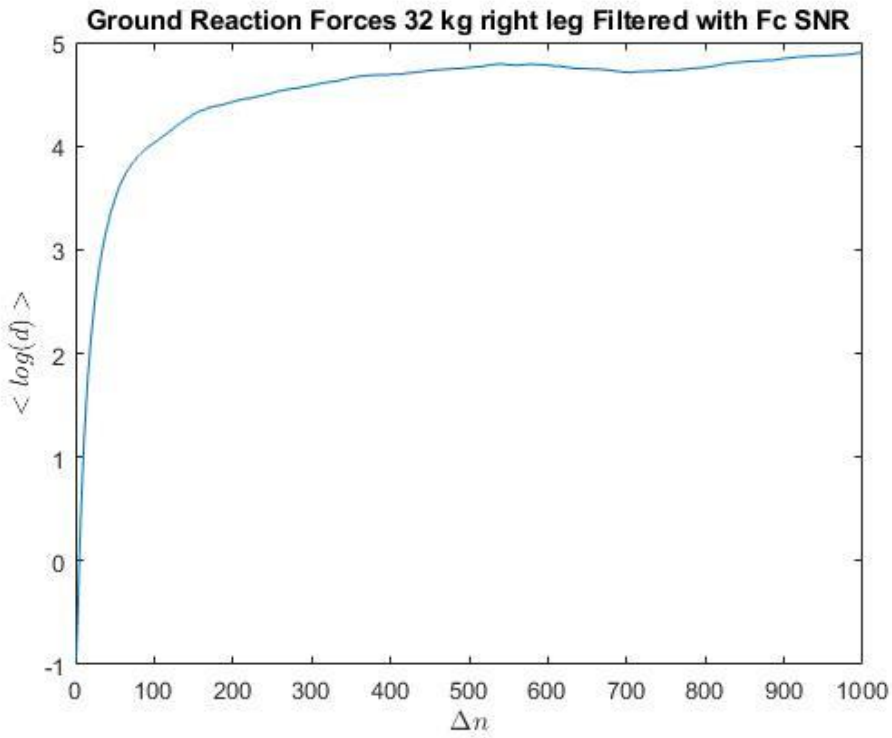

Figure 121 Divergence Curve of Ground Reaction Forces 32 kg right leg Filtered with cut off Frequency using SNR Analysis.

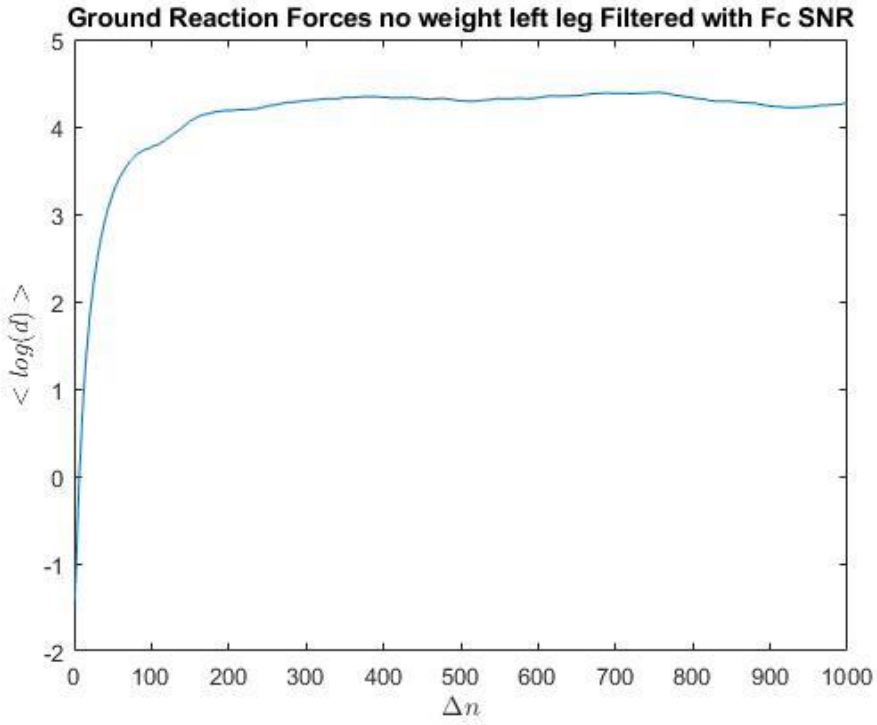

Figure 122 Divergence Curve of Ground Reaction Forces no weight left leg Filtered with cut off Frequency using SNR Analysis.

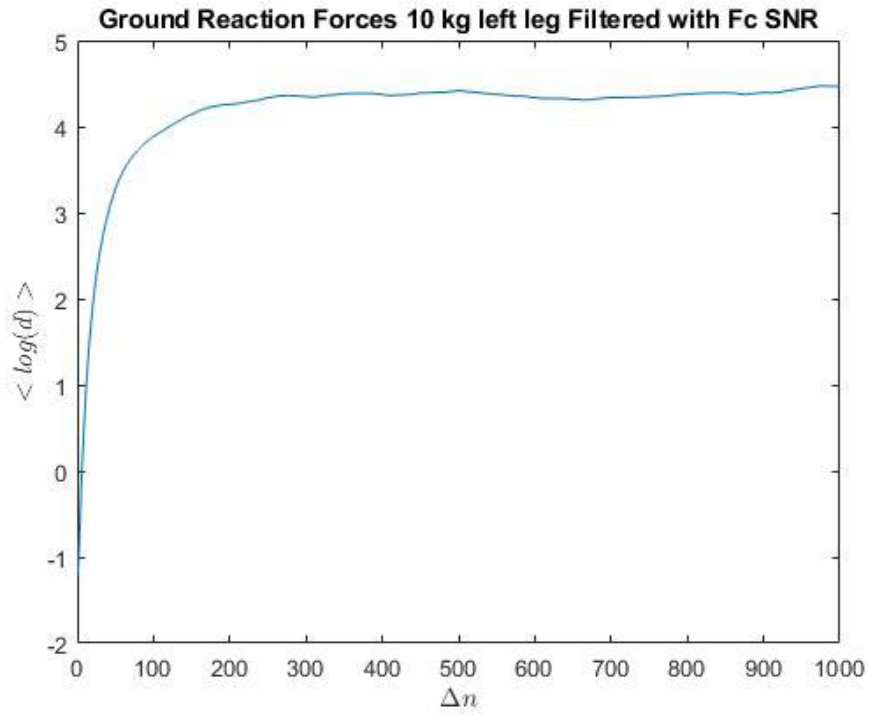

Figure 123 Divergence Curve of Ground Reaction Forces 10 kg left leg Filtered with cut off Frequency using SNR Analysis.

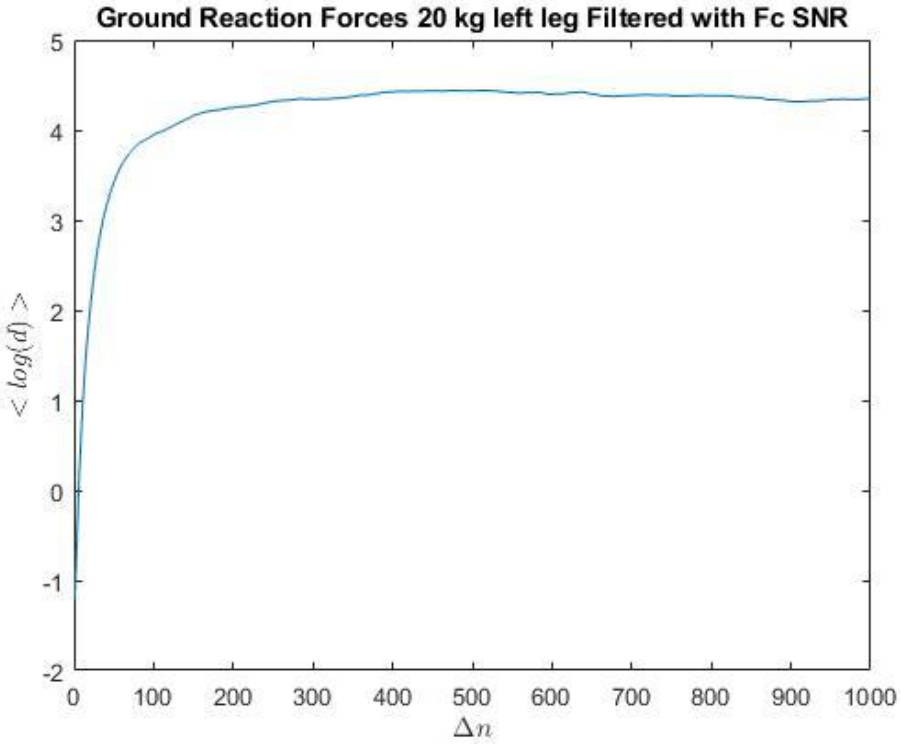

Figure 124 Divergence Curve of Ground Reaction Forces 20 kg left leg Filtered with cut off Frequency using SNR Analysis.

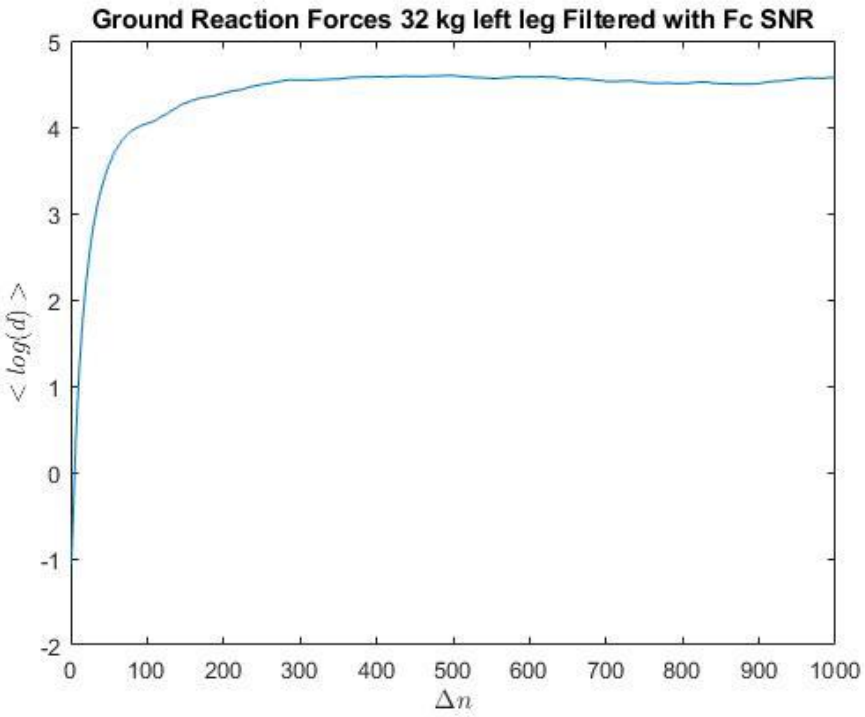

Figure 125 Divergence Curve of Ground Reaction Forces 32 kg left leg Filtered with cut off Frequency using SNR Analysis.

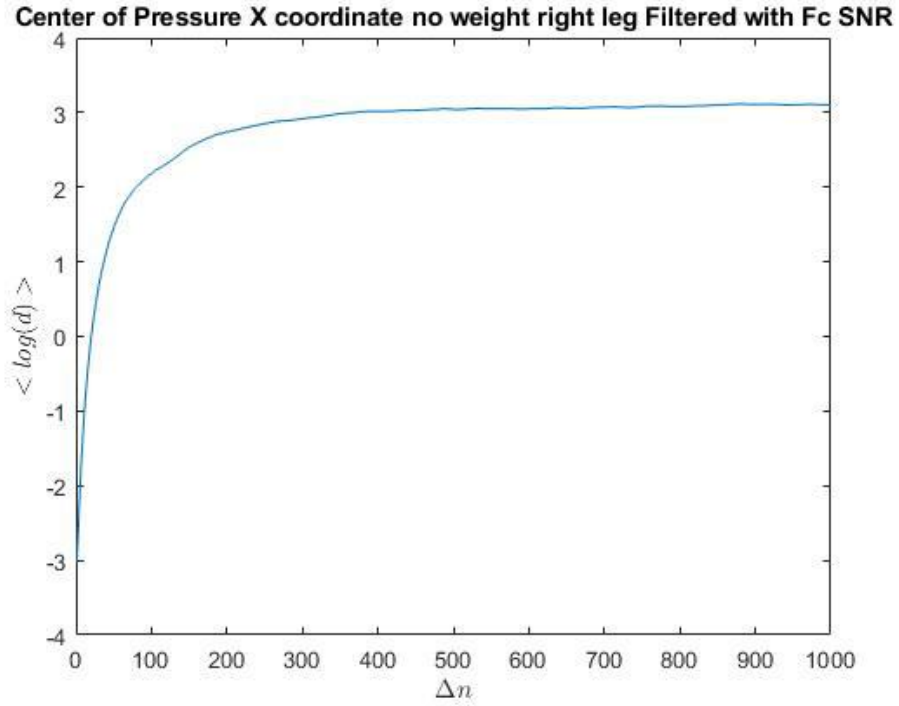

Figure 126 Divergence Curve of Center of Pressure X coordinate no weight right leg Filtered with cut off Frequency using SNR Analysis.

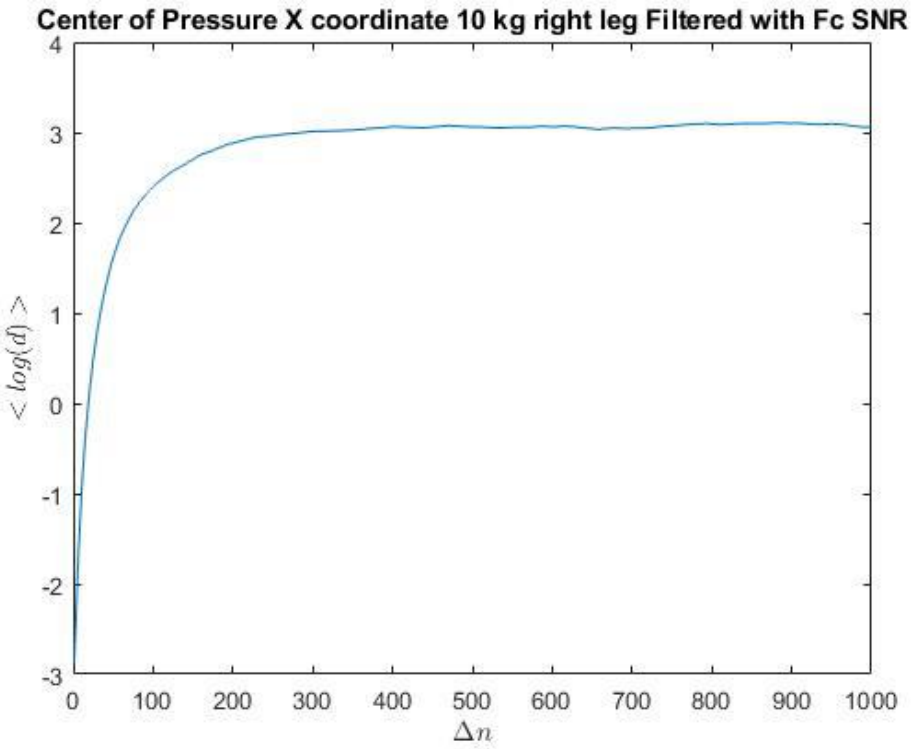

Figure 127 Divergence Curve of Center of Pressure X coordinate 10 kg right leg Filtered with cut off Frequency using SNR Analysis.

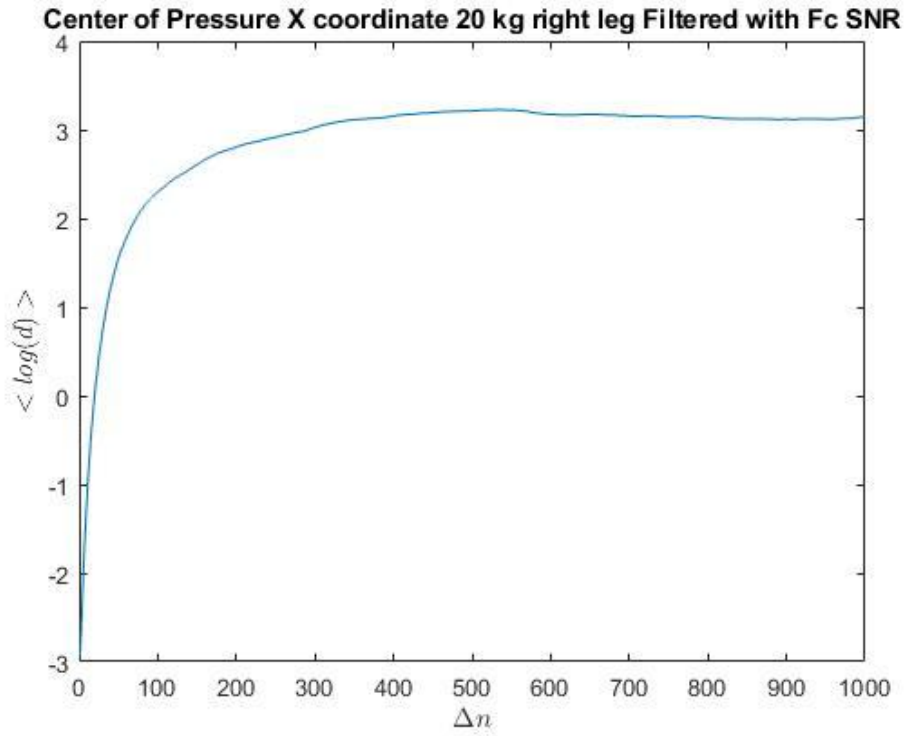

Figure 128 Divergence Curve of Center of Pressure X coordinate 20 kg right leg Filtered with cut off Frequency using SNR Analysis.

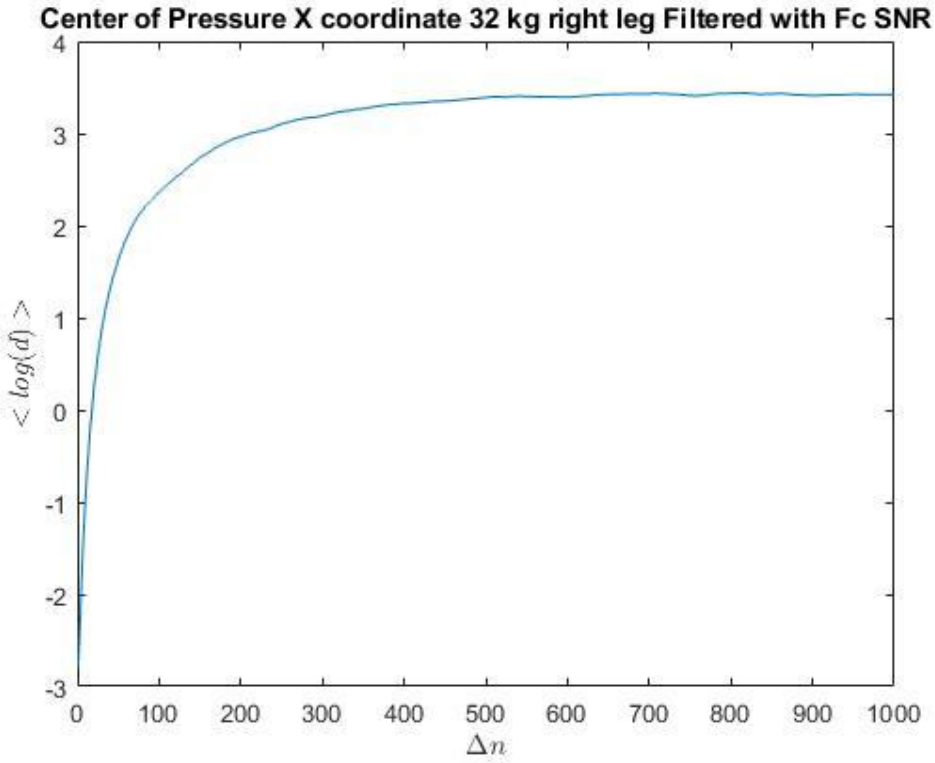

Figure 129 Divergence Curve of Center of Pressure X coordinate 32 kg right leg Filtered with cut off Frequency using SNR Analysis.

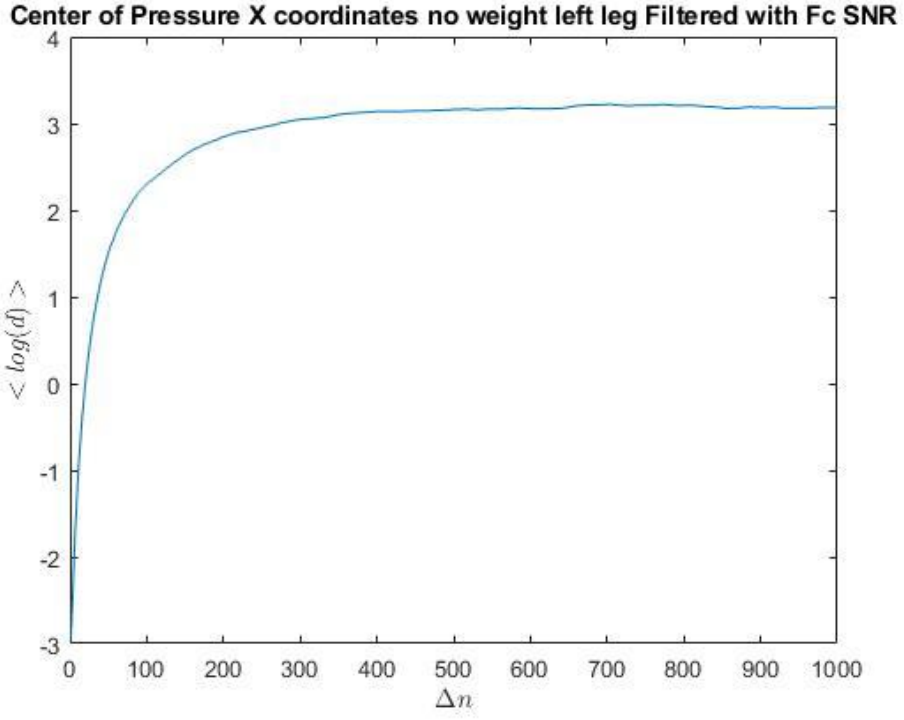

Figure 130 Divergence Curve of Center of Pressure X coordinates no weight left leg Filtered with cut off Frequency using SNR Analysis.

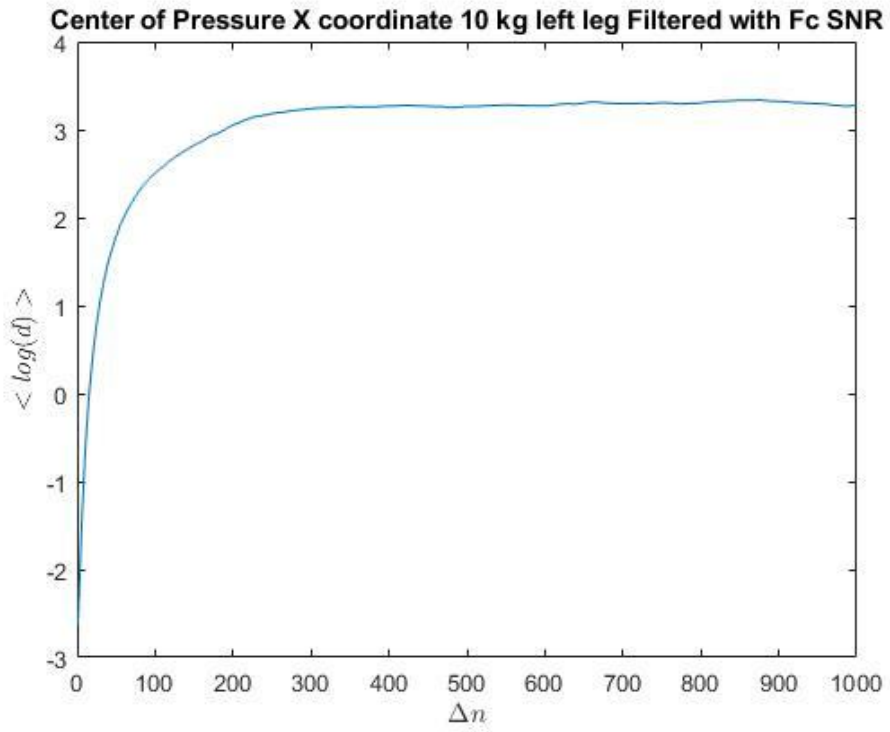

Figure 131 Divergence Curve of Center of Pressure X coordinate 10 kg left leg Filtered with cut off Frequency using SNR Analysis.

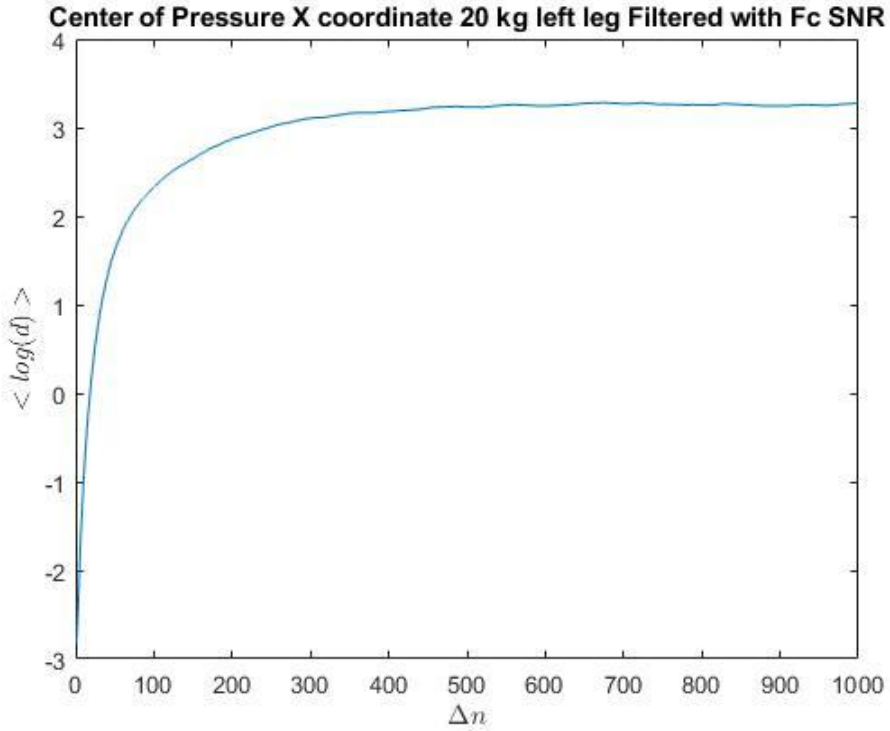

Figure 132 Divergence Curve of Center of Pressure X coordinate 20 kg left leg Filtered with cut off Frequency using SNR Analysis.

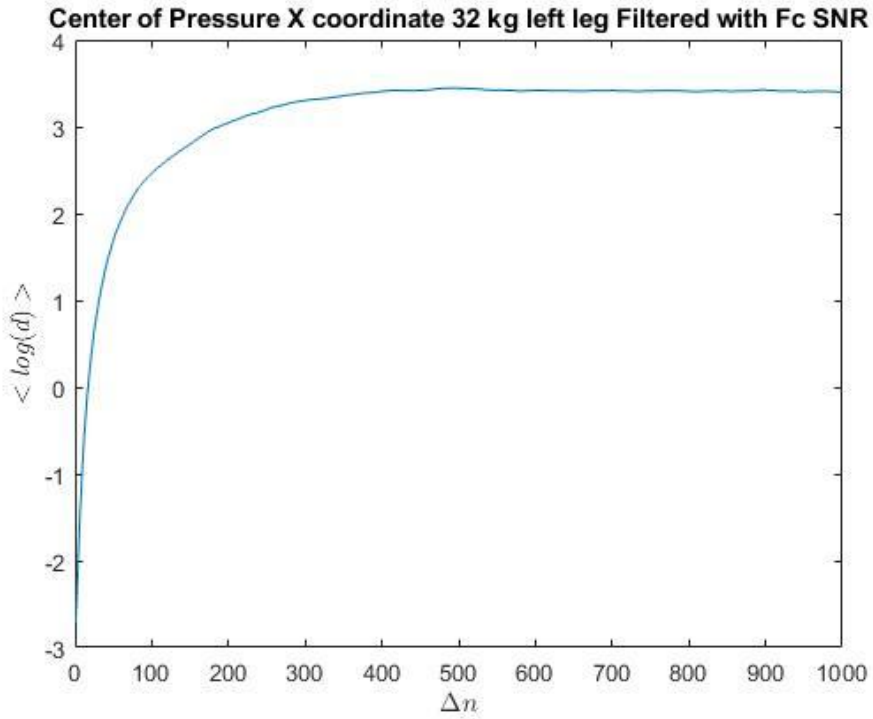

Figure 133 Divergence Curve of Center of Pressure X coordinate 32 kg left leg Filtered with cut off Frequency using SNR Analysis.

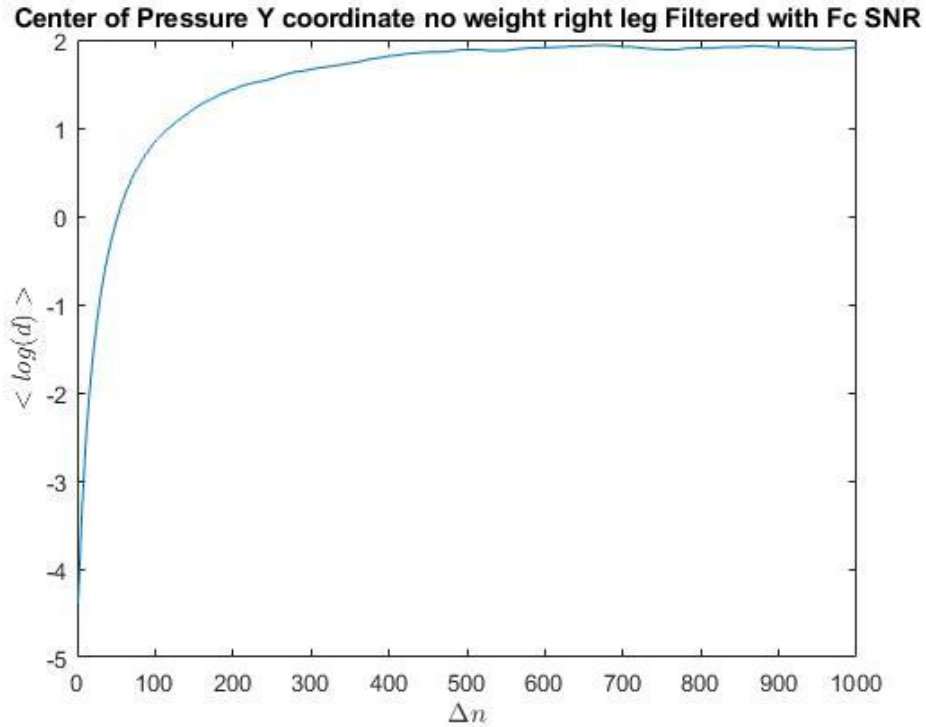

Figure 134 Divergence Curve of Center of Pressure Y coordinate no weight right leg Filtered with cut off Frequency using SNR Analysis.

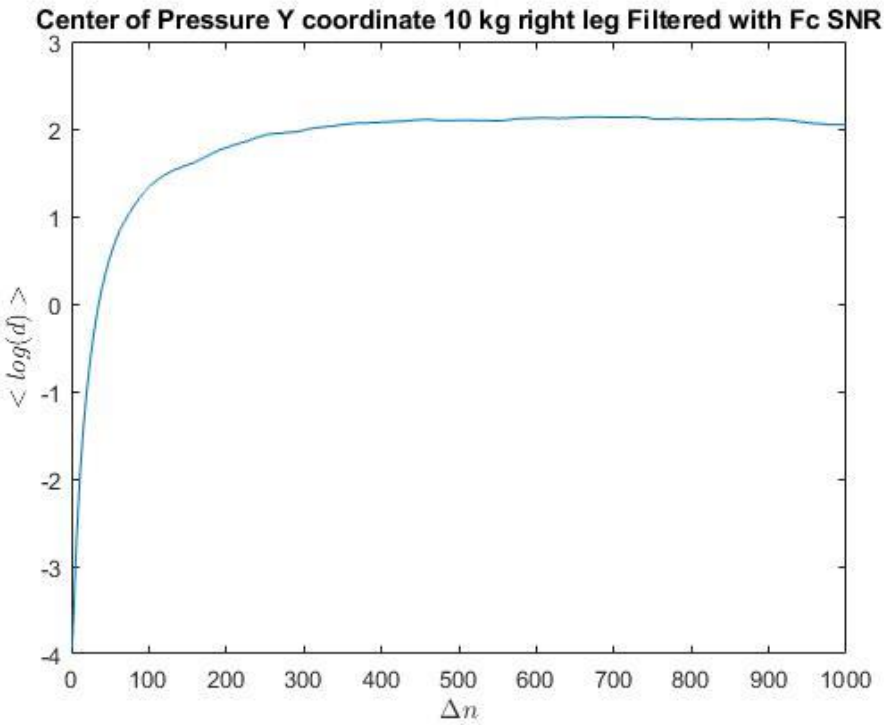

Figure 135 Divergence Curve of Center of Pressure Y coordinate 10 kg right leg Filtered with cut off Frequency using SNR Analysis.

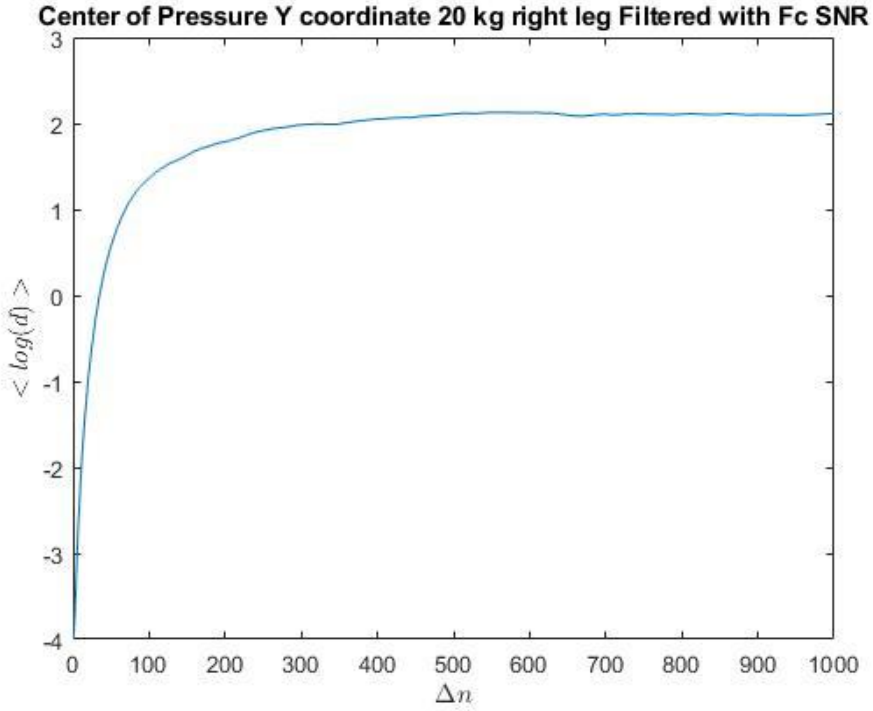

Figure 136 Divergence Curve of Center of Pressure Y coordinate 20 kg right leg Filtered with cut off Frequency using SNR Analysis.

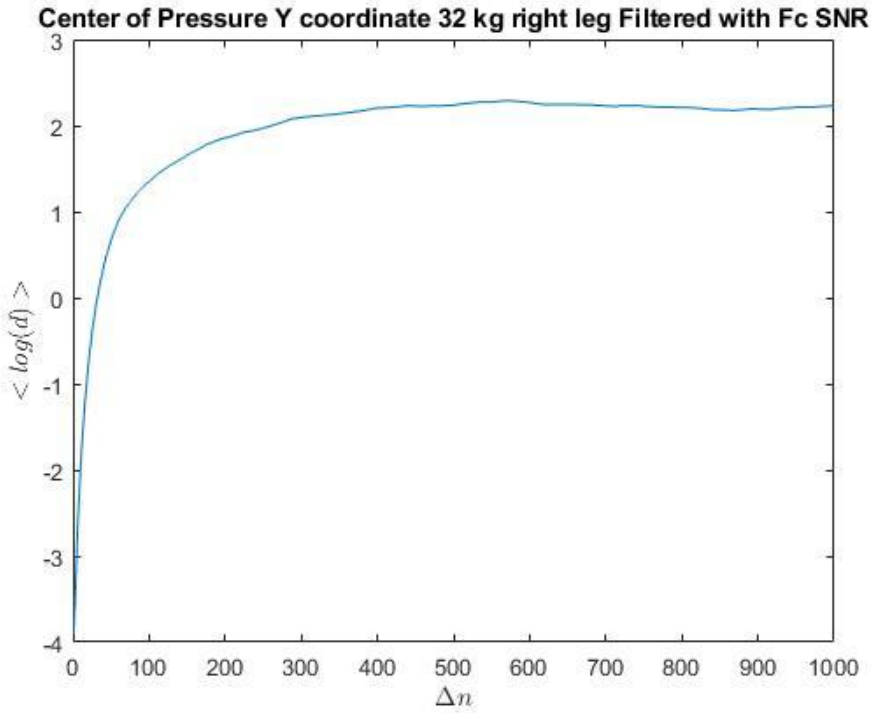

Figure 137 Divergence Curve of Center of Pressure Y coordinate 32 kg right leg Filtered with cut off Frequency using SNR Analysis.

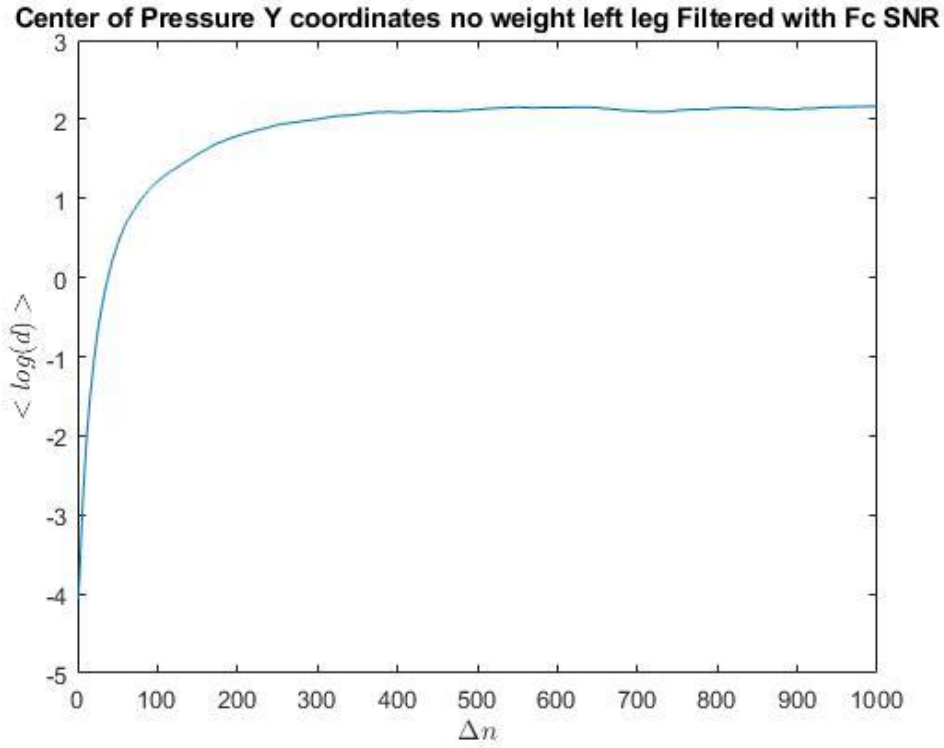

Figure 138 Divergence Curve of Center of Pressure Y coordinates no weight left leg Filtered with cut off Frequency using SNR Analysis.

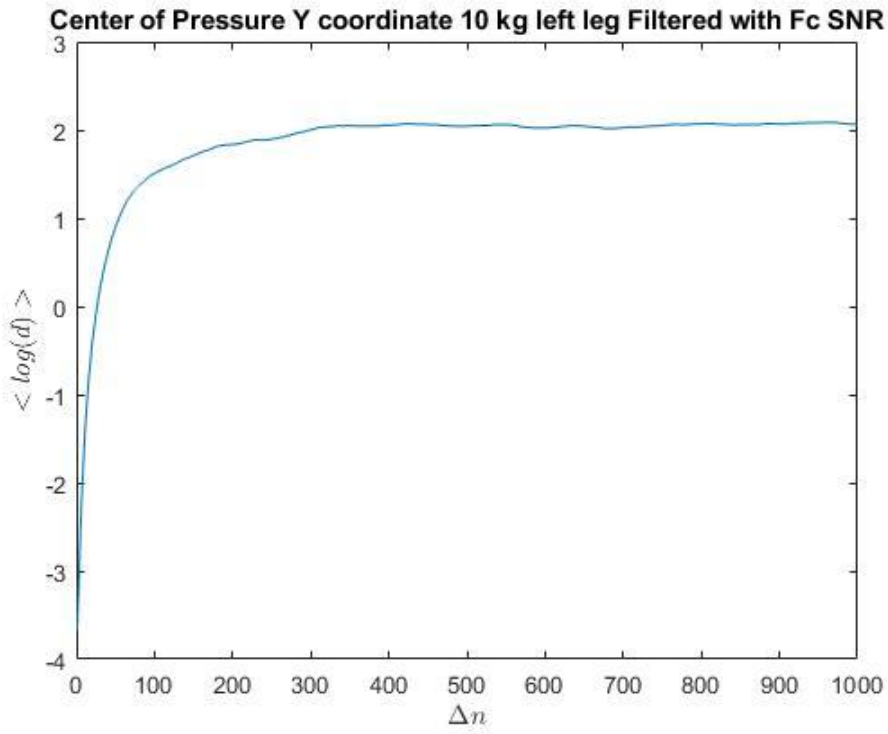

Figure 139 Divergence Curve of Center of Pressure Y coordinate 10 kg left leg Filtered with cut off Frequency using SNR Analysis.

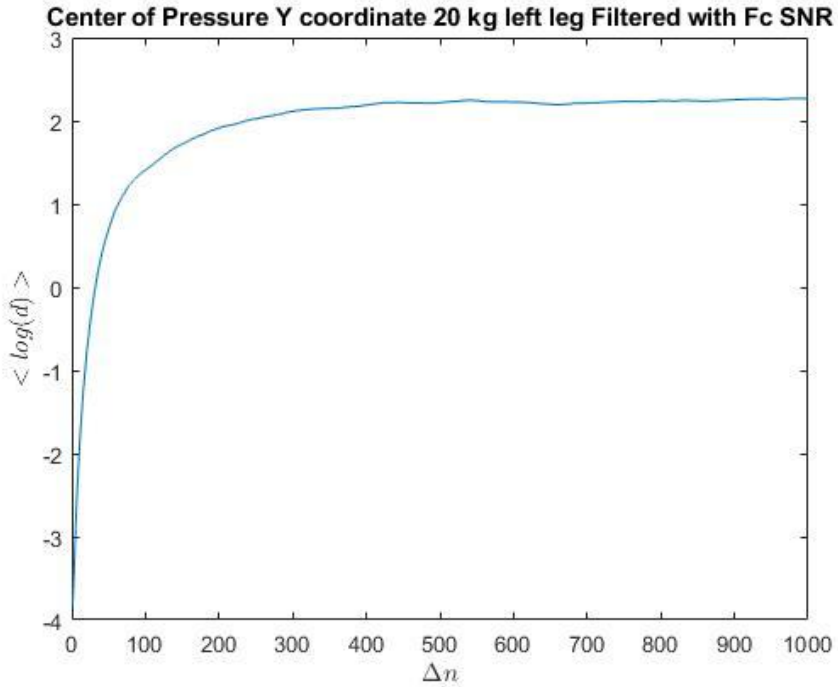

Figure 140 Divergence Curve of Center of Pressure Y coordinate 20 kg right leg Filtered with cut off Frequency using SNR Analysis.

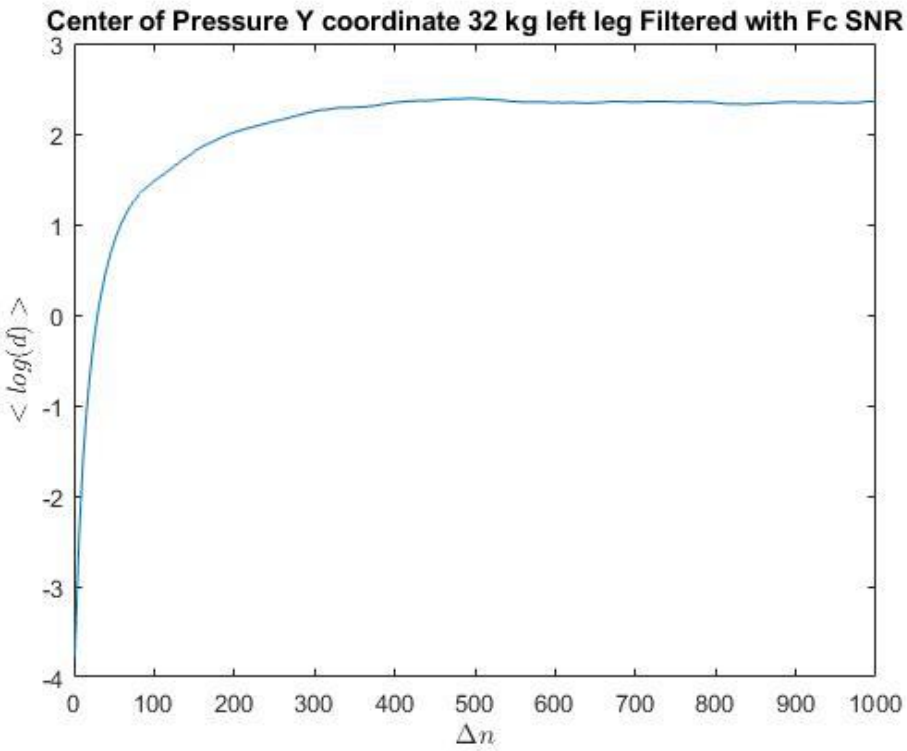

Figure 141 Divergence Curve of Center of Pressure Y coordinate 32 kg left leg Filtered with cut off Frequency using SNR Analysis.

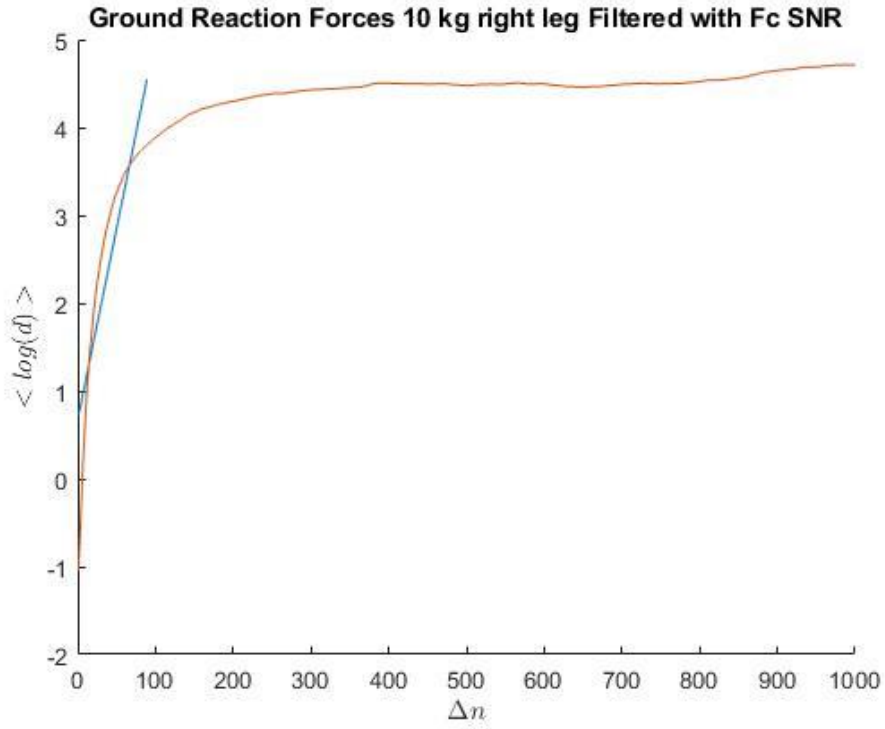

Figure 142 Divergence Curve of Ground Reaction Forces 10 kg right leg Filtered with Filtered with cut off Frequency using SNR Analysis and 0.9 Correlation Coefficient Regression Line.

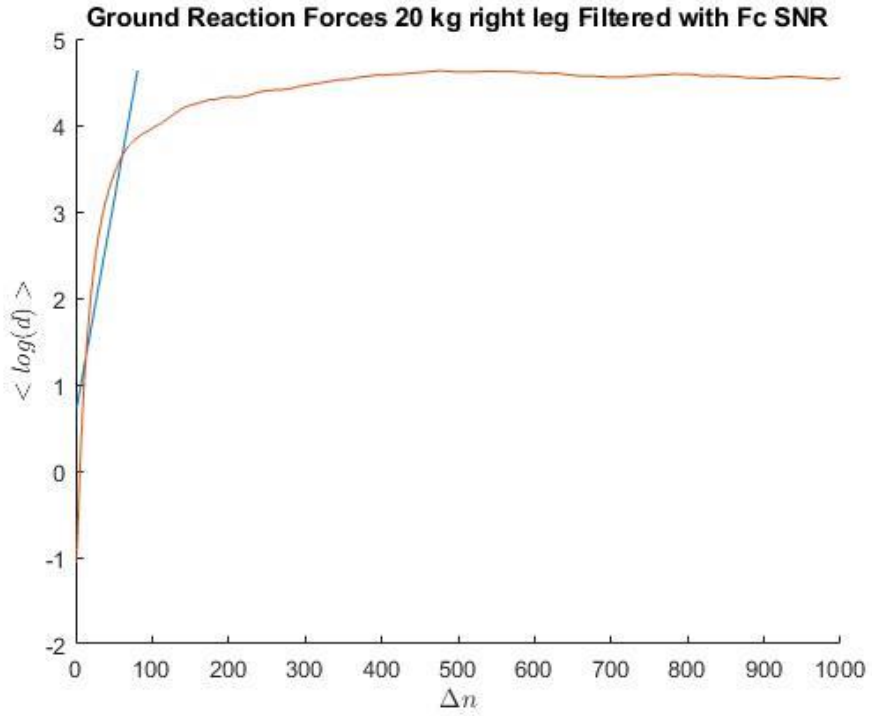

Figure 143 Divergence Curve of Ground Reaction Forces 20 kg right leg Filtered with cut off Frequency using SNR Analysis and 0.9 Correlation Coefficient Regression Line.

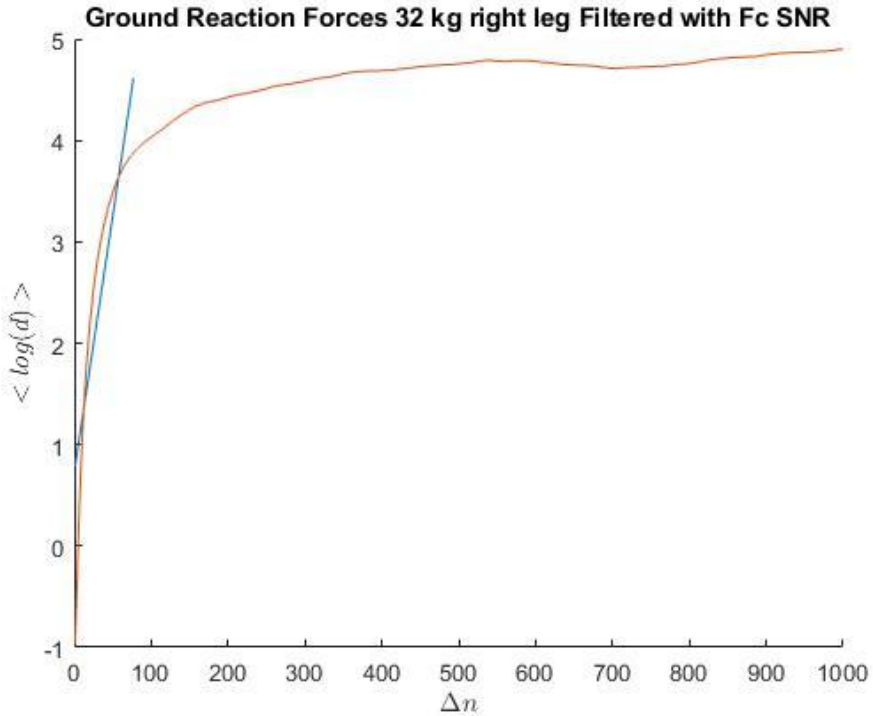

Figure 144 Divergence Curve of Ground Reaction Forces 32 kg right leg Filtered with cut off Frequency using SNR Analysis and 0.9 Correlation Coefficient Regression Line.

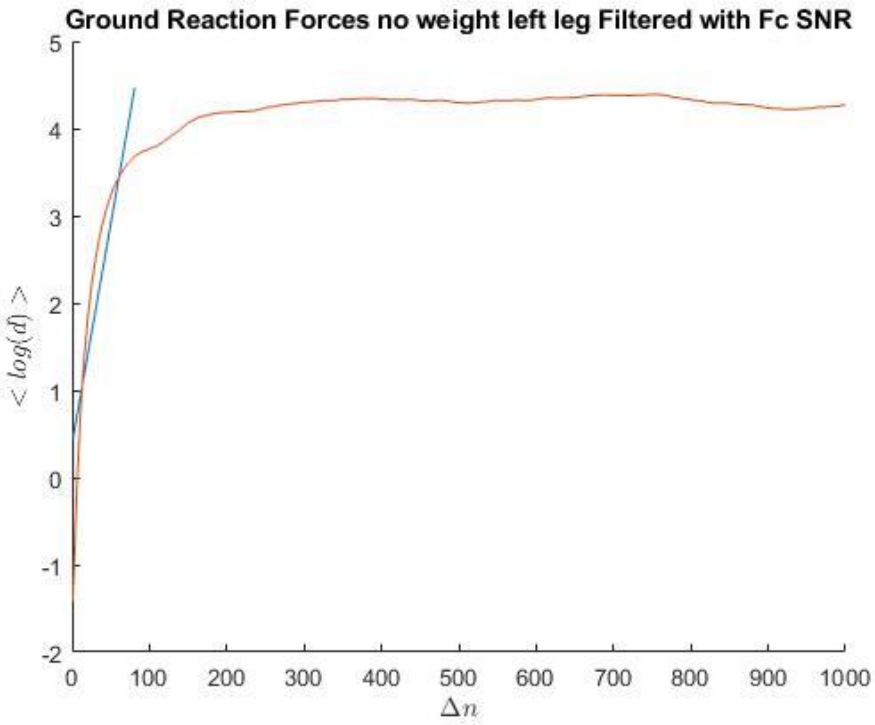

Figure 145 Divergence Curve of Ground Reaction Forces no weight left leg Filtered with cut off Frequency using SNR Analysis and 0.9 Correlation Coefficient Regression Line.

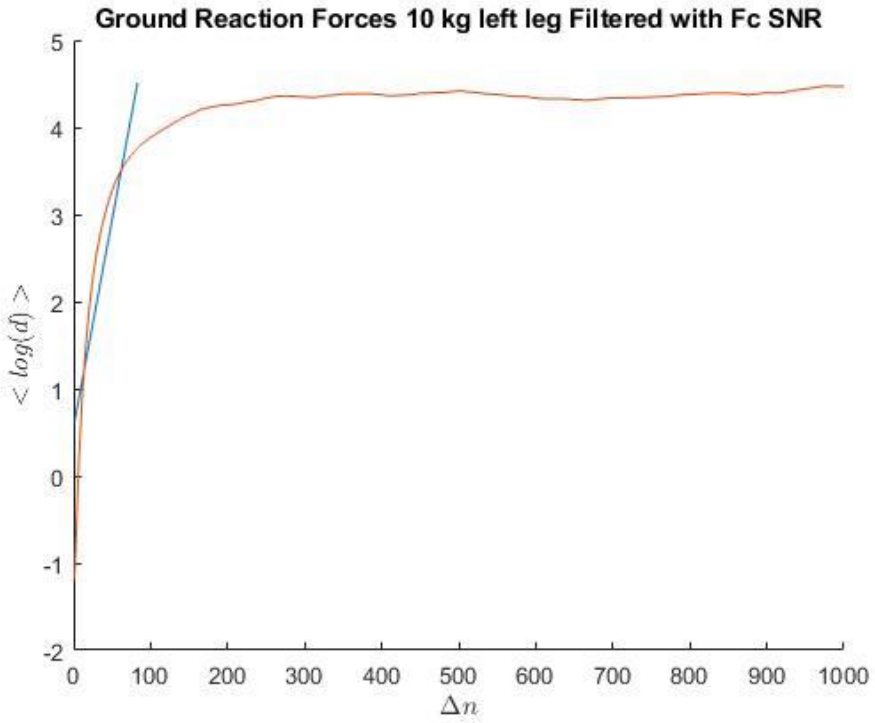

Figure 146 Divergence Curve of Ground Reaction Forces 10 kg left leg Filtered with cut off Frequency using SNR Analysis and 0.9 Correlation Coefficient Regression Line.

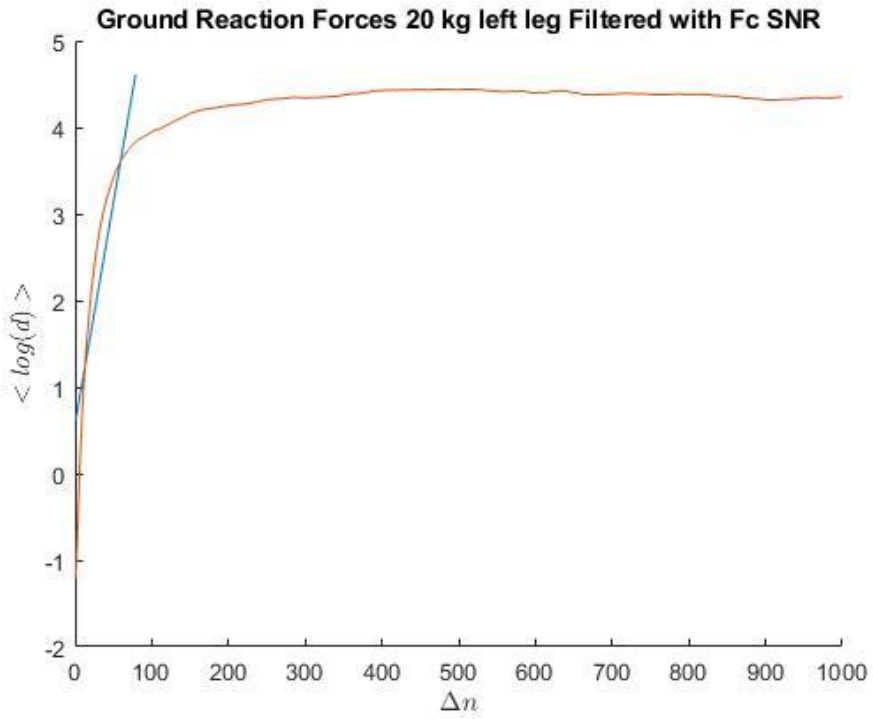

Figure 147 Divergence Curve of Ground Reaction Forces 20 kg left leg Filtered with cut off Frequency using SNR Analysis and 0.9 Correlation Coefficient Regression Line.

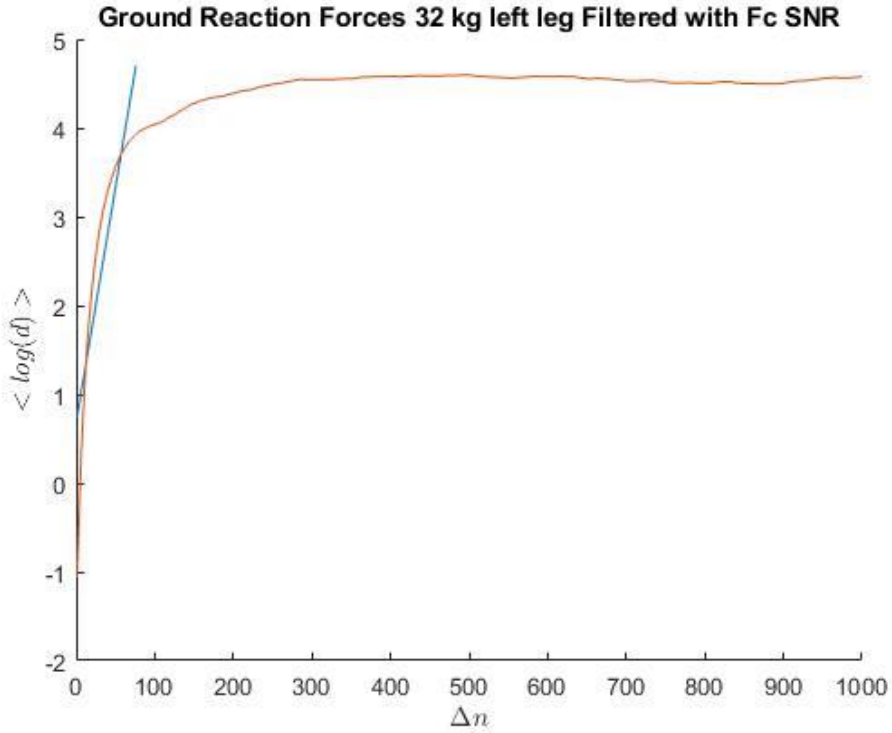

Figure 148 Divergence Curve of Ground Reaction Forces 32 kg left leg Filtered with cut off Frequency using SNR Analysis and 0.9 Correlation Coefficient Regression Line.

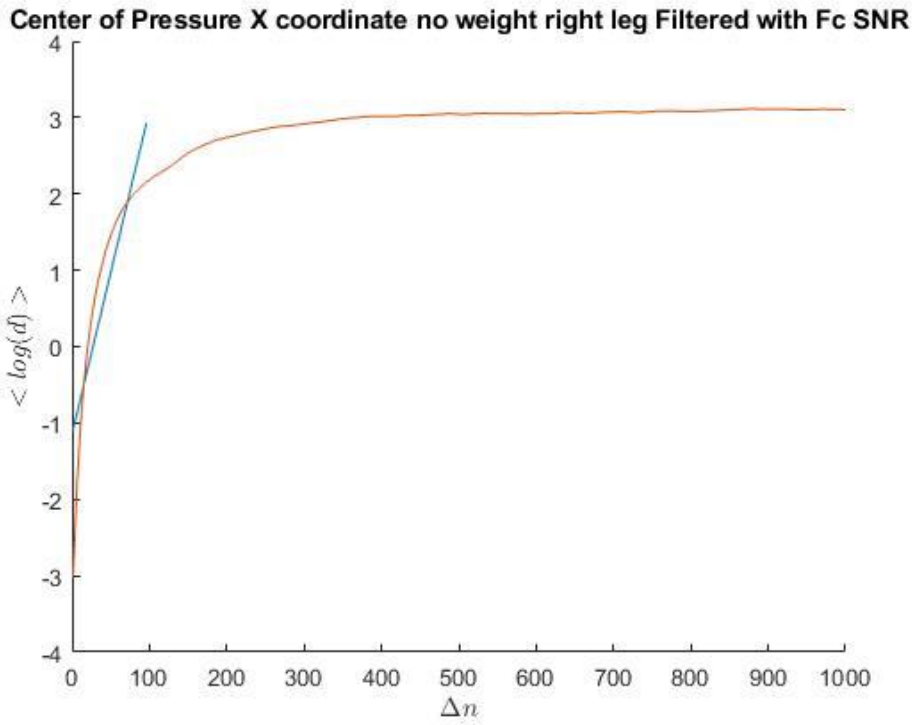

Figure 149 Divergence Curve of Center of Pressure X coordinate no weight right leg Filtered with cut off Frequency using SNR Analysis and 0.9 Correlation Coefficient Regression Line.

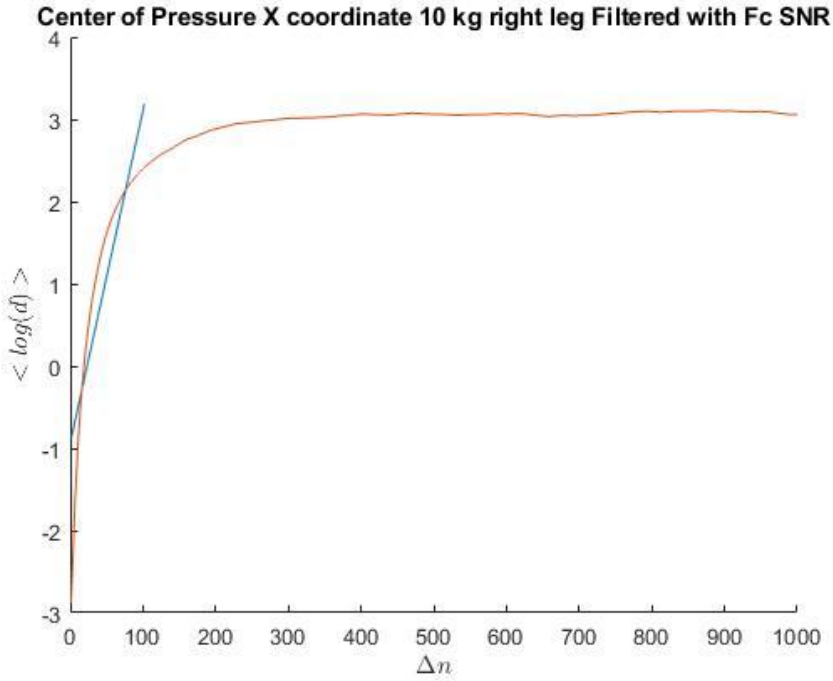

Figure 150 Divergence Curve of Center of Pressure X coordinate 10 kg right leg Filtered with cut off Frequency using SNR Analysis and 0.9 Correlation Coefficient Regression Line.

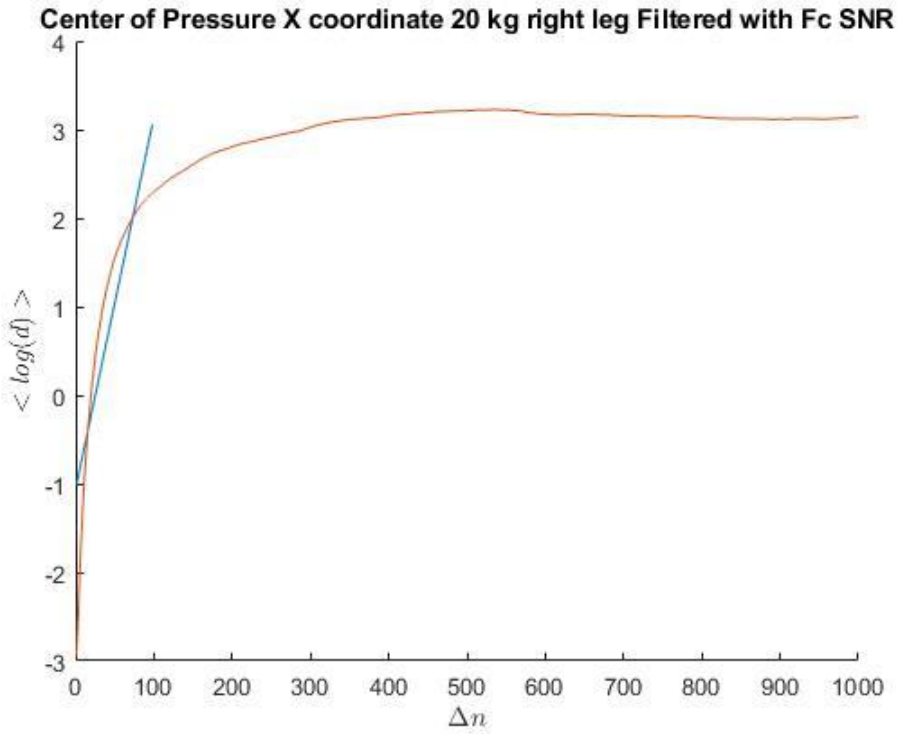

Figure 151 Divergence Curve of Center of Pressure X coordinate 20 kg right leg Filtered with cut off Frequency using SNR Analysis and 0.9 Correlation Coefficient Regression Line.

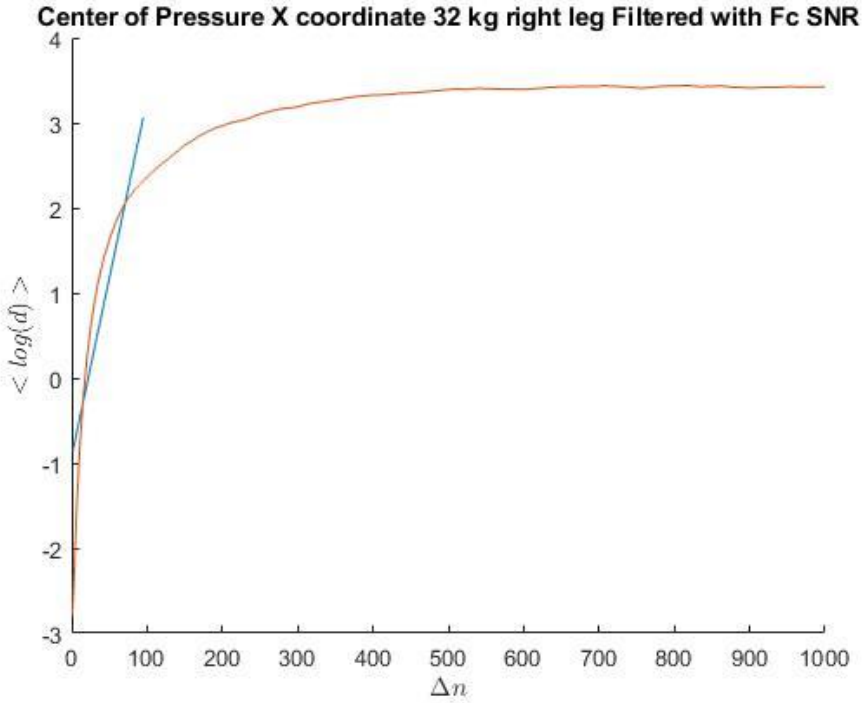

Figure 152 Divergence Curve of Center of Pressure X coordinate 32 kg right leg Filtered with cut off Frequency using SNR Analysis and 0.9 Correlation Coefficient Regression Line.

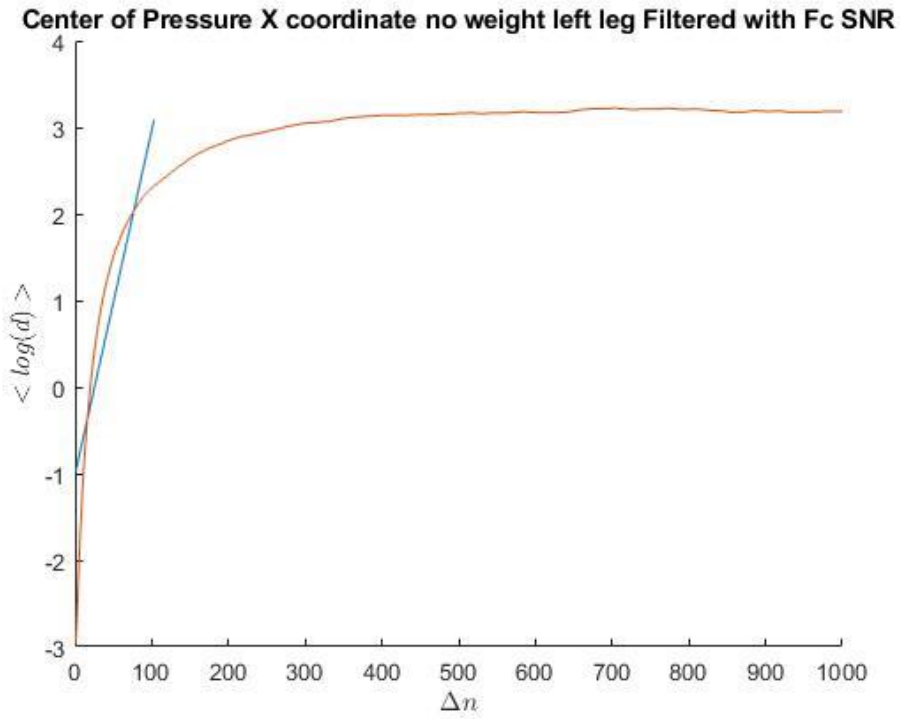

Figure 153 Divergence Curve of Center of Pressure X coordinates no weight left leg Filtered with cut off Frequency using SNR Analysis and 0.9 Correlation Coefficient Regression Line.

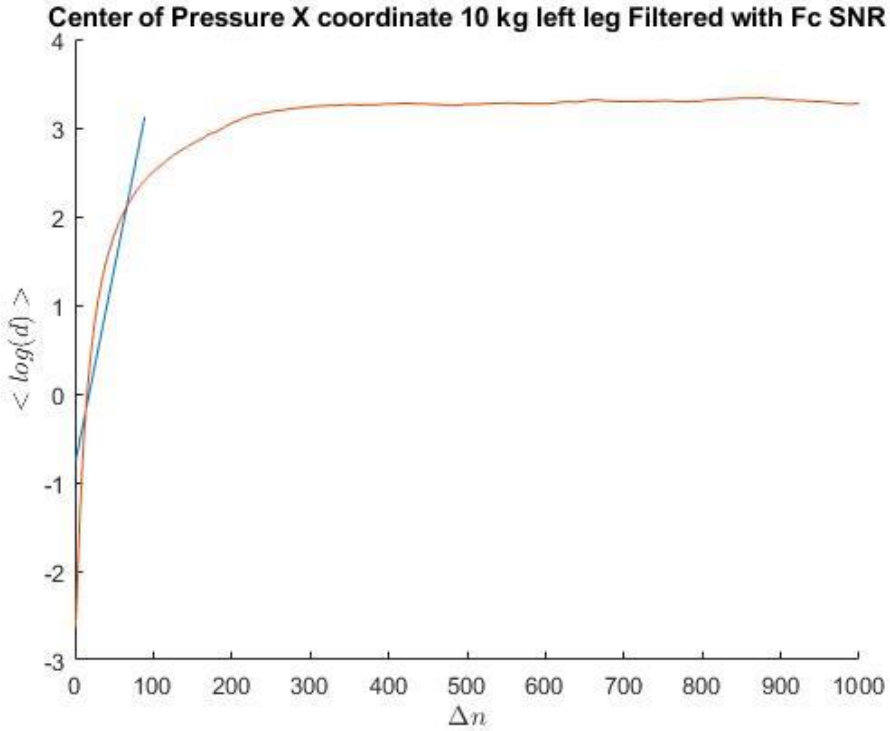

Figure 154 Divergence Curve of Center of Pressure X coordinate 10 kg left leg Filtered with cut off Frequency using SNR Analysis and 0.9 Correlation Coefficient Regression Line.

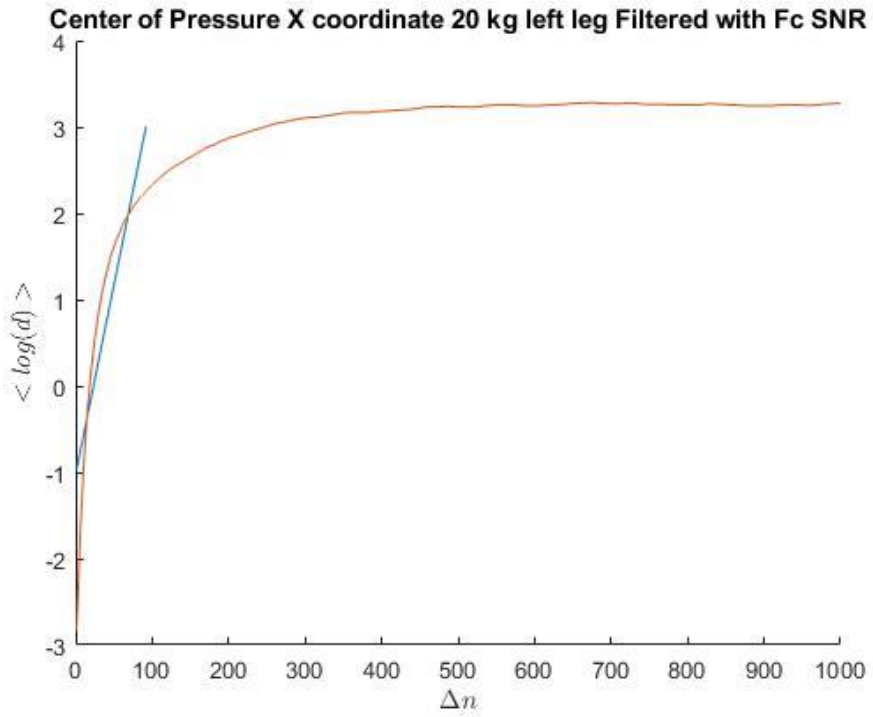

Figure 155 Divergence Curve of Center of Pressure X coordinate 20 kg left leg Filtered with cut off Frequency using SNR Analysis and 0.9 Correlation Coefficient Regression Line.

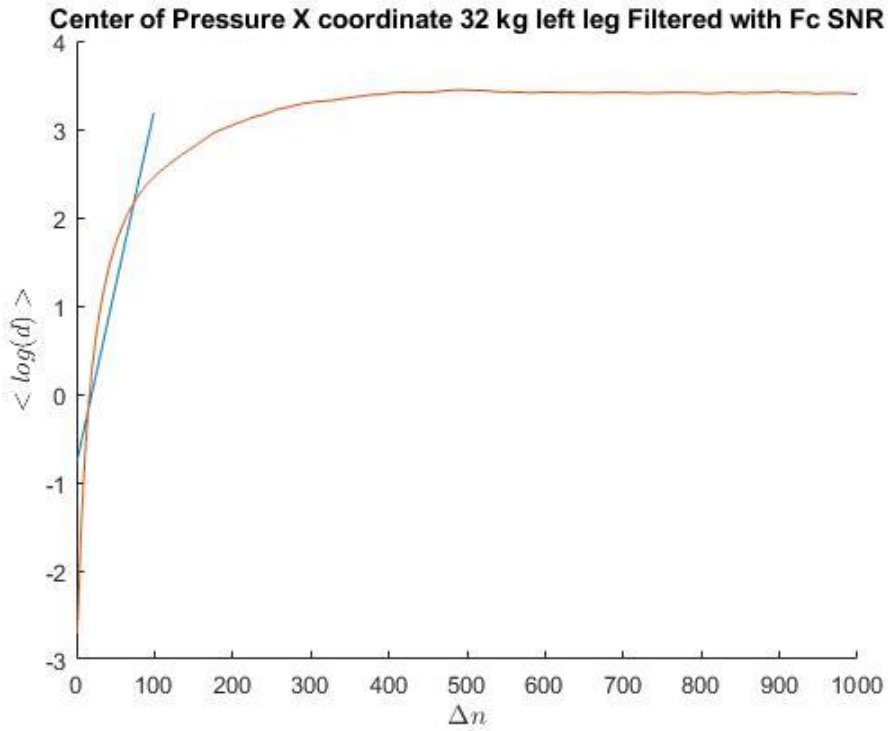

Figure 156 Divergence Curve of Center of Pressure X coordinate 32 kg left leg Filtered with cut off Frequency using SNR Analysis and 0.9 Correlation Coefficient Regression Line.

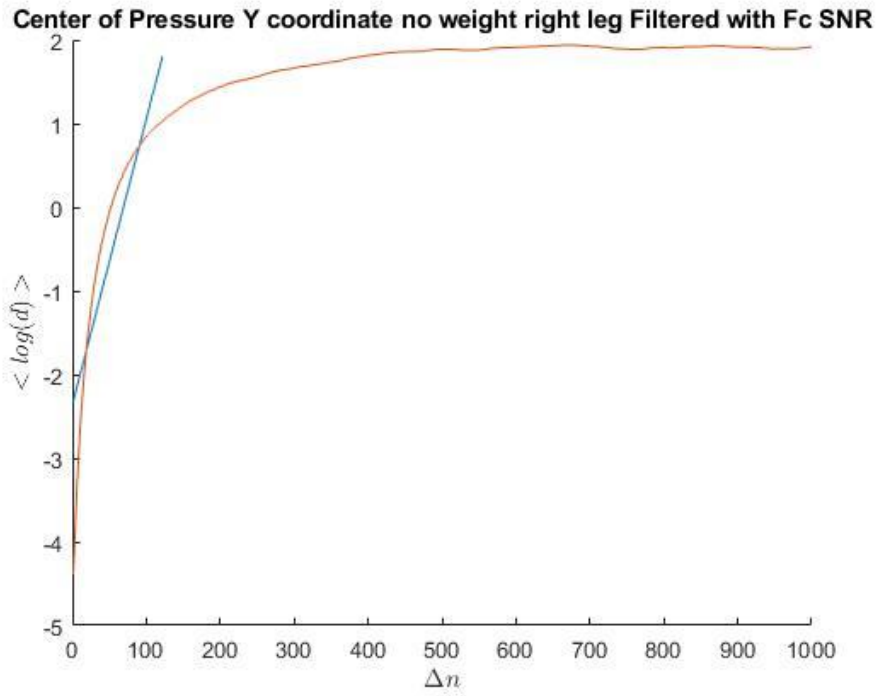

Figure 157 Divergence Curve of Center of Pressure Y coordinate no weight right leg Filtered with cut off Frequency using SNR Analysis and 0.9 Correlation Coefficient Regression Line.

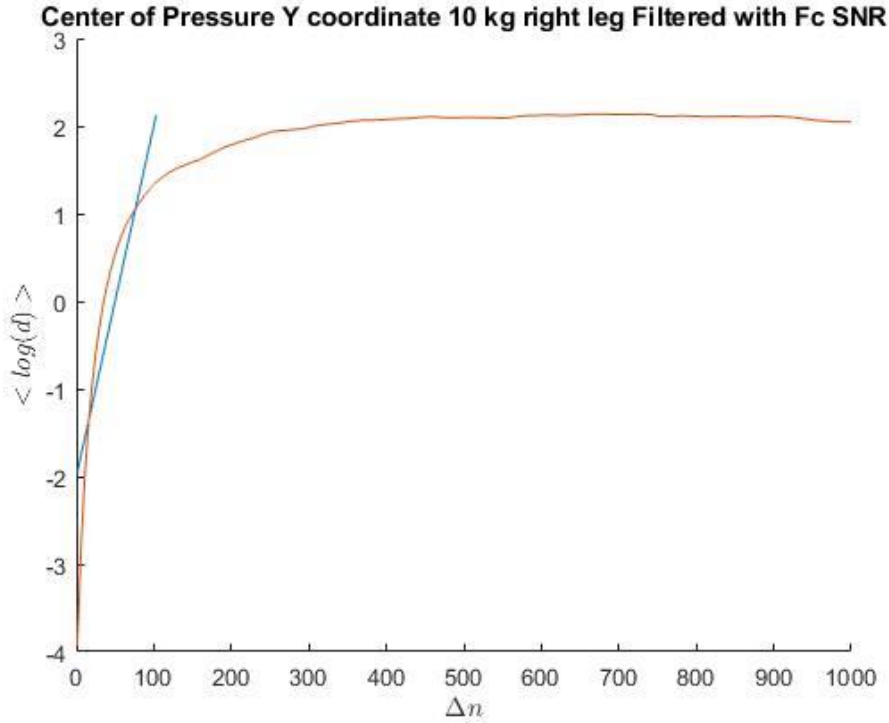

Figure 158 Divergence Curve of Center of Pressure Y coordinate 10 kg right leg Filtered with cut off Frequency using SNR Analysis and 0.9 Correlation Coefficient Regression Line.

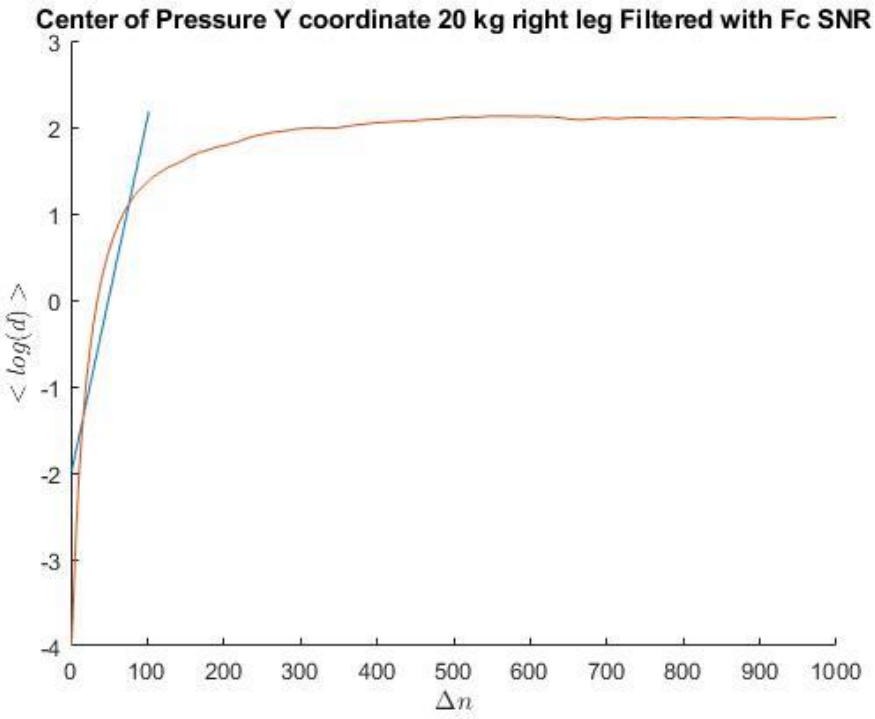

Figure 159 Divergence Curve of Center of Pressure Y coordinate 20 kg right leg Filtered with cut off Frequency using SNR Analysis and 0.9 Correlation Coefficient Regression Line.

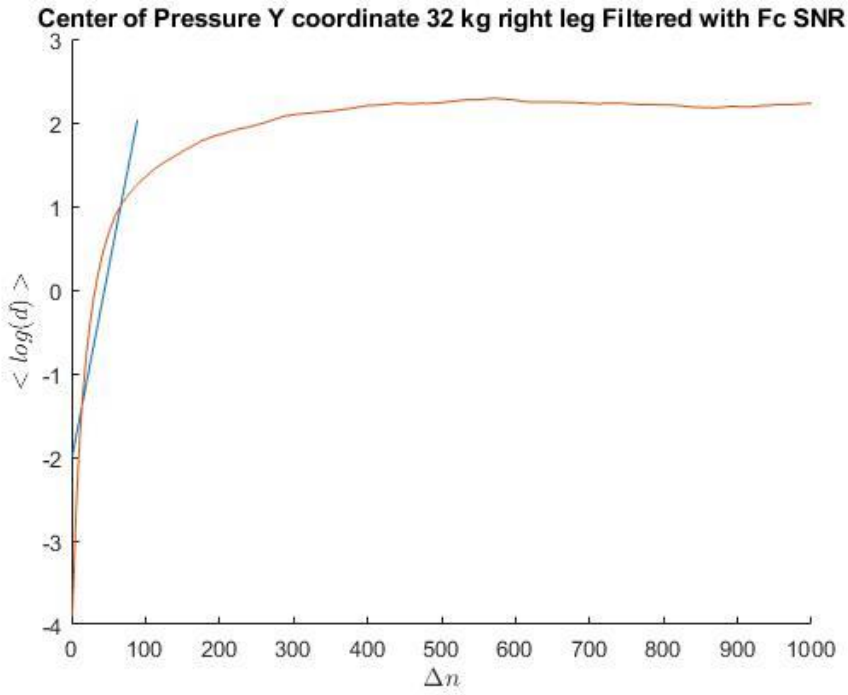

Figure 160 Divergence Curve of Center of Pressure Y coordinate 32 kg right leg Filtered with cut off Frequency using SNR Analysis and 0.9 Correlation Coefficient Regression Line.

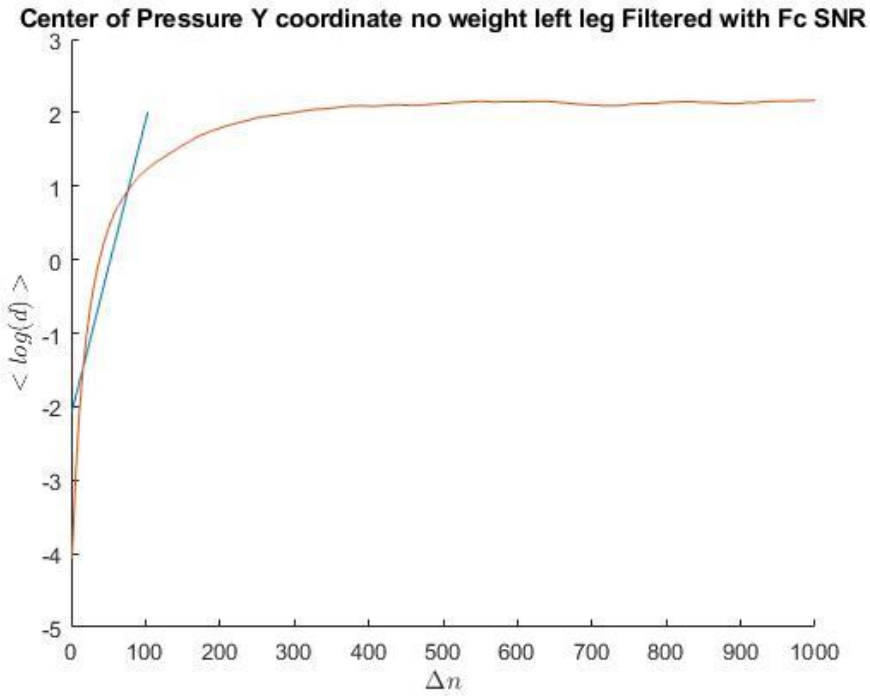

Figure 161 Divergence Curve of Center of Pressure Y coordinates no weight left leg Filtered with cut off Frequency using SNR Analysis and 0.9 Correlation Coefficient Regression Line.

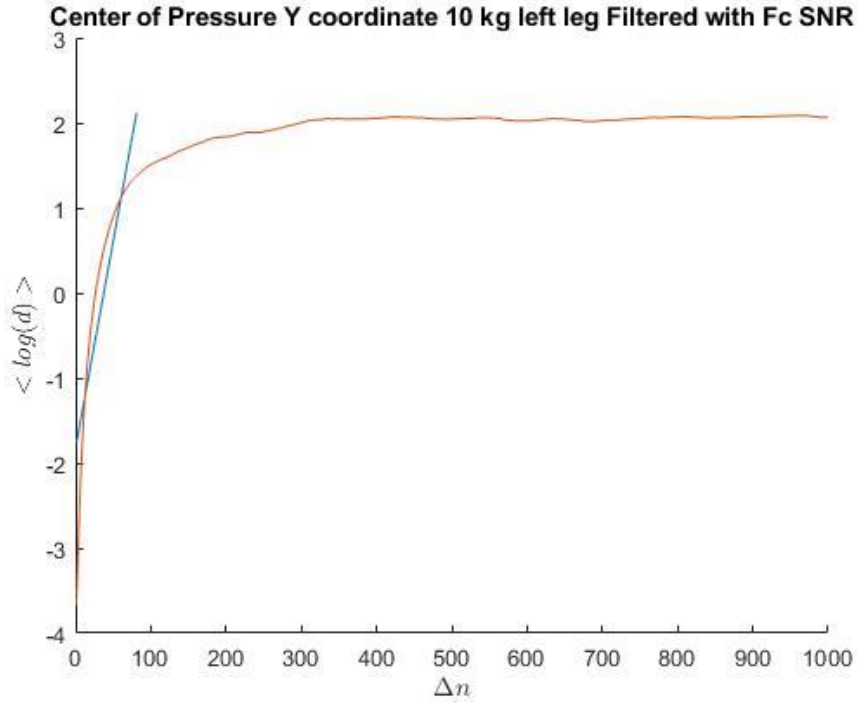

Figure 162 Divergence Curve of Center of Pressure Y coordinate 10 kg left leg Filtered with cut off Frequency using SNR Analysis and 0.9 Correlation Coefficient Regression Line.

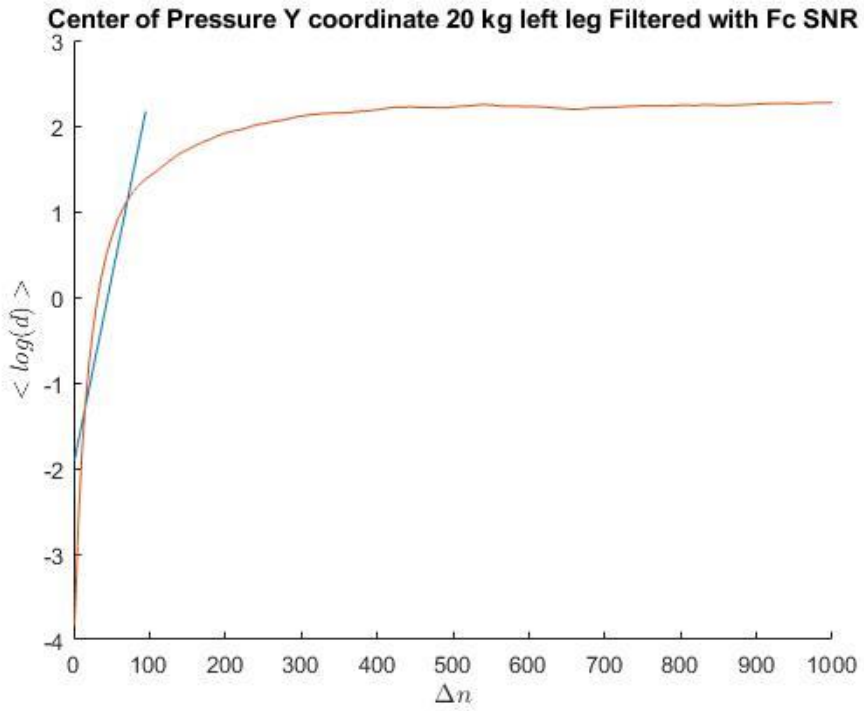

Figure 163 Divergence Curve of Center of Pressure Y coordinate 20 kg right leg Filtered with cut off Frequency using SNR Analysis and 0.9 Correlation Coefficient Regression Line.

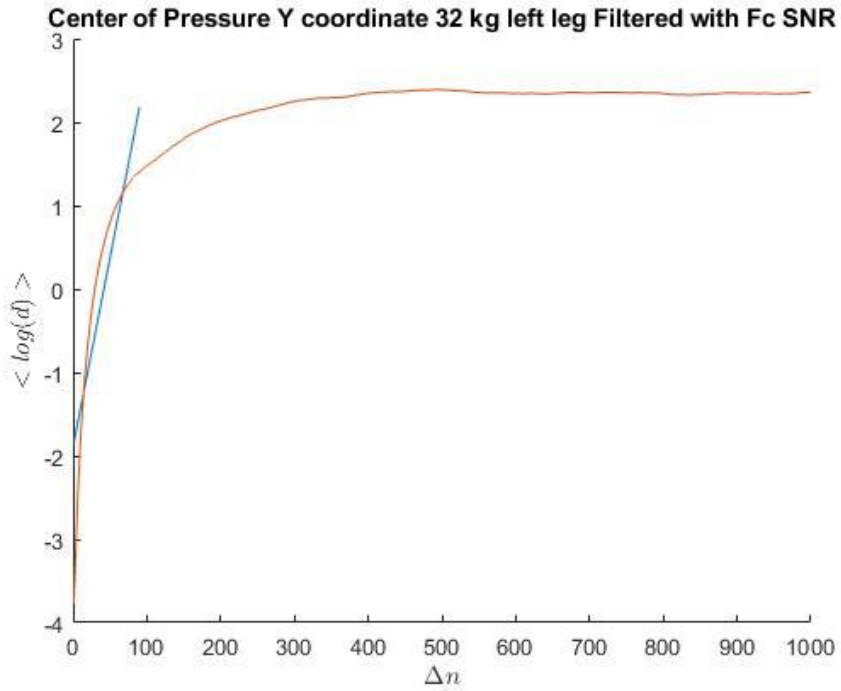

Figure 164 Divergence Curve of Center of Pressure Y coordinate 32 kg left leg Filtered with cut off Frequency using SNR Analysis and 0.9 Correlation Coefficient Regression Line.

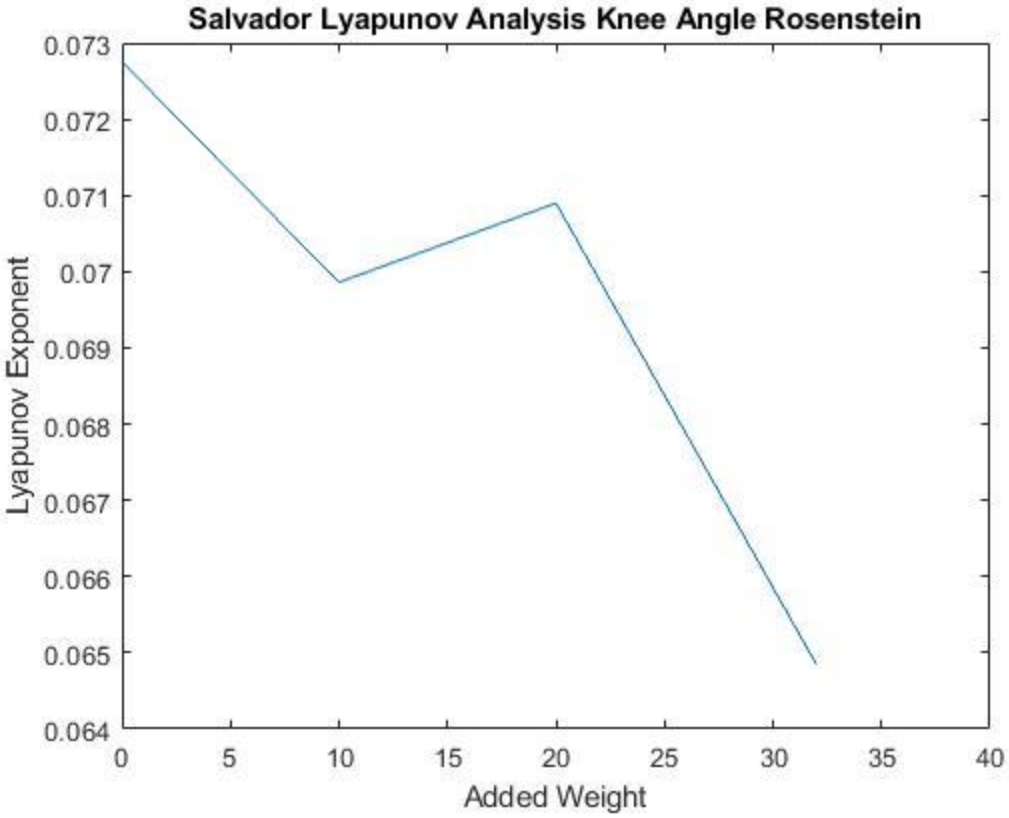

Figure 165 Subject Salvador Lyapunov Exponent Values

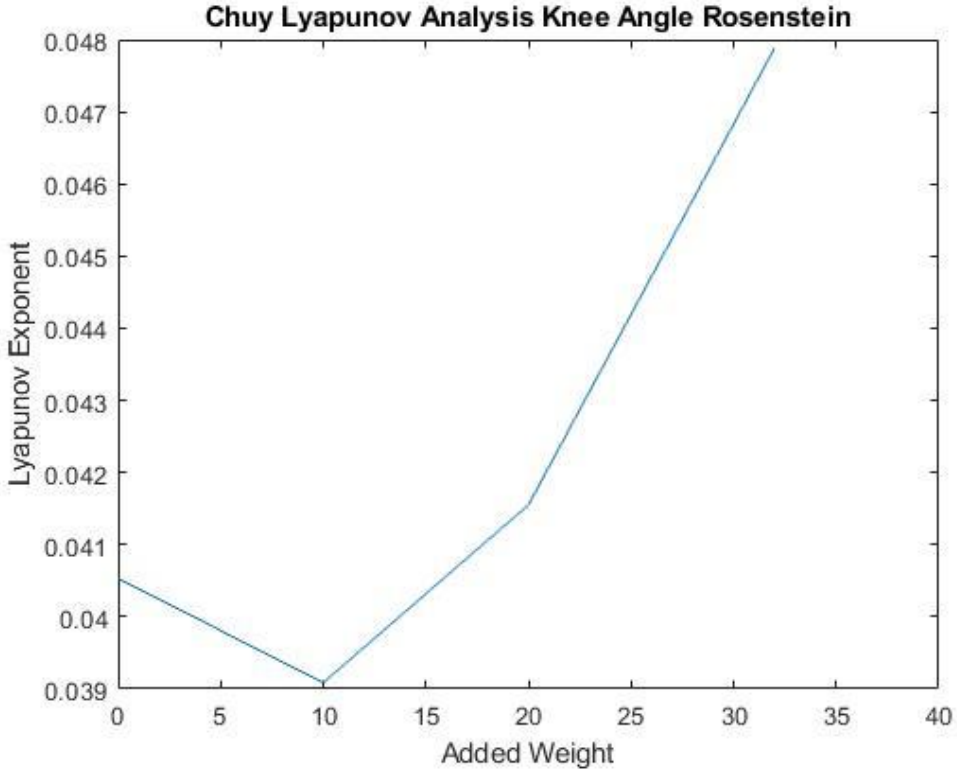

Figure 166 Subject Chuy Lyapunov Exponent Values

BIOGRAPHICAL SKETCH

Jose de Jesus Galarza was born in June 30th 1986. He earned a Bachelors in Engineering in Monterrey at the Universidad de Monterrey. He earned a Masters in Science in Mathematics from The University of Texas Rio Grande Valley in May 2017. He earned a Master of Science in Engineering from The University of Texas Rio Grande Valley in August 2021.

Contact email; jose.galarza01@utrgv.edu